AN INTERFEROMETRIC STUDY

OF

JUPITER'S DECIMETER RADIO EMISSION

Thesis by

Glenn LeRoy Berge

In Partial Fulfillment of the Requirements

For the Degree of

Doctor of Philosophy

California Institute of Technology

Pasadena, California

1965

(Submitted April 30, 1965)

ACKNOWLEDGEMENTS

I wish to thank G. J. Stanley, Director of the Owens Valley Radio Observatory, for suggesting this investigation and for providing the observing time necessary to conduct it. I am indebted to D. Morris and J. D. Wyndham for assisting with the observations and with some of the preliminary data reduction. I have benefited from discussions with several people, especially D. Morris and V. Radhakrishnan. J. A. Roberts has provided much useful information in advance of publication. J. F. Bartlett furnished invaluable assistance with the computer programming. I also wish to thank the many unnamed people who have been responsible for developing and maintaining the equipment at the Owens Valley Radio Observatory.

The research in radio astronomy at the Owens Valley Radio Observatory is supported by the United States Office of Naval Research under contract Nonr 220(19).

ABSTRACT

An interferometric study of the decimeter radio emission from the planet Jupiter has recently been carried out at the Owens Valley Radio Observatory. Using the two 90-foot paraboloids as an interference polarimeter, observations have been made with various east-west spacings ranging from 300 to 4700λ at 10.4 cm. and 300 to 2300λ at 21.2 cm. and also with some critical north-south spacings at 10.4 cm.

The visibility functions obtained are consistent with earlier measurements, which gave the polar and equatorial dimensions as one and three planetary diameters respectively, but they are more complete and extend to larger baselines. They permit the fitting of a rather detailed model for the decimeter brightness distribution. The observations are consistent with a symmetrical synchrotron emission source having the polarization properties one would expect with a dipole magnetic field. It probably is centered quite closely on the planetary disk, which is itself seen as a thermal radio source.

The observations also indicate the presence of a small circularly polarized component in the radiation which varies in magnitude and sense as Jupiter rotates. Another result is that the disk emission at 10.4 cm.

is about twice the thermal emission one would expect for a temperature of 130° K.

The implications of the various results are discussed.

Table of Contents

I. INTRODUCTION

For thousands of years the planet Jupiter has been a source of wonder to those who observed this "wandering star". In the past ten years Jupiter has again become a source of wonder - this time because of the nature of its radio emission. It has been known for some time that the equivalent black body temperature of Jupiter's disk at infrared wavelengths is about 130°K. (1). In the radio region, such a temperature would lead to a signal which could easily be detected by modern techniques at wavelengths of a few centimeters. However, the first radio observations of Jupiter had nothing to do with the thermal emission and were completely unexpected.

In 1955, B. F. Burke and K. L. Franklin discovered, by a combination of inspiration and accidental good fortune, that Jupiter sometimes emits very powerful bursts in the decameter region of the radio spectrum (2). Their frequency happened to be 22.2 Mc/s, and the bursts have since been observed throughout the range from about 5 to 40 Mc/s. The power and intermittent nature of the bursts definitely indicated a non-thermal origin. In addition to being an important discovery, this work called the attention of radio astronomers very dramatically to the planet Jupiter.

The next year (1956) C. H. Mayer, T. P. McCullough, and R. M. Sloanaker began a series of observations of Jupiter at a wavelength of 3.15 cm. (3),(4). They found that the equivalent black body disk temperature was about 140°K. for this wavelength. The agreement with the infrared temperature was therefore very good. Later observations in this wavelength region gave similar or slightly higher disk temperatures. There was no rush to go to somewhat longer wavelengths because it was assumed that the flux density would go as λ^{-2}, thus making detection difficult.

A surprise came in 1958 when R. M. Sloanaker and E. F. McClain made observations at 10.3 cm (5),(6) and discovered that the flux density was unexpectedly large, giving a disk temperature of 640°K. Observations at still longer wavelengths showed that the disk temperature continued to rise with wavelength. It is now thought that the enhanced emission in the decimeter range is due to synchrotron radiation from a Jovian Van Allen belt.

The radio emission of Jupiter can, as we have seen, be divided conveniently into three parts:

1) Decameter: non-thermal bursts,
2) Decimeter: mostly synchrotron emission,
3) Centimeter and shorter: mostly thermal emission from the disk.

The present observations were made at 10.4 and 21.2 cm. Hence, we will be concerned mainly with the second case,

plus a minor but important contribution from the third case.

Table I is an attempt to show the state of knowledge about the subject which existed while this project was being undertaken. It is a brief, but fairly comprehensive summary of the history of centimeter and decimeter observations of Jupiter. The entries are roughly in chronological order according to the time of observation. It is up-to-date except for information found by the present investigation, some of which has been published (7),(8). Table II, consisting of additional work of a theoretical or review nature, has been added for completeness.

It is clear that a great deal of single-dish (meaning unresolved in this case) work has been done on the centimeter and decimeter emission of Jupiter. At the present time, the latest publication of Roberts and Komesaroff (9) may be considered the definitive work, with regard to sensitivity and completeness, on the integrated decimeter emission of Jupiter. We may summarize the integrated emission results as follows:

a. The spectrum of the non-thermal emission is very flat over the range from 10 cm. to 100 cm. with a flux density of about $6.7 \times 10^{-26} \mathrm{Wm}^{-2}(\mathrm{c/s})^{-1}$.

b. Over this range, the percentage polarization is constant at 22 percent (linear polarization). The circular polari-

TABLE I A CHRONOLOGY OF CENTIMETER AND DECIMETER RADIO OBSERVATIONS OF JUPITER

Observers	Observing Period	Wavelength (cm.)	Flux Density(a)	T_D(K°) (a)	ϕ (Deg.)(b)	Additional Results, Comments, and Conclusions	References (c)
Mayer McCullough Sloanaker	May 13 & 31, 1956	3.15	15.9±6.4	140±56		The results agree with the infrared disk temperature (130°K).	(3),(4), (13)
	March 23-Apr. 1, 1957		16.5±3.0	145±26			
Drake Ewen	July 24, 1957	3.75	~16	~200			(14)
Mills Little Sheridan Slee	Before Oct., 1957	350	<5	<500,000			(15)
Giordmaine Alsop Townes Mayer	Apr.1958	3.18	18.4±1.9	165±17		They used a maser amplifier with the same antenna used by Mayer, McCullough and Sloanaker. There seemed to be detectable fluctuations not correlated with the rotation. On Apr. 30-May 1, 1958, a disk temperature of 268°K was observed at 3.36 cm.	(16),(17), (18),(19)
	Apr. 16-May 8, 1958	3.36	18.9±2.0	189±20			
	May 24-July 29, 1958; Jan 31-Feb. 7, 1959	3.17	19.4±2.2	173±20			
	Aug. 22-Sept. 4, 1958	3.03	21.0±2.5	171±20			

Observers	Observing Period	Wavelength (cm)	Flux Density(a)	T_D(K°) (a)	ϕ (Deg.)(b)	Additional Results, Comments, and Conclusions	References
Sloanaker McClain	June 10-Aug. 20, 1958	10.2 and 10.3	6.9±0.9	640±85	67±0.5	The flux density measured is far too large to be explained by a body at 130°K. There were no long-term trends over the observing period. There may be a cyclical variation of about 30 percent correlated with a rotational period 40^s to 2^m longer than System II. (One cycle per rotation period.)	(5),(6), (13),(20), (21)
Roberts, J. Stanley	Apr. 15-June 17, 1959	31.3	6.3±1.7	5500 ±1500	77	Large variations were noticed, but they were not significantly larger than the variations due to noise which were seen on other weak sources. There was no correlation with Jupiter's rotation or with solar activity. Two possible mechanisms are discussed: free-free emission in a Jovian corona and synchrotron emission in a Jovian Van Allen belt.	(22)
McClain Nichols Waak	May 15-July 31, 1959	21	6.4±1.2	2500 ±450	76	The emission seemed to be enhanced by about 15 percent near LCM=73° (System III). There was no correlation with solar activity except possibly a slightly elevated temperature following a flare and an intense aurorae. The disk temperature seemed to decrease	(23,)(24), (25

Observers	Observing Period	Wavelength (cm.)	Flux Density(a)	T_D(K°) (a)	φ (Deg.)(b)	Additional Results, Comments, and Conclusions	References (c)
McClain Nichols Waak, Continued						with time during the observing interval.	
Epstein	May 16-June 2, 1959	21	7.7	3000	14	There were variations of as much as a factor of two in a period of a few hours.	(26)
Drake Hvatum	May, 1959	22	~7.0	~3000	76	The data suggest variations of 30 percent in the flux over a period of several days. The variations are not correlated with Jupiter's rotation. It was suggested that the mechanism responsible for the decimeter emission was synchrotron emission in a Jovian Van Allen belt. Drake was the first to consider this mechanism.	(27),(28)
Drake Hvatum	May 26,27, 1959	68	~10.7	~44,000	14	There were no significant short period variations in the flux.	(28),(29)
	July 20-30, 1959	68	~8.3	~34,000	15		
	Oct., 1959	68	~2.4	~10,000	14		
Long Elsmore	Sept. 16, 17, 1959 Mar. 4-9, 1960, Mar. 15-18, 1960	73	<2(d)	<10,000 (d)			(30)

Observers	Observing Period	Wavelength (cm.)	Flux Density(a)	T_D(K°) (a)	ϕ (Deg.)(b)	Additional Results, Comments, and Conclusions	References (c)
Long Elsmore,Cont.	Mar. 20-23, 1960						
Sloanaker Boland	Oct. 16-30, 1959	10.2 10.3	3.4±0.7	315±65	79	The decrease by a factor of two since the 1958 observations is considered to be real and may be related to an increase in solar activity. The previous correlation with rotation may have been premature.	(20),(21)
Radhakrishnan Roberts, J.	April, 1960	31.3			Varied	There were two very important results: Measurements with different feed horn orientations indicated that the radiation at 31 cm. was highly polarized (~30 percent with the E-vector within 12 degrees of Jupiter's equator). Long baseline interferometer measurements showed that the equatorial extent of the source was about three times the planetary disk.	(10)
Morris Berge	Jan. 23-29 Feb.13-18,1961	31.3	6.7±0.9	5800± 800	Varied	Interferometer observations showed no significant difference in the brightness distribution or polarization between the two wavelengths. This supported the synchrotron	(7),(31)

Observers	Observing Period	Wavelength (cm.)	Flux Density	T_D(K°) (a)	ϕ (Deg.)(b)	Additional Results, Comments, and Conclusions	References (c)
Morris Berge, Cont.	June 1-10, July 8-10,22-29, 1961	21.6	8.2±1.2	3400± 500	Varied	mechanism. The 1/e gaussian size was about one and three planetary diameters for the polar and equatorial dimensions respectively. A time variation of the plane of polarization was noticed; one cycle with a peak-to-peak amplitude of about 18° for each rotation of the planet. This indicated that the magnetic axis was tilted by about 9° with respect to the rotational axis with the magnetic poles at λ_{III}=20° and 200° (A later analysis showed that the pole at 200° was in the northern hemisphere.). The integrated radiation went through a double cycle variation of a few percent for each rotation: the radiation was more intense when observed from Jupiter's magnetic equatorial plane.	
Roberts, M.	Apr. 25-Nov. 30, 1961	21.1	9.9	3900	15	The observations indicated variations of a factor of 2-1/2. Using the 10.7 and 20 cm. solar flux as an index of solar activity there was a strong correlation between Jupiter's flux density and solar	(32),(33), (34)
			10.4	4100	24		

Observers	Observing Period	Wavelength (cm.)	Flux Density	T_D(K°) (a)	ϕ (Deg.)(b)	Additional Results, Comments, and Conclusions	References (c)
Roberts, M. Continued						activity with a phase lag of 0 to 6 days.	
Bash Drake Gundermann Heiles	May 1-Aug. 8, 1961, Sept. 17, 1962-Feb. 25, 1963	10.0	7.0(±0.2)	620(±15)	74°	The disk temperatures were very constant. The peak-to-peak fluctuations between different 6-day intervals was about 5 percent and the difference between the 1961 and 1962 means was 3 percent. There were variations correlated with Jupiter's rotation which gave a rotational period only 0^s.5 different from that adopted for System III. A model which took account of the polarization, tilt of magnetic axis, and beaming with unknown parameters was fitted with the following results: 7.8 percent linear polarization, 24°.3 tilt of magnetic axis, north pole of magnetic axis at λ_{III}=186°.8, strong beaming. Roberts and Komesaroff have recently shown (9) that the data would also fit a model with a much larger percentage polarization and much smaller tilt of the magnetic axis.	(35)

Observers	Observing Period	Wavelength (cm.)	Flux Density	T_D(K°) (a)	ϕ (Deg.)(b)	Additional Results, Comments and Conclusions	References (c)
Miller Gary	Aug.,1961 Sept.,1961	20.8 20.8	9.5±0.8 5.7±1.0	3630±300 2190±400	14 77	The data were consistent with the observations of Morris and Berge (7) concerning the polarization, tilt of the magnetic axis and beaming except that it seemed that the magnetic pole near λ_{III}=20° was in the northern hemisphere.	(36),(37), (38)
Boischot Ginat Kazes	Oct.,1961- Dec.,1962	21.0	6.6±0.5	2570±20	90		(39),(40)
Morris Bartlett	Apr. 4-21, 1962	10.6	8.3±1.0	830±100	Varied	20±5 percent linear polarization. 20°±11° tilt of magnetic axis. Magnetic pole at 260° ±70°.	(41)
Roberts, J. Komesaroff	Apr. 1, 1962	74			~90	This was an occultation of Jupiter by the moon. It showed that the radiation came from a region much larger than Jupiter's disk and that it had a limb brightened or double structure. There were signs of asymmetry, but the noise was too great to allow a definite model to be determined.	(9),(12), (42)

Observers	Observing Period	Wavelength (cm.)	Flux Density	T_D(K°) (a)	ϕ (Deg.)(b)	Additional Results, Comments and Conclusions	References (c)
Roberts, J. Komesaroff	May 29-30 June 1-4 Aug. 28, 29,31 Sept. 24, 27, 1962 Aug. 2-7, 1963	21	7.4	2900	Varied	The sensitivity was high enough to show that the curve of direction of polarization vs. LCM departed markedly from a sinusoid. This asymmetry was interpreted as being due to an asymmetry in the radiating region, either because of an off-center magnetic dipole, or else a non-dipole component in the field. This curve, observed over a range of one year, gave a rotation period which was within $0^s.5$ of that adopted for System III. The variation of flux density and percentage polarization with LCM was accurately determined. The flux density variation was closely correlated with the magnetic latitude of the earth as seen from Jupiter, and was explained by beaming of the synchrotron emission. It allowed a rough estimate of the electron pitch angle distribution to be made. The flux density was apparently 5 percent lower in 1963 than in 1962 and this change may have been real.	(9),(42), (43)

Observers	Observing Period	Wavelength (cm.)	Flux Density	$T_D(K°)$ (a)	ϕ (Deg.)(b)	Additional Results, Comments, and Conclusions	References (c)
Roberts, J. Komesaroff	May 30,31 June 1,3, 4 Sept. 24, 1962	74	6.4	31,000	Varied	The direction of polarization is severly affected by ionospheric Faraday rotation. The flux density variations due to beaming seem to be less than at 21 cm.	(9),(42)
Rose Bologna Sloanaker	July 8- Oct. 7, 1962	9.4	8.6±0.5	670±40	0,45,90, 135	19±2 percent linear polarization. 10°.5±2° tilt of magnetic axis. Magnetic poles: λ_{III}= 170°±20°(northern hemisphere) 350°±20°(southern hemisphere). There was some evidence for beaming with an enhancement of a few percent in the plane of the magnetic equator.	(44),(45) (e)
Roberts, J. Komesaroff	Aug. 24, 25,1962	10.0	9.8	870	Varied		(9)
Boischot Ginat Kazes	Sept.- Dec., 1962	13.0	6.8 ± 0.7	1010±100	90		(40)
Roberts, J. Komesaroff	Sept.26, 1962	100	8.2	73,000			(9)
Korolkov Parijsky Timofeeva	Oct.,Nov. 1962	3.02				95 percent of the radiation comes from a region with radius $R<1.1R_{Jup}$. The non-thermal component which they deduce is only $6\times10^{-27}Wm^{-2}(c/s)^{-1}$.	(46)

Observers	Observing Period	Wavelength (cm.)	Flux Density	$T_D(K°)$ (a)	ϕ (Deg.)(b)	Additional Results, Comments and Conclusions	References (c)
Parijsky	1962-63	3.02 6.5	22.7 ± 3.7 8.7	185 ± 30 324			(47)
Gary	Nov.,Dec., 1962 Jan.,1963	21.4	~7.5	~3000	24 and 66	22±2 percent linear polarization. 10°±1° tilt of magnetic axis. Magnetic pole: $\lambda_{III}=195°\pm3°$(northern hemisphere). The beaming effect is confirmed. There was a long term (few weeks) variation which may be correlated with solar activity and short term variations which may be due to confusion by background sources.	(48),(49)
Haddock Dickel	1963	3.75			Varied	5.8 percent linear polarization. 15 degree tilt of magnetic axis. Magnetic pole: $\lambda_{III}=187°$(northern hemisphere). The scatter was too great to detect variations in flux density as a function of LCM. The presence of polarization indicates that there is a significant fraction of non-thermal radiation at this wavelength.	(50)
Roberts, J. Komesaroff	June 10-12,1963	31.3	7.7	6700		The purpose of these observations was to look for circular polarization. The mean	(9)

Observers	Observing Period	Wavelength (cm.)	Flux Density	T_D(K°) (a)	ϕ (Deg.)(b)	Additional Results, Comments, and Conclusions	References (c)
Roberts, J. Komesaroff, Continued						circular polarization is ≤1 percent and at any given LCM it is ≤3 percent.	
Gower	June 22-July 1, 1963	169	5.7±0.6	144,000 ±15,000		The conclusion is that the spectrum of the non-thermal radiation is very flat. The observations set an upper limit of 3 planetary diameters for the (Gaussian) size of the source and an upper limit of 20 percent for the polarization.	(51)
Roberts, J. Komesaroff	Nov. 1,2, 1963	6	10.5	340	Varied	~9 percent linear polarization.	(9)
Roberts, J. Komesaroff	Nov. 6-11, 1963	11.3	7.5	850	Varied	The variations of polarization direction, flux density, and percentage polarization as a function of LCM are similar to those found at 21 cm. On the basis of all their Jupiter measurements, the authors conclude that the non-thermal spectrum is flat, thus revising Roberts' earlier estimate for the spectral index (66).	(9),(43)

NOTES - TABLE I

(a) The flux density is given in units of $10^{-26} Wm^{-2}(c/s)^{-1}$ for a standard Earth-Jupiter distance of 4.04 A.U. (polar semi-diameter = 22".75 and equatorial semi-distance = 24".38). The conversion between flux density (S) and equivalent black body disk temperature is accomplished by using the formula $T_D = \frac{S\lambda^2}{2K\Omega}$ where $\Omega = 4.096 \times 10^{-8}$ steradians.

(b) ϕ is the angle between Jupiter's equator and the E-vector of the antenna. In the papers describing some of the earlier observations, the plane of polarization of the antenna was not specified. In some of these cases, the information was taken from Roberts and Huguenin (34).

(c) The references given here, together with those in Table II, are intended to be a comprehensive listing of the literature available. Therefore, no attempt was made to avoid duplication in cases where a paper appears in a similar form in two or more places. Some references have certainly been overlooked, but most of these will be similar to ones which are cited.

(d) These limits for the flux density and disk temperature are for a source diameter of two minutes of arc. If the source were larger, the upper limits would be larger.

(e) The different references give somewhat different results. The results quoted are from the latest reference.

TABLE II ADDITIONAL WORK OF A THEORETICAL OR REVIEW NATURE

Authors	Date	Title	Comments	References
Roberts, J. Stanley	1959	"Radio Emission From Jupiter at a Wavelength of 31 cm."	In addition to presenting new observational results, the authors consider two possible mechanisms for the large decimeter emission: free-free emission in a Jovian corona, and synchrotron emission in a Jovian Van Allen belt.	(22)
Field	1959	"The Source of Radiation From Jupiter at Decimeter Wavelengths" 1.	Four mechanisms are considered: a) Thermal radiation from Jupiter's atmosphere. b) Free-free emission in an ionosphere. c) Cyclotron emission in a Van Allen belt. d) Synchrotron emission in a Van Allen belt.	(52)
	1960	2. "Cyclotron Radiation by Trapped Electrons"	Part (c) in the first paper is explored in more detail.	(53)
	1961	3. "Time Dependence of Cyclotron Radiation"	Field concludes, from theoretical considerations, that the cyclotron mechanism could not explain the variations with time which had been reported. (The interferometer observations, which dealt a severe blow to the cyclotron mechanism were not yet available.)	(54)

Authors	Date	Title	Comments	References
Davis Chang	1961	"Synchrotron Radiation as the Source of Jupiter's Polarized Decimeter Radiation"	The authors decide that the synchrotron mechanism is the most likely and they compute roughly what the magnetic field strength, electron energies, and electron density must be in the radiating region.	(55)
	1962	"On the Effect of Geomagnetic Fluctuations on Trapped Particles"		(56),(57)
Chang	1960 1962	"Synchrotron Radiation as the Source of the Polarized Decimeter Radiation from Jupiter"	The author derives a Stokes parameter description for synchrotron radiation from relativistic electrons trapped in a planetary dipole magnetic field. For a range of specified models, he computes the transforms one would obtain by observing with an interferometer. He also considers the problem of accelerating the electrons.	(58),(59)
Chang Davis	1962	"Synchrotron Radiation as the Source of the Polarized Decimeter Radiation from Jupiter"	This is essentially a summary of Chang's thesis (59).	(60)
Roberts, M. Huguenin	1963	"The Radiation Belt of Jupiter"	The authors maintain that Jupiter's decimeter radiation consists of three components: a) A thermal component corresponding to the infrared temperature of 130°K. b) A non-thermal, non-polarized component, perhaps originating in an ionosphere.	(34)

Authors	Date	Title	Comments	References
Roberts, M. Huguenin, Continued			c) A non-thermal, polarized component due to synchrotron emission. This component undergoes large variations correlated with solar activity.	
Thorne	1963	"The Theory of Synchrotron Radiation From Stars with Dipole Magnetic Field"	Although this investigation was concerned with stars, it can also be applied to Jupiter. The author has since done some computations specifically for Jupiter.	(61)
Korchak	1963	"The Polarization of Synchrotron Radiation in a Dipole Field"		(62)
Mayer	1961	"Radio Emission of the Moon and Planets"		(63)
	1962	"General Report on Planetary Radio Astronomy"		(64)
Drake	1961	"Radio Emission From the Planets"		(65)
Roberts, J.	1963	"Radio Emission From the Planets"	This comprehensive summary includes some unpublished (at the time) data by Roberts and Komesaroff. The author concludes that the flux increases with the wavelength as $\lambda^{0.3}$. He also concludes that many of the reported time variations were caused by signal-to-noise or stability limitations, by confusion, or by the source polarization.	(66)

Authors	Date	Title	Comments	References
Wildt Smith, H. Salpeter Cameron	1963	"The Planet Jupiter"	This is a summary of a conference sponsored by NASA and held at the Institute for Space Studies in New York in October, 1962.	(67)
Smith, A. Carr	1964	"Radio Exploration of the Planetary System"		(68)
Warwick	1964	"Radio Emission From Jupiter"	In addition to his review, Warwick investigates some new ideas. One is an attempt to explain the asymmetry noticed by Roberts and Komesaroff (43) by the shadowing of a synchrotron emission region by Jupiter's disk.	(69)

zation is <1 percent on the average and is always <3 percent at 31 cm., according to Roberts and Komesaroff (9).

c. Studies of the change of polarization direction with longitude of the central meridian have shown that the magnetic axis is tipped by about 9° with respect to the rotational axis. The non-sinusoidal character of this variation indicates an asymmetry of the source.

d. Studies of the variation of total flux density with longitude of the central meridian have shown that the radiation is strongly beamed in the plane of the magnetic equator. The variation is obtained as the magnetic axis apparently rocks to and fro.

e. Observations of (c) and (d) over a long time range indicate that the rotational period based on the rocking of the magnetic axis is the same as the System III period to within $0^{s}.5$.

f. There is now a large suspicion that the spectacular variations reported earlier, whether correlated with solar activity or not, were ficticious and that the only variations are those identified with the rotation and perhaps small, long-term changes (on the order of a year or years). However, the most precise measurements were made at solar minimum, and it is possible that at solar maximum there are striking changes.

In contrast to this detailed picture of the integrated emission, high resolution studies of Jupiter

were still at a rather primitive level when the present investigation was begun. The interferometric work at Caltech by Radhakrishnan and Roberts (10) and Morris and Berge (11) had established that the radiation came from a region larger than the planetary disk. An elliptical gaussian fitted to the observations had polar and equatorial dimensions of about one and three planetary diameters respectively at both 21 and 31 cm. An occultation observation at 74 cm. with the 210-foot CSIRO antenna (9), (12), (42) tended to confirm the large extent of the source. The angular size data together with the polarization data provided a strong indication that the non-thermal decimeter radiation was caused by the synchrotron mechanism (55), (59), (60).

At the time of the opposition of Jupiter in 1963, it was deemed worthwhile to begin a new and extensive high resolution observing program of the planet at the Caltech Owens Valley Radio Observatory. There were several reasons for thinking that the previous observations could be greatly improved upon:

a) Receivers and associated equipment were now available for a wavelength of 10 cm., thus doubling the largest possible baseline as measured in wavelengths.

b) It was now possible to obtain lower system noise temperatures, due largely to a parametric amplifier operating at 10 cm. and a travelling-wave maser operating at 21 cm.

c) A mechanical integration system was now available. It greatly increased the accuracy of obtaining amplitude and phase information from the interference fringes produced by weak signals. This, in effect, improved the sensitivity.
d) The method for rotating the feed horns had been improved, both in ease of operation and in setting accuracy.

This thesis is to be a discussion of all the Caltech radio observations of Jupiter from October, 1963 to the present time, together with the results and implications of these observations.

II. OBSERVATIONS

A. Equipment

All of the observations to be described were made with the two-element interferometer at the Caltech Owens Valley Radio Observatory. Each of the elements is an equatorially-mounted, 90-foot diameter, parabolic antenna. The feed of each antenna can be rotated remotely from the observing room, and the resulting position angle is displayed in this room. Each antenna can be moved along tracks to a maximum separation of 1800 feet east-west and 1600 feet north-south. While in use, each is fixed at one of a number of possible discrete stations located along the tracks. For the wavelengths used in this investigation, 10.4 cm. and 21.2 cm., the antenna beamwidth, between half-power points, was 18' and 33' respectively.

Figure 1 is a block diagram which describes the receiving equipment. Although its details evolved during the course of the observations, it was always similar, in general concept, to that used by Clark and Kuz'min (70) for their observations of Venus. The boxes outlined with dashed lines in the upper left and right corners indicate what was located at the antennas, namely, a klystron local oscillator with a phase-lock system, occasionally a RF preamplifier, a crystal mixer, and a low-noise intermediate

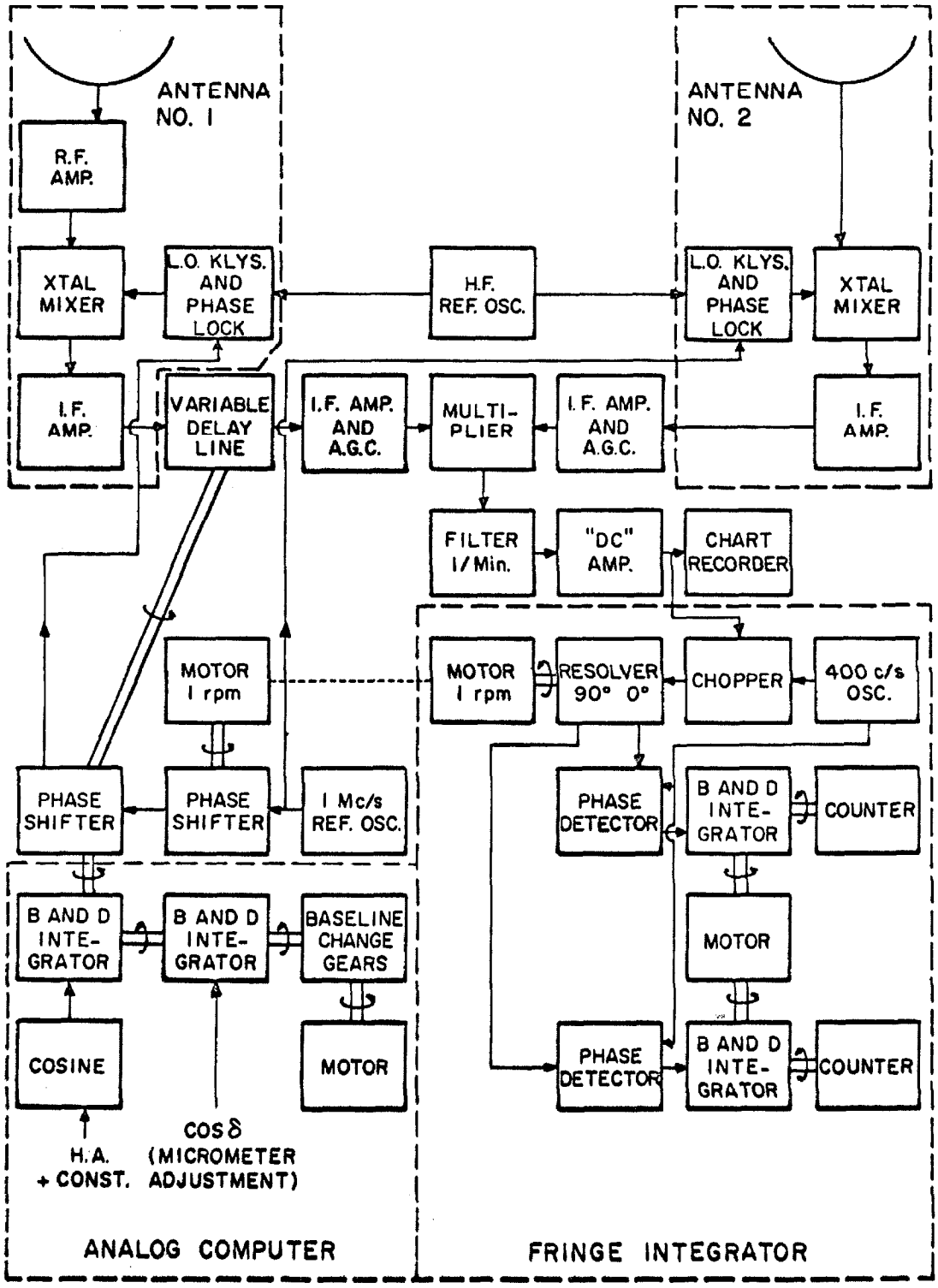

Figure 1. Block diagram of the receiving equipment.

frequency amplifier. Everything else was located in the observing room. The noise temperature of the receivers was about 500° K. at 10.4 cm. and about 400°K. at 21.2 cm. However, for most of the 10.4 cm. observations, a low-noise parametric amplifier was used as a RF amplifier preceding the crystal mixer of one antenna. This reduced the system temperature to about 250°K. For some of the 21.2 cm. observations, a travelling wave maser provided by the Bell Telephone Laboratories, was used in the same way to provide a system temperature of about 180°K.

Each local oscillator was phase-locked to the sum of frequencies provided by a central high frequency reference oscillator and a 1 Mc/s low frequency reference. The high frequency reference was usually not crystal stabilized, but the frequency drift over a period of several days was less than 1 Mc/s. The intermediate frequency was 10 Mc/s. The bandwidth was 5 Mc/s, and the image was not rejected. After arriving at the observing room, the signals from the two antennas underwent more IF amplification, at which time an automatic gain control stabilized the gain of each channel by keeping the total noise constant in each. The two IF signals were then correlated in a diode multiplier.

A mechanical analogue computer was used to provide a continuous computation of the instantaneous

fringe rate for the source being observed. Its output was used to drive a phase shifter which changed the phase of the local oscillator in one arm of the interferometer at the natural fringe rate. The purpose of this was to move the interferometer fringes in the sky at the same rate as the source. In addition, another phase shifter added an exact 1 RPM phase change in the local oscillator. The resulting interferometer fringe frequency was one per minute (within the mechanical tolerances of the computer) regardless of the baseline or source position. In addition to providing a convenient fringe rate, this system eliminated the need for making a correction for filter attenuation as a function of fringe rate.

The computer output also controlled the tracking of a variable delay line in the IF path from one antenna. The delay error was never more than a few nanoseconds, that is, very much less than the deviation required to produce complete cancellation between the two sidebands ($\Delta t \approx \frac{1}{2} \frac{1}{\Delta f} \approx 25$ ns).

The one per minute fringe was filtered and, after amplification, was fed to a chart recorder and a mechanical integrator. In the integrator, the output signal was multiplied by a one per minute sine wave and also by a one per minute cosine wave, that is, a second sine wave shifted by 90° with respect to the first. The

two outputs were then integrated by two ball and disk integrators operating mechanical counters. The reason for having two correlators is that there is, in general, a constant (within the computer tolerances) phase difference between the sine wave and the fringe pattern. The fringe amplitude is proportional to the square root of the sum of the squares of the integrator outputs. By considering one output as a sine channel and the other as a cosine channel, one can obtain the phase of the natural fringes with respect to the computer fringes.

B. Observing Procedure

Table III summarizes the observations which were made for this investigation. The total integration time on Jupiter was about 235 hours. This does not include the time spent on such things as rotating the feed horns between integrations or observing other sources for calibration purposes. To do such a study on a typical radio source with a similar size would require only a fraction of this observing time. However, as we saw in the introduction, Jupiter is not a typical radio source. It changes its radio appearance as a function of the longitude of the central meridian, and this added dimension is a great complication.

One type of calibration which must be done is

TABLE III SUMMARY OF OBSERVATIONS

Dates (U.T.)	Antenna Positions #1	#2	Wavelength (cm.)	Antenna Spacing (Wavelengths)	Useful Observing Time (Min.)
Oct. 17-19, 1963	0	400'E	10.4 cm.	1172 E-W	1090
Oct. 20-22, 24-28, 1963	0	100'E	10.4 cm.	293 E-W	1120
Oct. 30-Nov. 5, 1963	0	800'E	10.4 cm.	2345 E-W	2000
Nov. 7-11, 26-27, 1963	0	1600'E	10.4 cm.	4689 E-W	2320
Nov. 20-25, 1963	0	1600'E	21.2 cm.	2300 E-W	2130
Dec. 19-23, 1963	0	800'E	21.2 cm.	1150 E-W	1540
Jan. 23-24, 26-29, Feb. 1-2, 1964	0	200'E	21.2 cm.	288 E-W	2200
July 4-7, 1964	1600'N	1600'E	10.6 cm.	6507 E-W	340
July 11, 1964	1600'N	200'N	10.6 cm.	4026 N-S	72
Feb. 28, Mar. 3, 1965	0	800'E	10.6 cm.	2300 E-W	320
Mar. 9-11, 1965	0	200'E	10.6 cm.	575 E-W	960

the determination of pointing corrections. Errors in antenna pointing result from polar axis misalignment, sagging of the reflecting surface and feed support, and permanent imperfections built into each antenna. In general, the errors depend on where the antenna is pointed, that is, they are a function of hour angle and declination. In addition, they are likely to change when the antenna is moved to a different station because the polar axis alignment will be changed somewhat.

The procedure was to determine the pointing corrections after each antenna move or feed horn change. This was accomplished by doing position finding measurements on the radio sources M87 and, particularly at long baselines, 3C273, both of which had declinations near that of Jupiter at the time. Since Jupiter was usually observed over a large range of hour angles, the corrections were also determined over a large range of hour angles. It was found that the pointing errors never varied by more than a minute of arc as a function of feed horn position angle so that horn rotation effects could be ignored. The pointing corrections to be applied to the dial readings were typically a few minutes of arc. It was concluded that after applying these corrections, the antenna pointing on Jupiter was rarely off by more than 2 minutes of arc. The pointing was adjusted every

two hours to take account of the hour angle dependence of the corrections and to allow for Jupiter's motion.

The other important calibration is that of the fringe amplitude. This is a gain calibration. The primary amplitude calibrator for the east-west spacings was 3C147, and for the others it was 3C48. These were chosen because they are reasonably strong sources and they are not resolved at long baselines. This can be seen from the latest size information given by Anderson, Donaldson, Palmer, and Rowson (71) who find a size of 0".6 for 3C147 and 0".5 for 3C48. The calibrator was observed each day immediately after the Jupiter observations. The flux densities adopted were those given by Kellermann (72):

3C147	$11.6 \pm 0.8 \times 10^{-26} \mathrm{Wm}^{-2}(\mathrm{c/s})^{-1}$	for 10.6 cm.
	$21.4 \pm 0.5 \times 10^{-26} \mathrm{Wm}^{-2}(\mathrm{c/s})^{-1}$	for 21.2 cm.
3C48	$8.2 \pm 0.4 \times 10^{-26} \mathrm{Wm}^{-2}(\mathrm{c/s})^{-1}$	for 10.6 cm.

One problem encountered during the observations was that of gain stability. The long term stability, found from calibration measurements on the same source at the same position day after day, was quite good, but there seemed to be short-period variations of up to 10 percent. These may have been correlated with where the antennas pointed. The errors produced were only serious for the short baseline (unresolved) measurements. At larger spacings the accuracy was limited by the noise and

not by the gain stability. It was determined that the gain changed little with horn rotation. The upper limit on this change was about 1 percent.

Various studies were made of the instrumental polarization at the time of these observations. To give some idea of the importance of the instrumental polarization, a small unpolarized source observed by the interferometer would seem to have 0.5 percent or less of linear polarization and 0.5 percent or less of circular polarization. Jupiter has such a high degree of linear polarization that errors produced by the instrumental polarization were generally negligible compared to other errors. However, there are one or two types of measurements where this was not true, and that will be discussed later.

For many of the observations in this study, the fringe amplitudes were small, and hence it is important to examine the possible effects of confusion by background radiation. Planetary observers have a distinct advantage when the problem of confusion arises, and that is that the objects they study move in the sky. This allows them to study the area where the planet has been or will be in order to check separately for possible confusion in that place. However, this method was not used. The observing time was limited, and checks for confusion would have subtracted from the time available to observe Jupiter.

There were no known discrete sources in the antenna beam while Jupiter was observed, and at the time, Jupiter was well away from the galactic plane. In addition, each observing run lasted several days, during which the planet moved a couple of beamwidths, typically. This should help cancel out any confusion. Other than these arguments, one can only consider the problem statistically. Kellermann (72) has computed rough values for the RMS confusion level for the Caltech interferometer. He gets 0.15 and 0.05 x $10^{-26} Wm^{-2}(c/s)^{-1}$ for 21 cm. and 10 cm. wavelengths respectively. The linearly polarized component will be a small percentage of this. If anything, the confusion will decrease, statistically, as the baseline is increased, but its resolution behavior is not well known. Cases where there may be a confusion limitation will be noted later.

The integration scheme which has been described depends on the integrator "knowing" what the fringe rate is. In practice the fringe rate differed a slight amount from the exact one per minute rate which was fed to the integrator, and this produced a slow drift in the measured phase. The deviation was due to changes in electrical path lengths and mechanical errors in the analogue computer. The phase drift caused by the computer error, which proved to be the more important of the two at large baselines,

was roughly some constant per natural fringe (of the order of 0.2). Therefore, the fringe drift per unit time was proportional to the natural fringe rate which, in turn, is proportional to the effective baseline. The fringe amplitude error which this produces is

$$\text{Fractional error} = 1 - \frac{\sin \frac{1}{2}\Delta\phi}{\frac{1}{2}\Delta\phi} \qquad (2\text{-}1)$$

where $\Delta\phi$ is the phase drift during the integration. The drift can be found by comparing the phases obtained from successive integrations.

At short and moderate baselines the amplitude error due to this cause was always less than 1 percent and was neglected. At long baselines it was always less than 5 percent, and was again neglected because it was much smaller than the random error due to noise.

The system noise of the interferometer produces random noise in each channel of the integrator. This noise has a normal distribution centered at zero if there is no signal and at the signal level in that channel if there is a signal. When the outputs of the two channels are combined in quadrature the noise is no longer completely random. It produces a systematic error which becomes quite important when the signal and noise levels are comparable. Clark and Kuz'min (70) have applied a simple correction to help allow for this error.

Because the Jupiter investigation often involved the observation of very small fringe amplitudes, it was felt advisable to examine this error in detail in order to obtain the most information possible from the data. The derivation of the corrections which were applied to the data is discussed in the appendix. It can be concluded that when the measured amplitude is equal to or less than the RMS noise it does not contain much information about the true signal amplitude although the phase information is valuable.

The observations themselves were made by taking repetitious integrations with four successive feed horn orientations. These were: both horns parallel with the E-vector parallel to Jupiter's axis (‖), both horns parallel with the E-vector perpendicular to Jupiter's axis (=), horns perpendicular (or crossed) with one in each of the previous directions (⊥) and horns crossed, 45° on each side of the equatorial direction (⟩). This choice of feed combinations was made in order to obtain a variety of information about the brightness and polarization distributions across the face of the source. For future reference let us examine the interferometer response for different feed combinations.

Moffet (73) has described the response of a two-element interferometer with identically polarized

feeds to an unpolarized source. In complex notation the response as a function of time is

$$\underline{R}(t) = \tfrac{1}{2} GA \exp\left[i(-2\pi s_x \Omega t + \psi) \right] S'_I \underline{\beta}_I(s_x, s_y)$$

where G is the receiver gain.

ψ is an instrumental phase constant.

A is the geometric mean of the antenna collecting areas.

s_x and s_y are the x- and y- components of the effective baseline measured in wavelengths (x and y are expressed in radians and are measured east-west and north-south respectively in celestial coordinates with east and north positive.)

Ω is the earth's angular velocity.

$\underline{\beta}_I(s_x, s_y)$ is the complex visibility function:

$$\underline{\beta}_I(s_x, s_y) = V(s_x, s_y) \exp\left[i\Phi(s_x, s_y) \right]$$

$$= \frac{\iint I(x,y) \exp\left[2\pi i (s_x x + s_y y) \right] dx dy}{\iint I(x,y)\, dx dy}$$

$I(x,y)$ is the source brightness distribution as smoothed by the antenna beam patterns.

S'_I is the integrated flux density of the source.

Morris, Radhakrishnan, and Seielstad (74) have generalized the result to include other feed combinations

for observing polarized sources. They describe the polarization in terms of the four Stokes parameters, I, Q, U, and V, as defined by Chandrasekhar (75). Let $\underline{I}$ be the unnormalized complex visibility function of $I(x,y)$. $\underline{I} = S'_I \underline{\beta}_I(s_x, s_y)$. $\underline{Q}$, $\underline{U}$, and $\underline{V}$ can be defined similarly for the visibility functions of Q, U, and V. Then the response with identical linearly polarized feeds is

$$\underline{R}(t) = \tfrac{1}{2}k\ (\underline{I} + \underline{Q} \cos 2\phi + \underline{U} \sin 2\phi) \qquad (2\text{-}2)$$

where $k = GA \exp\left[i(-2\pi s_x \Omega t + \psi)\right]$.

$\phi = \phi_1 = \phi_2$ is the orientation of the plane of polarization of the feeds with respect to the ℓ-axis of the coordinate system defining the Stokes parameters.

With "crossed" linearly polarized feeds $(\phi_2 = \phi_1 + \frac{\pi}{2})$ we get

$$\underline{R}(t) = \tfrac{1}{2}k\ (-\underline{Q} \sin 2\phi_1 + \underline{U} \cos 2\phi_1 \pm i\underline{V}) . \qquad (2\text{-}3)$$

There are many other possible combinations, but these are the only ones which interest us in the present study. The plane of polarization of the integrated flux density of a source is often used to define the ℓ-axis of the coordinate system. As we saw in the introduction, the plane of polarization, in the case of Jupiter, is always within 9° or 10° of the equatorial direction.

The individual integrations were usually of ten minutes duration, but occasionally they were only five minutes long. It was not practical to make an absolute phase calibration for the observations. Therefore, absolute phases (Φ) were not determined, only phases relative to some slowly drifting instrumental phase. However, as we shall see, it has proven very valuable to compare the relative phases obtained with the different horn orientations.

Table III shows that there were large gaps in the antenna spacing series used. For the east-west observations these gaps were filled in to a large extent by observing over a wide range of hour angles (the limit was $\pm 4^h$) and thus obtaining foreshortening of the effective baseline. For a source at the celestial equator the effective baseline is decreased to 1/2 of its transit value at $\pm 4^h$. To compute the effective baseline ($s = \sqrt{s_x^2 + s_y^2}$) one can use the general formula given by Moffet (73):

$$s = s_o \cos \theta \qquad (2\text{-}4)$$

where $\sin \theta = -\sin a \cos \delta \sin h + \cos a (\cos \phi \sin \delta - \sin \phi \cos \delta \cos h)$.

s_o is the antenna spacing in wavelengths.

a is the baseline azimuth.

δ is the declination.

h is the hour angle.

ϕ is the geographic latitude.

This expression is greatly simplified for the special cases of east-west and north-south baselines.

When a radio source is observed over a large hour angle range there is also another important effect, and this is that the projected baseline rotates with respect to celestial coordinates. Moffet (73) also gives a general formula for the position angle (p) of the projected baseline:

$$\frac{s_x}{s_y} = \tan p = \frac{\sin a \cos h - \cos a \sin\phi \sinh}{\sin a \sin\delta \sinh + \cos a (\cos\phi \cos\delta + \sin\phi \sin\delta \cosh)} \quad (2\text{-}5)$$

This also simplifies for the special cases of east-west and north-south baselines. Notice that for an east-west baseline ($a = \pi/2$) with $\delta = 0^{\circ}$, the position angle is a constant 90° regardless of the value of h. Fortunately, this was nearly the case for the east-west observations of Jupiter. The added complication of baseline rotation would have made the problem more difficult.

Because the distance to Jupiter is variable, the effective baseline must be modified in order to make it a physically meaningful quantity. Different investigators use different conventions in dealing with this variation. The convention used here is to normalize the baseline to the standard distance for Jupiter (4.04 A.U.)

by multiplying the effective baseline by the ratio of the standard distance to the actual distance. Hence, $s' = s \frac{4.04 \text{ A.U.}}{D}$ is the baseline we will use. It is still measured in wavelengths.

The observed flux densities must also be modified for the same reason. They have also been normalized to the standard distance, in this case by multiplying them by the factor $\left(\frac{D}{4.04_{\text{A.U.}}}\right)^2$.

III. SHORT BASELINE RESULTS

Since the Caltech discovery, in 1961, that the plane of polarization of Jupiter's decimeter radiation rocks back and forth in position angle as the planet rotates (11), presumably because the magnetic axis is not parallel to the rotational axis, several observers at various observatories have verified the effect. It is now universally agreed that there is an angle of 9° or 10° between Jupiter's magnetic and rotational axes. As pointed out in the introduction, there are two side effects of this "wobbling", each of which results from the beaming properties of the synchrotron radiation. They are that the observed flux density and the observed degree of polarization both depend on the longitude of the central meridian (LCM).

The present investigation included short baseline observations at 10.4 and 21.2 cm. One reason was to obtain a "zero baseline", or single dish, normalization for the visibility functions, and the other was to study the integrated radiation from Jupiter and, in particular, extend our information about the longitude dependence of the flux density and the direction and degree of linear polarization. It has since become obvious that recent observations by Roberts and Komesaroff (9),

using very low noise receivers and a very large collecting area have provided these dependences with a greater accuracy than we have obtained. However, within the limits of error, the two sets of data are consistent with each other and with the earlier results.

Figure 2 shows the results obtained at 10.4 cm. with an east-west antenna spacing of 100 feet, and Figure 3 shows the results obtained at 21.2 cm. with an east-west antenna spacing of 200 feet. Because of the scatter due to noise, means have been taken over each 30° interval of longitude. The error brackets are standard deviations. In each case the observations cover many days of observing so that the variations shown are thought to be correlated with LCM only and not other observing variables such as hour angle. In each case the flux densities are based on the calibration source 3C147 as explained in the last chapter. They are normalized to correspond to a standard distance for Jupiter of 4.04 A.U. The System III LCM (ℓ_{III}) plotted is that based on the period and epoch defined by the International Astronomical Union and tabulated by B. Morrison (76). The flux densities are obtained from the sum of the parallel horn measurements, and the percentage polarizations are obtained from the difference of the parallel horn measurements $\left(\frac{R_{=}-R_{\shortparallel}}{R_{=}+R_{\shortparallel}}\right)$. The fact that the direction of polarization may differ

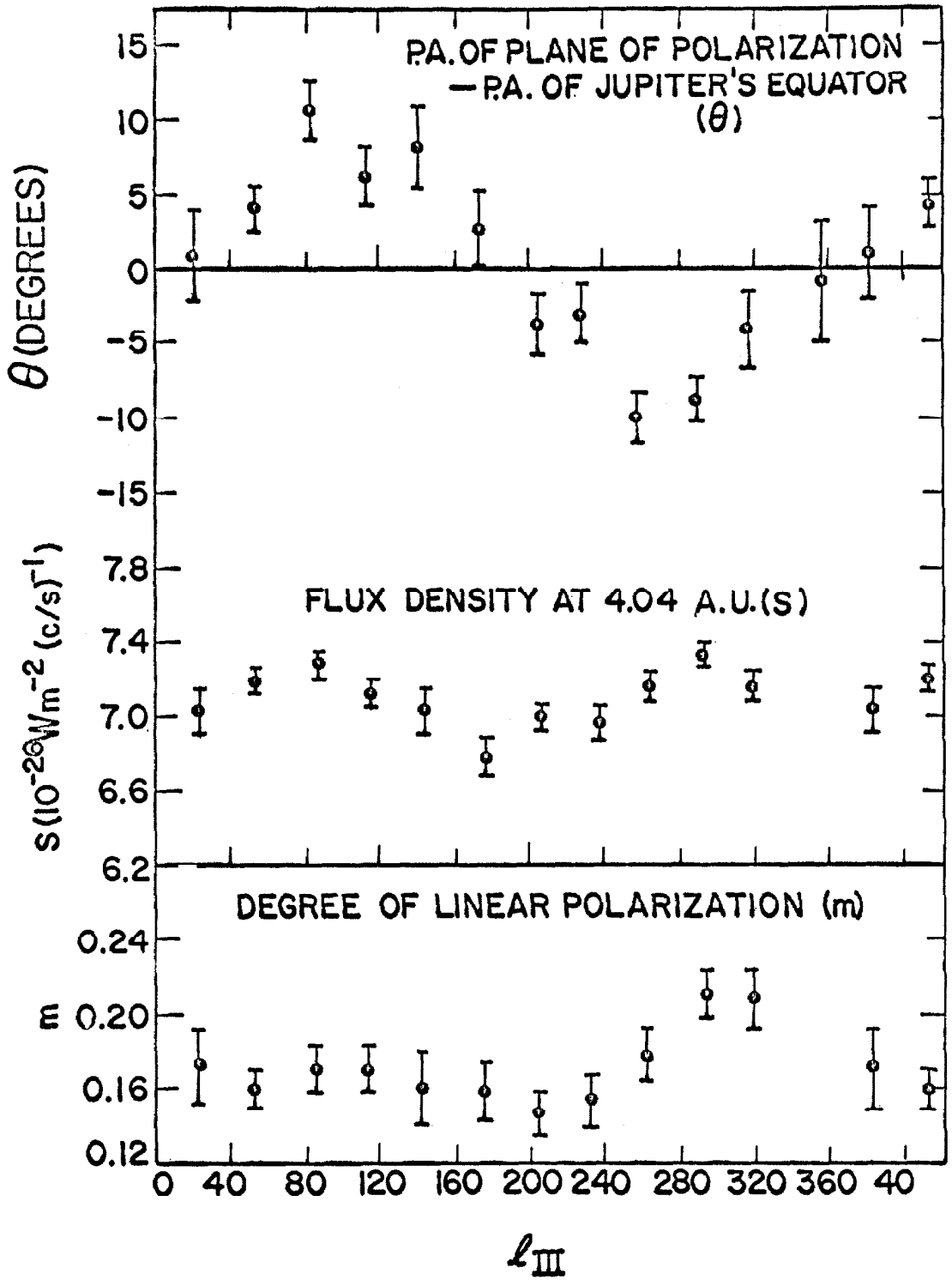

Figure 2. Orientation of the plane of polarization, the flux density, and the degree of linear polarization, each as a function of ℓ_{III} at 10.4 cm. (100' E-W, Oct., 1963)

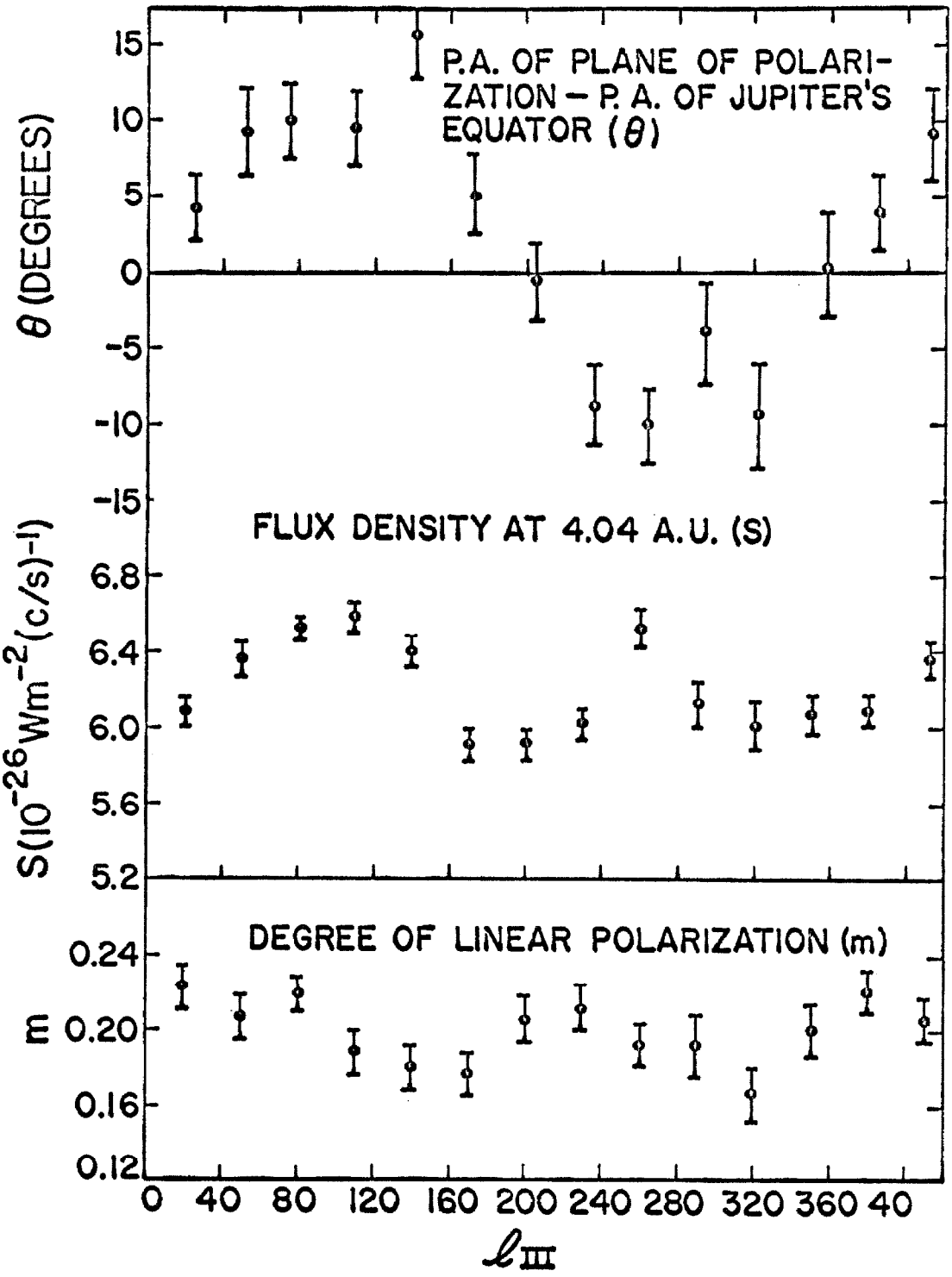

Figure 3. Orientation of the plane of polarization, flux density, and degree of linear polarization, each as a function of ℓ_{III} at 21.2 cm. (200' E-W, Jan./Feb., 1964)

by as much as 9° from the equatorial direction produces a small error which has been corrected for in the percentage polarization determinations.

The determination of the plane of polarization depends on a unique interferometer technique which was also used in the initial work of Morris and Berge (11). The feed horns are crossed with one parallel to Jupiter's equator and one parallel to Jupiter's rotational axis ($\perp$). With crossed horns the interferometer does not respond to the unpolarized radiation. If the plane of polarization were exactly parallel to the equatorial direction, then with this horn combination the interferometer would not respond to the linearly polarized radiation either. However, interference fringes are seen from time to time which indicate that the plane of polarization does deviate from the equatorial direction. Let θ = P.A. of plane of polarization - P.A. of equator. Then

$$\text{(Fringe Ampl.) } (\cos \Phi) = \pm mS \sin \theta \cos \theta$$

$$\text{or} \quad \sin 2\theta = \pm \frac{2(\text{Fringe Ampl.})(\cos \Phi)}{mS} \qquad (3\text{-}1)$$

where Φ is the fringe phase with crossed horns minus the fringe phase with parallel horns. The sign in front can be uniquely determined by a knowledge of which horn is rotated and in which direction to get to the crossed

horn position. In the absence of noise, circular polarization, instrumental effects, or asymmetry between the polarized and unpolarized components, the angle Φ must be 0° or 180° depending on the sign of θ. We know that any instrumental effects are small and that at this baseline any possible asymmetry is negligible. The cos Φ term helps correct for noise, takes out the effect of any possible circular polarization (which would be added in phase quadrature), and provides the sign of θ .

With a sufficiently long time base, observations of the variation of the plane of polarization can define an accurate rotation period for Jupiter's magnetic field. The present observations at 21 cm. combined with those made in 1961 (11) provide a baseline of 2-1/2 years. It is possible to say, from a comparison of the two, that this rotation period does not differ from that defined for System III by more than one part in 80,000, that is, 0.4 or 0.5 seconds. This substantiates, but does not improve on the limit given by Roberts and Komesaroff (9), who had a shorter time base, but more precise data.

The flux density at 4.04 A.U. was not significantly different from that found by earlier Caltech studies (11), (41) at similar frequencies.

Although the short baseline observations have been considered equivalent to single dish observations

there may be a question of whether this is really true, inasmuch as the baseline was obviously not zero. At a baseline of 300λ the decimeter radiation of Jupiter is resolved by 4 or 5 percent at most when the distance is 4.04 A.U. This can be estimated from the visibility functions which will be presented later. Thus at this and smaller baselines we are, in fact, examining the integrated radiation.

The observations presented so far are mostly a repetition of earlier work. They are worthy of consideration as a check on the earlier results and to look for time variations, but they are no longer very exciting. There was one exciting result of the short baseline observations, however, and that was the discovery of a small circularly polarized component in Jupiter's decimeter radiation. Because of its importance and because its detection was not confined to short baseline observations, a separate chapter will be devoted to the circular polarization.

IV THE CIRCULARLY POLARIZED COMPONENT

In the history of radio astronomy there has never been a report of the detection of circularly polarized radiation from a synchrotron emission source. A few attempts have been made to detect circular polarization from some discrete sources, but they have only resulted in upper limits for the percentage of circular polarization (usually a percent or a few percent).

The radiation from a relativistic electron in a magnetic field is, in general, elliptically polarized. The polarized component can be decomposed into a linear part and a circular part. The sense of the circular part depends on whether the angle between the magnetic field and the direction of observation is greater than or less than the electron pitch angle. For a synchrotron emission radio source, consisting of a large number of such electrons, one would expect that the fraction of circular polarization would be very small and, hence, undetectable. The reason is that for the usual sort of source the electron energies are extremely high so that the beaming cones are very small. The observer will not see the radiation of a given electron unless the direction of its motion passes very close to the observation direction. For such a

small beaming cone, the electron pitch angle distribution will be nearly isotropic over a range equal to a typical beaming cone. Hence, the circular components for the electrons one can see will nearly cancel out.

Recently, however, there have been suggestions (77), (9) that it might be possible to detect circular polarization in the decimeter radiation from Jupiter. This is because the electron energies are relatively low (a few Mev probably) for the Jupiter source and the beaming cones are correspondingly large. [The reason that there is emssion at a few thousand Mc/s is that the magnetic field is very large (of the order of a gauss).] In addition, the electron pitch angle distribution is very anisotropic with a large fraction of the electrons in flat helicies near the equatorial plane.

According to equation (2-2), an interferometer with parallel, linearly polarized feeds will respond to half the circularly polarized component. The phase of the interference fringes produced will be the same as for the unpolarized and linearly polarized components. We see from equation (2-3) that with crossed horns the interferometer again responds to half the circularly polarized component, but in this case the phase is different by 90°. It can either lead or lag by 90° depending on the sense of the circular polarization.

Figure 4 shows the data from which the existence of a circularly polarized component was first recognized. The points plotted were obtained during the period 26 Jan. to 3 Feb., 1964, at a wavelength of 21.2 cm. and an antenna spacing of 200 feet east-west. They represent the difference in phase between a crossed horn measurement with the E-vectors of the horns at 45° on either side of the equatorial direction and a parallel horn measurement. Two different cases are shown, one with the horns parallel to the polar axis and the other with the horns parallel to the equator. Both give very nearly the same average and the same variation as a function of the longitude of the central meridian. The systematic deviation of the phase difference from zero is interpreted as being due to a small variable amount of circularly polarized radiation adding in phase quadrature to the linearly polarized radiation (Figure 6a).

The fact that there is a large periodic variation which is correlated with Jupiter's rotation probably rules out an instrumental effect being responsible for the result. The only other possible explanation of the phase deviation is an intrinsic asymmetry of the source. However, at this baseline, it would be necessary to have an extremely large difference in the centroid positions for the radiation seen with crossed horns and the radiation seen with parallel

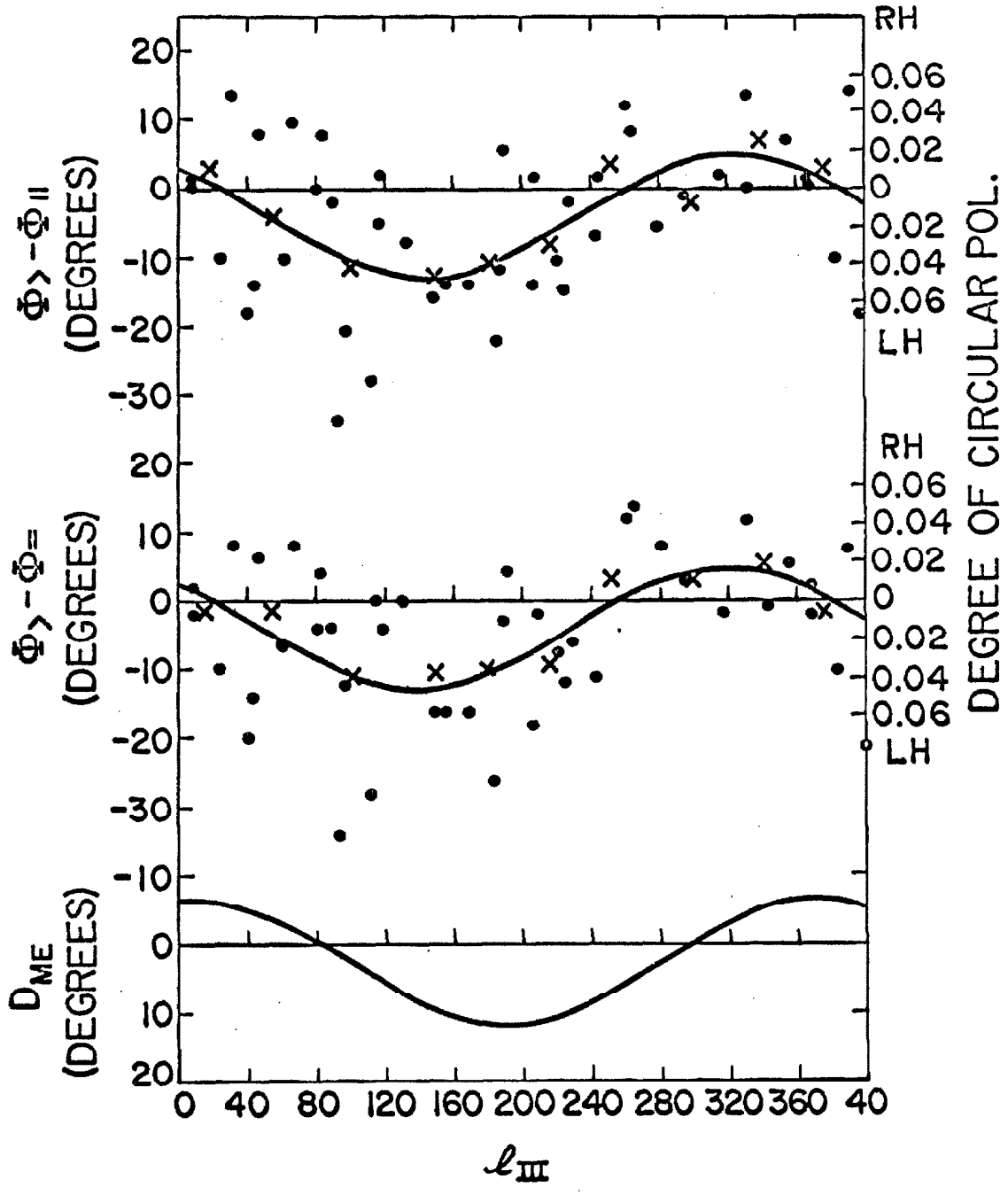

Figure 4. The upper graphs show the evidence for circular polarization at 21.2 cm. (200' E-W, Jan./Feb., 1964) The filled circles are the data points, the x's are means for each 40° of longitude, and the curves are least squares fits of a sinusoid to the data. The lower curve represents the magnetic latitude of the earth.

horns. Also, the fact that Figures 4a and 4b give the same result means that the centroid positions for the two parallel horn measurements, only one of which responds to the linearly polarized radiation, are the same. Thus, most of the phase variation in Figure 4 must be due to circular polarization. It is true, however, that the base level of the curves can be altered by instrumental effects. From tests made on the instrumental polarization for an unpolarized source, it was found that the maximum amount which the baseline can be shifted corresponds to about ±0.005 of circular polarization. The degree of circular polarization is given by m $\tan(\Phi_{>} - \Phi_{<})$. For the maximum deviation (12°.8) and m=0.20, this is 0.045 ±0.015.

Figure 4c shows the magnetic latitude of the earth as seen from Jupiter. It is clear that the variation of circular polarization, as a function of the longitude of the central meridian, is quite well correlated with the magnetic latitude of the earth. This is an expected result and will be described in more detail later. The agreement in phase is not perfect, however, and there may be a real phase difference between the curves representing the degree of circular polarization and the curve representing the magnetic latitude of the earth.

The earlier short baseline work at 10.4 cm. did

not include the particular crossed horn observation utilized above. Therefore, observations were carried out at 10.6 cm., 200 feet east-west in March, 1965 to look for the effect at this wavelength. The result obtained was very similar to the 21.2 cm. result shown in Figures 4a and 4b except that the amplitude was only three-fourths as great and the phase was earlier by 30°. The base level deviated from zero by a greater amount than at 21.2 cm. However, it was found that during these observations the instrumental elliptical polarization was as large as 1.5 percent so this probably accounts for the different base level. There was not enough time to make calibration observations to correct for this, and thus the base level found at 21.2 cm. is assumed to be true for 10.6 cm. Then for the maximum deviation (10°.3) and $m = 0.17$, the degree of circular polarization is 0.031 ± 0.015.

The other crossed horn combination used should also respond to half the circularly polarized radiation. Because of the large variation in the amount of linearly polarized radiation seen with this feed combination (due to the rocking of the plane of polarization) it is necessary to treat each integration separately. For each, the degree of circular polarization, *ignoring noise*, is

$$\frac{2(\text{fringe ampl.}) \sin \Phi}{S}$$

where Φ is the phase difference between the crossed horn and parallel horn measurements. However, there were problems in using this data. The scatter of the points was large, and although the results did not contradict the curve shown in Figure 4, they were not very accurate or useful in themselves.

The detection of circular polarization was not confined to the short baseline measurements. It has also been found at longer baselines. Berge and Morris (7) presented data of the same type as shown in Figure 4 except that the wavelength was 10.4 cm., and the antenna spacing was 800 feet east-west. At this large baseline the radiation seen with parallel horns was thought to be largely thermal emission from the disk of the planet, and the radiation seen with crossed horns was, of course, non-thermal emission from the radiation belts. There was a variable phase effect much like that shown in Figure 4 except that it had a larger amplitude. It was centered on 180° instead of 0° phase because the radiation seen with crossed horns was past the first null of the visibility function so that, for complete symmetry, its phase should be 180° with respect to its short baseline phase. At the time there was no reason to suspect the existence of circular polarization, and so the suggestion was made that Jupiter's magnetic dipole might be displaced away

from the center of the planet. This would cause the radio centroids of the thermal and non-thermal components to have different positions, thus producing a different fringe phase for each.

However, it now appears that most of this phase effect was due to circular polarization because a similar effect was found at a wavelength of 21.2 cm. and an antenna spacing of 1600 feet east-west. At this wavelength the thermal component should be much less important so that the peculiar phase effect for this baseline must be due mainly to circular polarization. From measurements of this sort it has been possible to obtain rough visibility functions for the circularly polarized radiation. Figure 5 shows the visibility function at each wavelength for the longitude at which the circularly polarized radiation is greatest ($\ell_{III} \approx 150°$).

A possible complication is that there may still be a difference in the positions of the thermal and non-thermal components which would distort the phase results at large baselines, particularly at the shorter wavelength. This would cause an error in the circular polarization inferred from the phase measurements. The relative phase of the two parallel horn combinations can provide a clue for solving this problem. Figure 6b is a vector diagram showing the situation at 10.4 cm., 800 feet

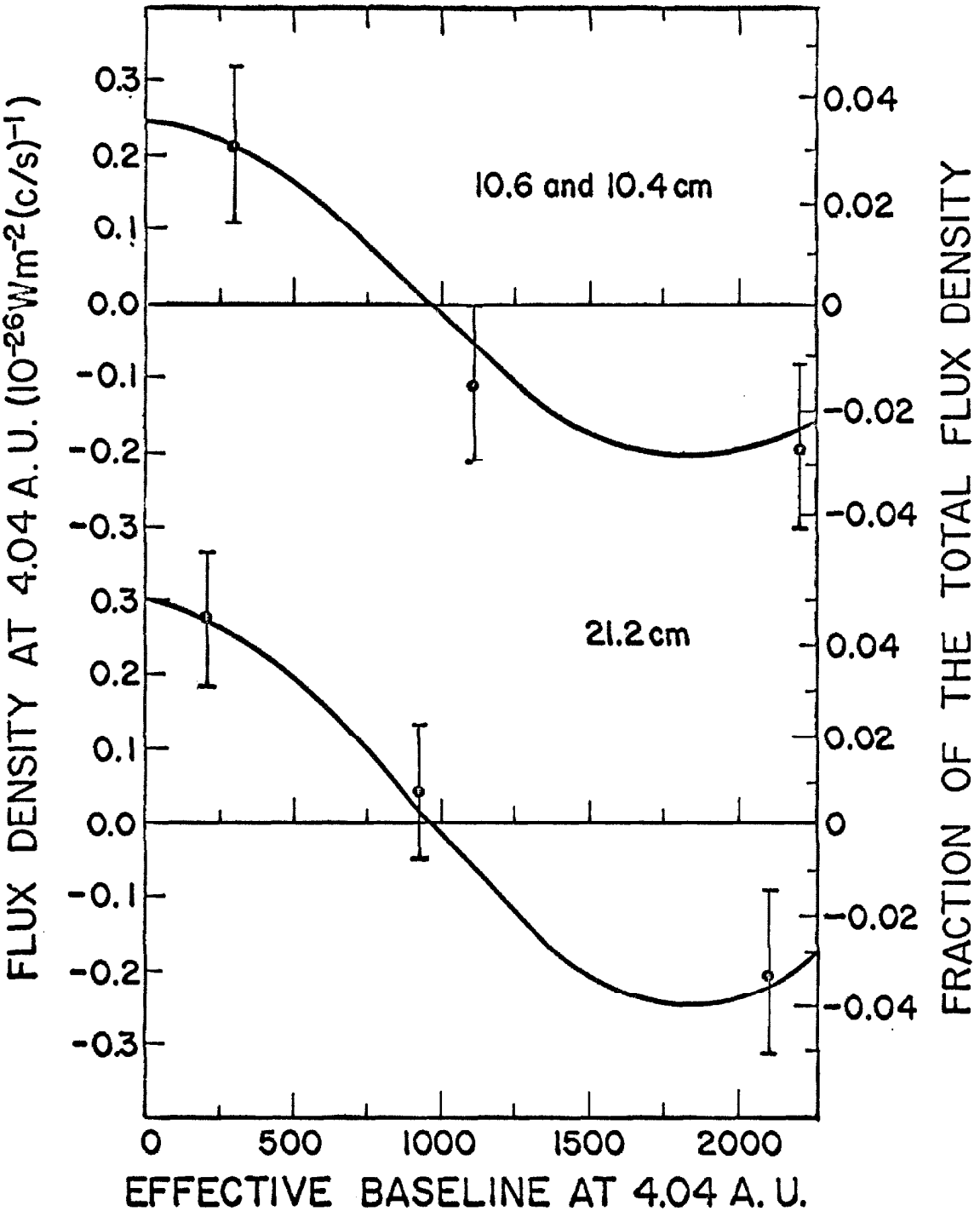

Figure 5. Visibility functions for the circularly polarized component at the longitude for which it is maximum. The curves, differing only by a scale factor, represent the visibility function of a double source with rather small components.

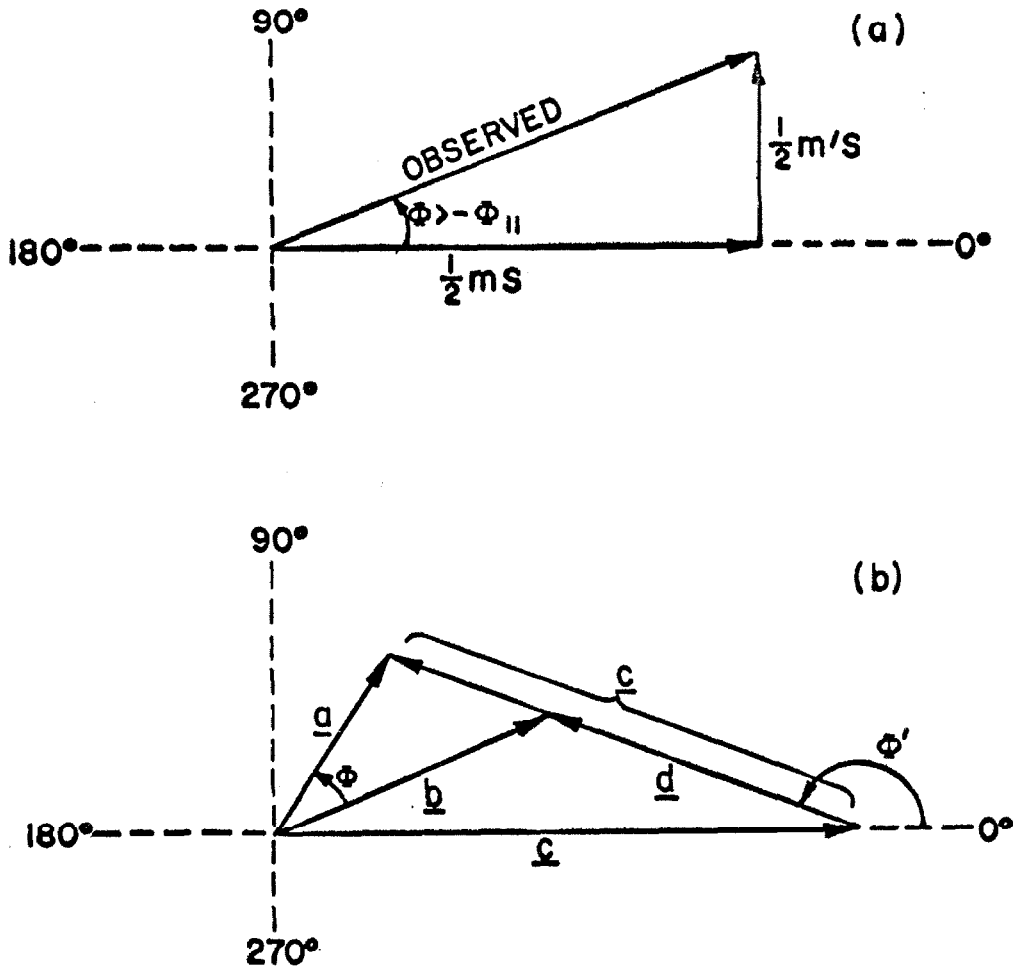

Fig. 6 a) Vector diagram showing the interferometer response to the linearly and circularly polarized components (mS and m'S) with crossed horns (›).

b) Vector diagram for studying the parallel horn measurements at 10.4 cm., 800' E-W.

a Observed visibility function with parallel horns (=).

b Observed visibility function with parallel horns (||).

c Visibility function for parallel horns (=) if there were no thermal component.

d Visibility function for parallel horns (||) if there were no thermal component.

e Visibility function for the thermal component.

$\Phi' = \Phi_= - \Phi_{||}$

Φ' Measures the relative position, in the east-west direction, of the thermal and non-thermal radiation.

east-west. If $a \neq b$ and $\Phi = 0°$ then $\Phi' = 180°$ and there is no displacement between the thermal and non-thermal components. However, Φ does seem to depart systematically from zero, and if Φ' is calculated for each set of data (assuming some reasonable value for the thermal contribution) it is found to vary periodically with ℓ_{III}. The variation suggests a shift of the non-thermal component in the direction of longitude 100°, latitude 0°. However, the amount of displacement inferred is less than a tenth of Jupiter's radius. This small amount should not seriously affect the circular polarization measurements.

If the points in Figure 5 are correct, then the circularly polarized component, when it appears, must be a rather well defined double source with a separation of about 5 equatorial radii. We conclude that most of it comes from a region near the equatorial plane on either side of the planet.

If we know the place of origin of the circularly polarized radiation, the direction in which the magnetic dipole is tipped, and the sense of circular polarization, all at some given longitude, then we can, in principle, determine the direction of Jupiter's magnetic field. In the region of $\ell_{III} \approx 150°$ or $200°$, the sense is left-handed and the dipole is tipped towards the earth at the

north. The result is that the magnetic pole in the northern hemisphere is a north magnetic pole, and the one in the southern hemisphere is a south magnetic pole. This is opposite the polarity of the earth's field, but it agrees with the result inferred by Warwick (78) from his observations of the decameter radio emission of Jupiter.

A final word of caution should be added with regard to these measurements. The circular polarization results should still be regarded with some suspicion because instrumental effects haven't been completely ruled out as the cause of the observed circular polarization. The checks of instrumental polarization were made on unpolarized sources, and it isn't entirely clear what instrumental effects would be produced by linearly polarized radiation. It is conceivable that in the case of Jupiter, a circular component could be produced instrumentally by the linearly polarized radiation and that it might appear to vary as the plane of linear polarization rocks back and forth within the crossed horn directions. However, it seems very improbable that such a large effect could be produced. Unfortunately there are no reasonably strong, highly polarized radio sources on which this can be checked.

V. THE OBSERVED VISIBILITY FUNCTIONS

The purpose of this chapter is to present the bulk of the information obtained by the present investigation. It is shown plotted in the form of visibility functions near the end of the chapter. First, however, let us see how the points were extracted from the raw data and also what the visibility functions represent.

We have seen that for an ordinary radio source the complex visibility function depends only on s_x and s_y [$\underline{\beta} = \underline{\beta}\ (s_x, s_y)$] or alternately, s and p. For a given source declination and interferometer configuration s_x and s_y are functions of hour angle only. However, for Jupiter $\underline{\beta} = \underline{\beta}\ (s_x, s_y, \ell_{III})$. The added dependence occurs because the magnetic axis and polar axis are not parallel to each other. The variation with ℓ_{III} comes about in two ways. The first is that as the planet rotates, the plane of the magnetic equator wobbles in position angle with respect to the interferometer baseline. The second is that the rocking back and forth of the magnetic axis causes the earth to change its position within the non-isotropic radiation pattern of the synchrotron emission. Figure 7 illustrates these two cases. The solution is to consider each longitude separately and obtain $\underline{\beta}\ (s_x, s_y, \ell_{III})$ for each.

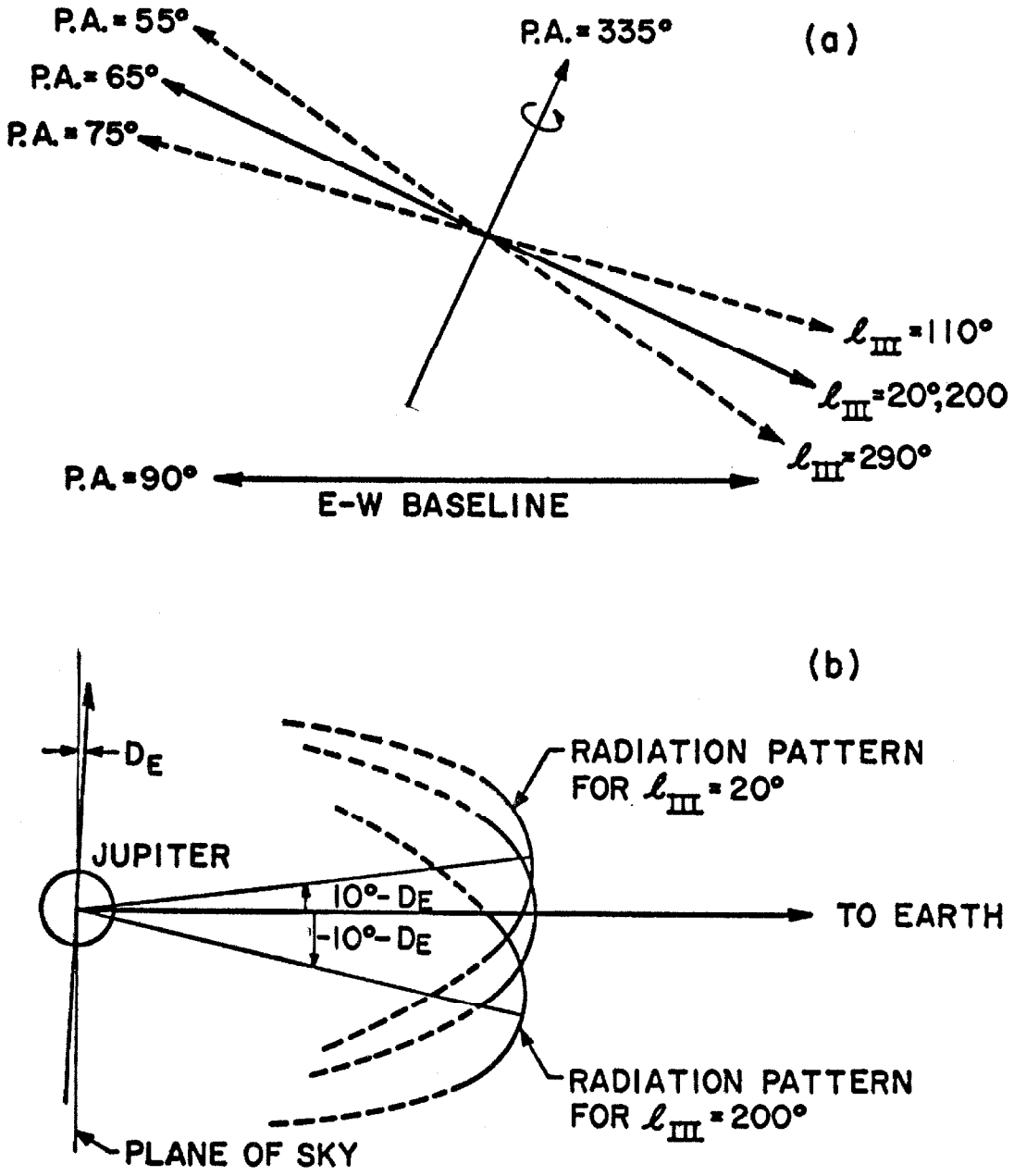

Figure 7. a) Orientation of the plane of polarization (and major axis) for different longitudes, and the baseline orientation for the east-west observations.
b) Geometry of the beaming effect.

One observing cycle of four feed combinations usually took about 50 minutes or 30° of Jupiter's rotation. Therefore, it was decided to consider discrete longitudes separated by 30°. The measured amplitudes were changed to flux densities by applying the necessary corrections and the calibration. It was straightforward to find the exact times that a given longitude was on the central meridian. The fringe amplitudes and relative phases were then obtained for those times by interpolating between the two nearest data points, and the effective baselines were found from the hour angles corresponding to those times.

When the resulting numbers were plotted for each of the twelve longitudes, it was found that the visibility functions were not well determined because there were too few points and the points had too much scatter due to noise. This was remedied by combining groups of three longitudes so that there were now only four longitude ranges. This made the division of longitudes much cruder and probably introduced some scatter because of variations with ℓ_{III} within each range, but at least there were enough points to determine the visibility functions with some accuracy. The longitude ranges were chosen as follows: One was centered on the longitude at which the north end of the magnetic axis

was tipped toward the earth (200°); one was centered on the longitude at which the north end of the magnetic axis was tipped away from the earth (20°); one was centered on the longitude at which the magnetic equator had the smallest position angle (290°) and one was centered on the longitude at which the magnetic equator had the largest position angle (110°).

It was pointed out earlier that during the east-west observation the declination of Jupiter was nearly 0° so that $p \approx 90°$ ($s_y \approx 0$) for all of these observations. Therefore, the main cause of the variation of major axis (or magnetic equator) position angle is due to the wobbling of Jupiter's magnetic axis. For a given longitude of the central meridian, the position angle with respect to the baseline is almost the same for all the points.

The motion of Jupiter in the sky and the change of apparent direction of the polar axis were slow enough so that they didn't produce any significant changes during the observing period.

Let us choose the ℓ-axis of the coordinate system defining the Stokes parameters as the plane of polarization of the integrated radiation from the source. If, in the case of Jupiter, this plane always coincided with the equatorial plane instead of wobbling by ±9°,

then the responses we would get would be

$$\underline{R}_{\shortparallel}(s_x, s_y, t, \ell_{III}) = \tfrac{1}{2}k\ (\underline{I} - \underline{Q}) \qquad \underline{R}_{=} - \underline{R}_{\shortparallel} = k\underline{Q}$$

$$\underline{R}_{=}(s_x, s_y, t, \ell_{III}) = \tfrac{1}{2}k\ (\underline{I} + \underline{Q}) \qquad \underline{R}_{=} + \underline{R}_{\shortparallel} = k\underline{I}$$

$$\underline{R}_{\lrcorner}(s_x, s_y, t, \ell_{III}) = \tfrac{1}{2}k\ (-\underline{U} + i\underline{V}) \qquad (5\text{-}1)$$

$$\underline{R}_{>}(s_x, s_y, t, \ell_{III}) = \tfrac{1}{2}k\ (\underline{Q} + i\underline{V})$$

where $k = GA \exp\left[i\ (-2\pi s_x \Omega t + \psi)\right]$.

In the real case, where there is wobbling, we can define the observed visibility amplitudes (V) and phases (Φ) which make up the observed visibility functions ($\underline{\beta} = V_e^{\,i\underline{\Phi}}$) by

$$\tfrac{1}{2}S_{\shortparallel}' V_{\shortparallel}(s_x, s_y, \ell_{III}) \exp\left[i\underline{\Phi}_{\shortparallel}(s_x, s_y, \ell_{III})\right] = \frac{\underline{R}_{\shortparallel}(s_x, s_y, t, \ell_{III})}{k}$$

$$\approx \tfrac{1}{2}\ (\underline{I} - \underline{Q})$$

$$\tfrac{1}{2}S_{=}' V_{=}(s_x, s_y, \ell_{III}) \exp\left[i\underline{\Phi}_{=}(s_x, s_y, \ell_{III})\right] = \frac{\underline{R}_{=}(s_x, s_y, t, \ell_{III})}{k} \qquad (5\text{-}2)$$

$$\approx \tfrac{1}{2}\ (\underline{I} + \underline{Q})$$

$$\tfrac{1}{2}S_{\lrcorner}' V_{\lrcorner}(s_x, s_y, \ell_{III}) \exp\left[i\underline{\Phi}_{\lrcorner}(s_x, s_y, \ell_{III})\right] = \frac{\underline{R}_{\lrcorner}(s_x, s_y, t, \ell_{III})}{k}$$

$$\approx \tfrac{1}{2}\ (-\underline{U} + i\underline{V})$$

(5-2 cont.)

$$\tfrac{1}{2}S_{\rangle}V_{\rangle}(s_x, s_y, \ell_{III})\exp[i\Phi_{\rangle}(s_x, s_y, \ell_{III})] = \frac{R_{\rangle}(s_x, s_y, t, \ell_{III})}{k}$$

$$\approx \tfrac{1}{2}\,(\underline{Q} + i\underline{V}) \quad .$$

It is still true that $\tfrac{1}{2}S_{\shortparallel}'V_{\shortparallel}\,e^{i\Phi_{\shortparallel}} + \tfrac{1}{2}S_{=}'V_{=}\,e^{i\Phi_{=}} = \underline{I}$.

The gain calibration represents the real part of k, and the visibility amplitudes plotted are the quantities $\tfrac{1}{2}S'V(s_x, s_y, \ell_{III})$. This represents only that part of the radiation which the interferometer responded to. Since there was no calibration for the instrumental phase ($\psi = \psi_1 + \psi_2$), where ψ_1 is the known artificial phase shifting and ψ_2 is some slow unknown function of time, the measured phases represent $\Phi + \psi_2$. The unknown instrumental phase has been removed by considering only the phase differences between different feed combinations.

It might be argued that, in making the observations, it would be better to let the position angles of the various feed combinations follow the wobbling of the plane of polarization so that strict equalities could be used in (5-2). This would be possible because the wobble is known quite accurately. However, it would make the observations more difficult and provide

more opportunity for operator error. As it is, the deviations due to the wobble are easily accounted for in the analysis described in the next chapter.

The visibility amplitudes and relative visibility phases are plotted in Figures 8 to 25. All of the observations listed in Table III are included except those made in 1965 which were done primarily to determine special phase effects. All of the figures except 16 and 17 are for an east-west baseline. Figures 16 and 17 show the data obtained at 10.4 cm. using north-south and north-east baselines. There was not much observing time available at these baselines, but it was possible to choose those times at which the projected baseline was parallel to the minor axis of the synchrotron emission region. The points plotted were obtained when the angle between the projected baseline and the minor axis was less than 5°. Because this part of the investigation was rather crude anyway, no distinction is made according to ℓ_{III}.

Figures 8 to 17 are for a wavelength of 10.4 cm., and Figures 18 to 25 are for a wavelength of 21.2 cm. The even-numbered ones show the visibility amplitudes and the odd-numbered ones show the relative visibility phases. These are not the only relative phases possible, but they are the ones which seem to be

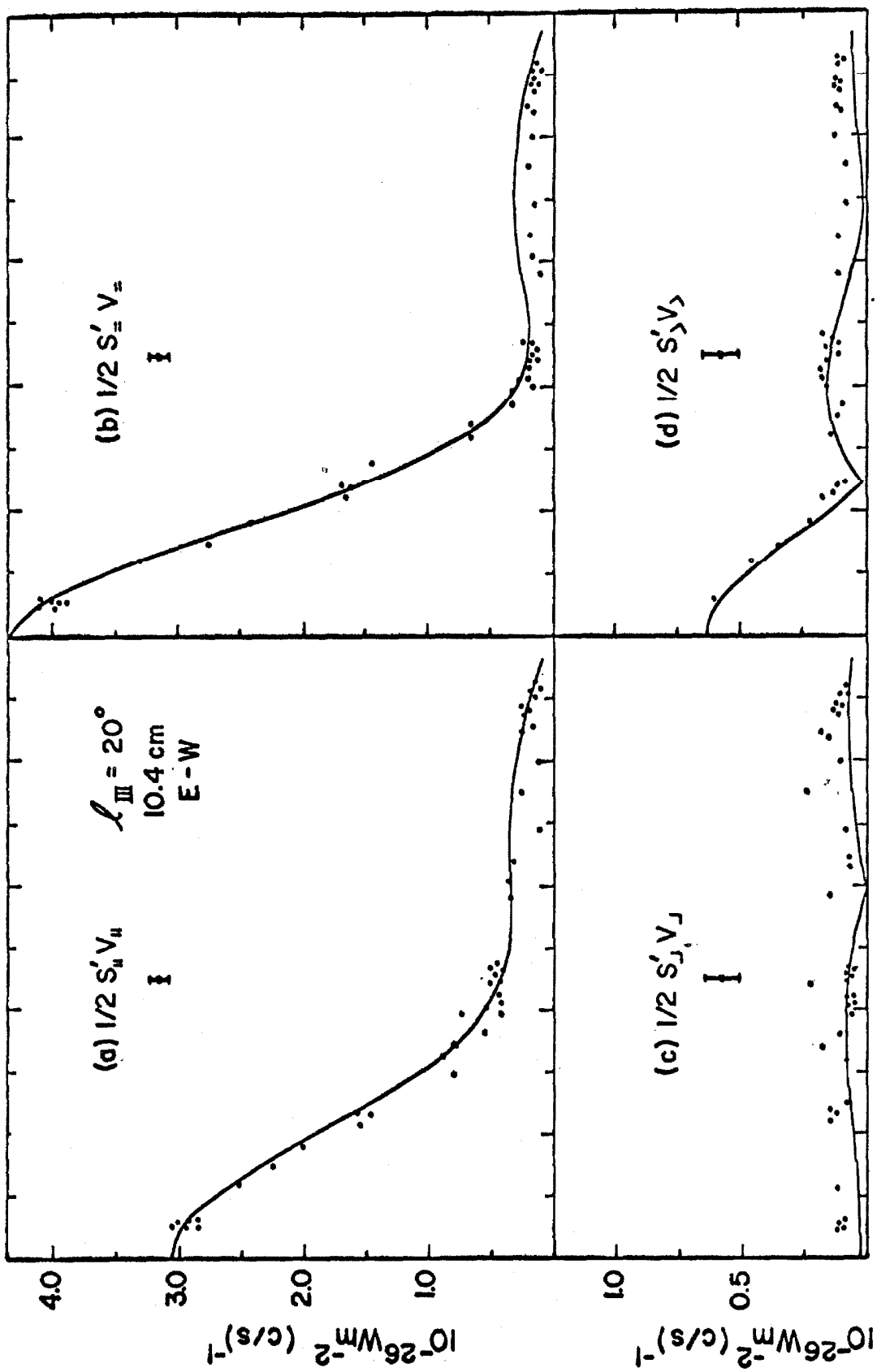

Fig. 8. Visibility amplitudes for $\ell_{III}=20°$ at 10.4 cm (E-W baseline Oct.-Nov., 1963).

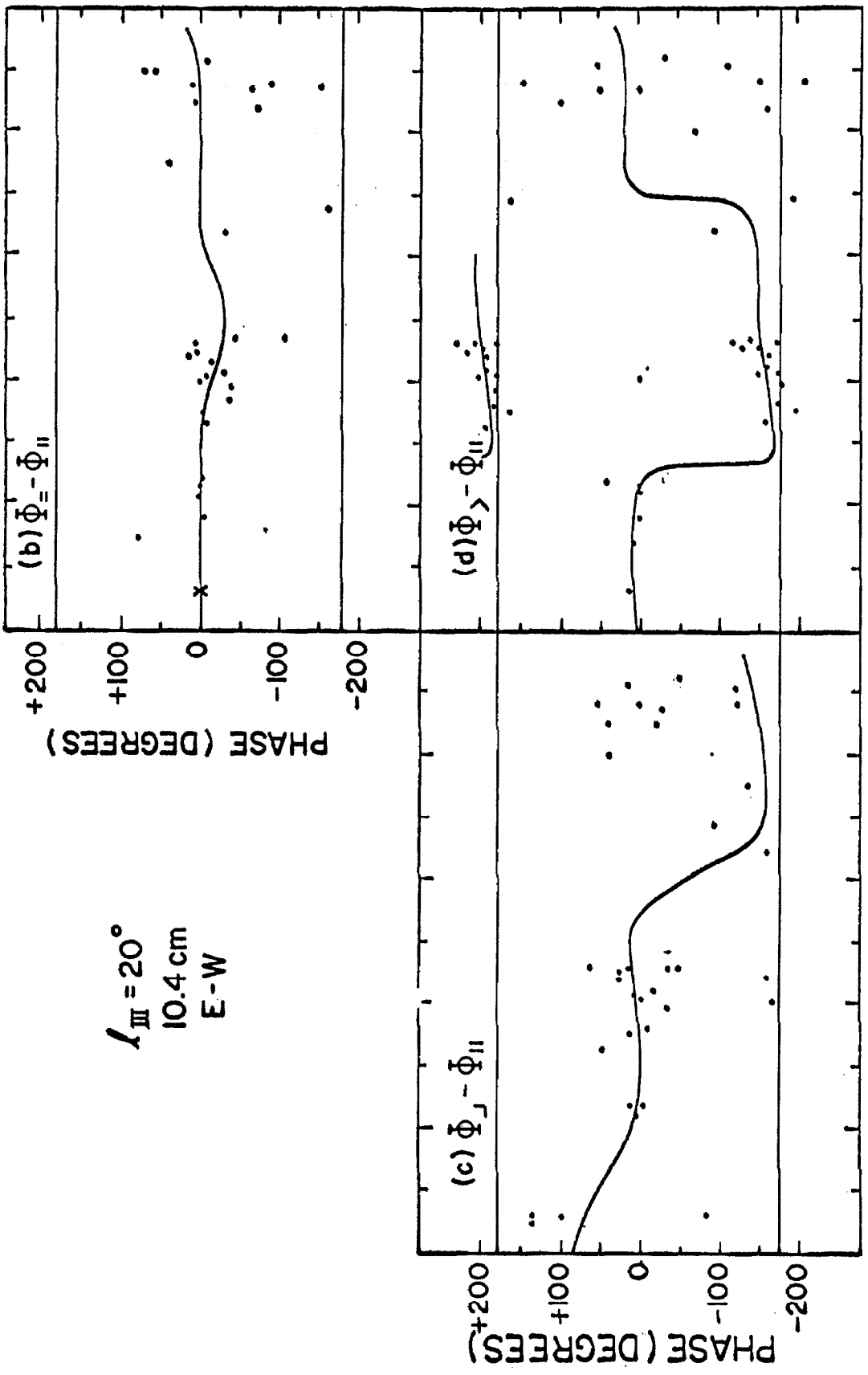

Fig. 9. Relative visibility phases for $l_{III}=20°$ at 10.4 cm(E-W baseline Oct.-Nov., 1963)

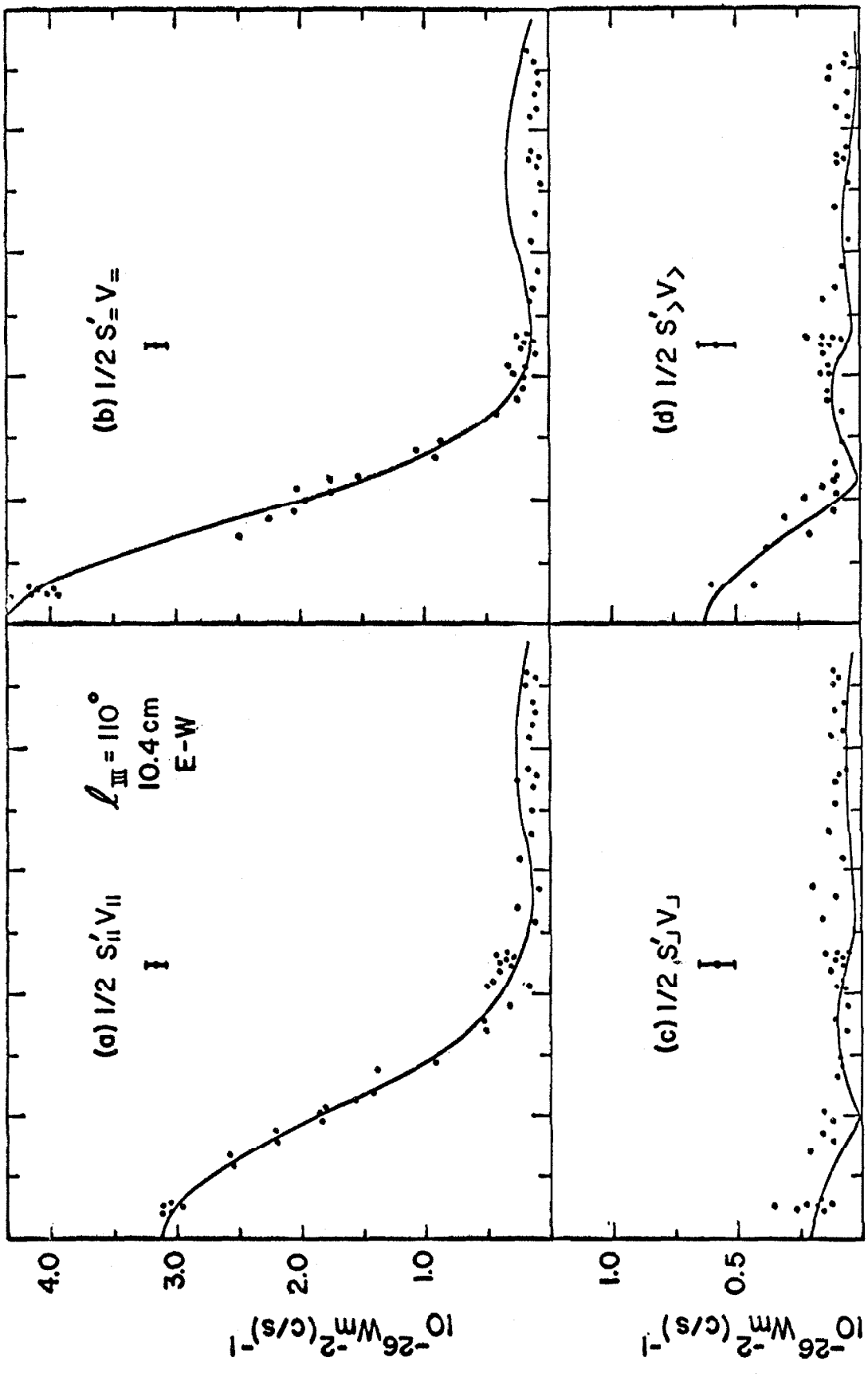

Figure 10. Visibility amplitudes for $\ell_{III}=110°$ at 10.4 cm(E-W baseline, Oct.-Nov., 1963)

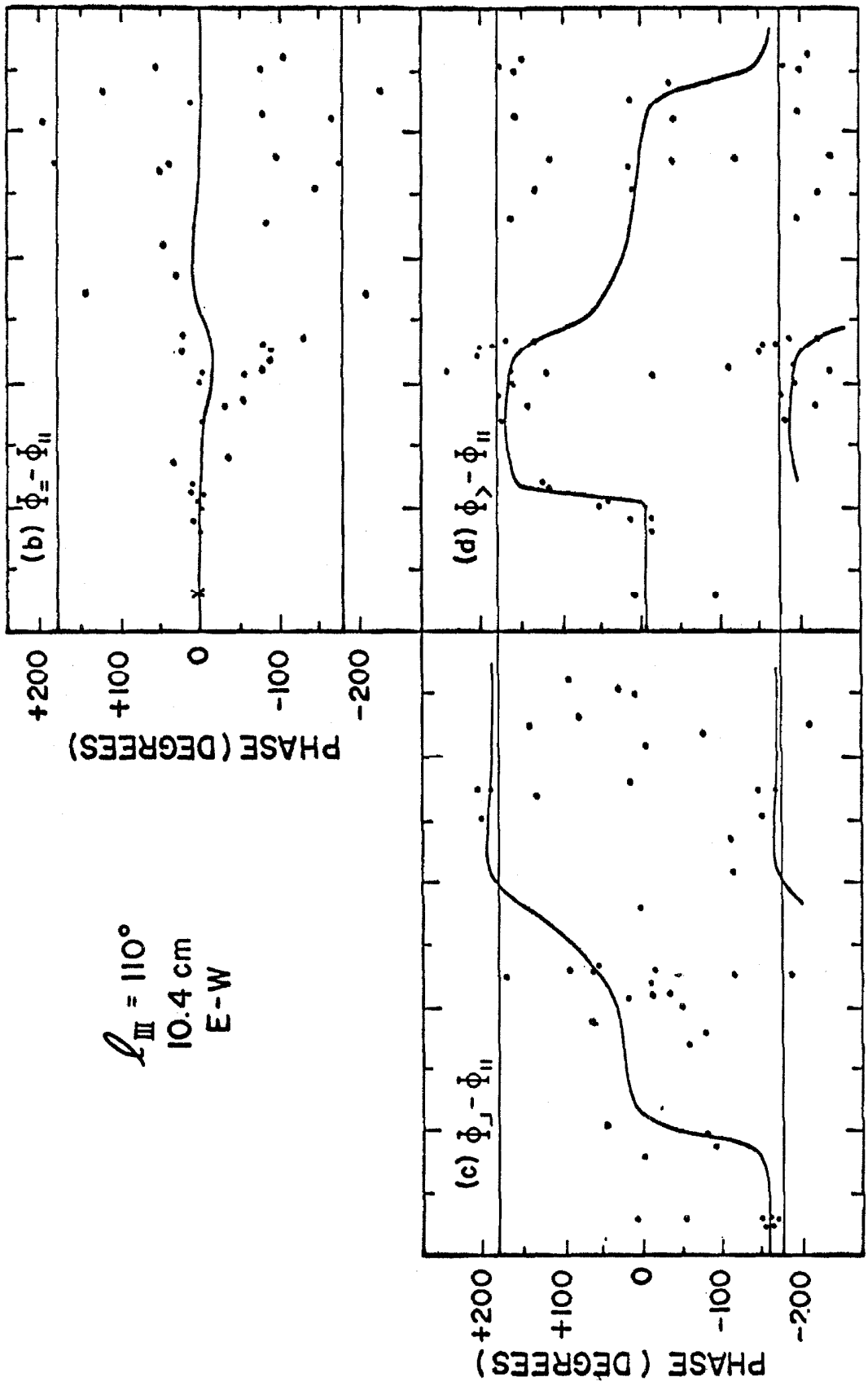

Figure 11. Relative visibility phases for $\ell_{III}=110°$ at 10.4 cm(E-W baseline, Oct.-Nov.1963).

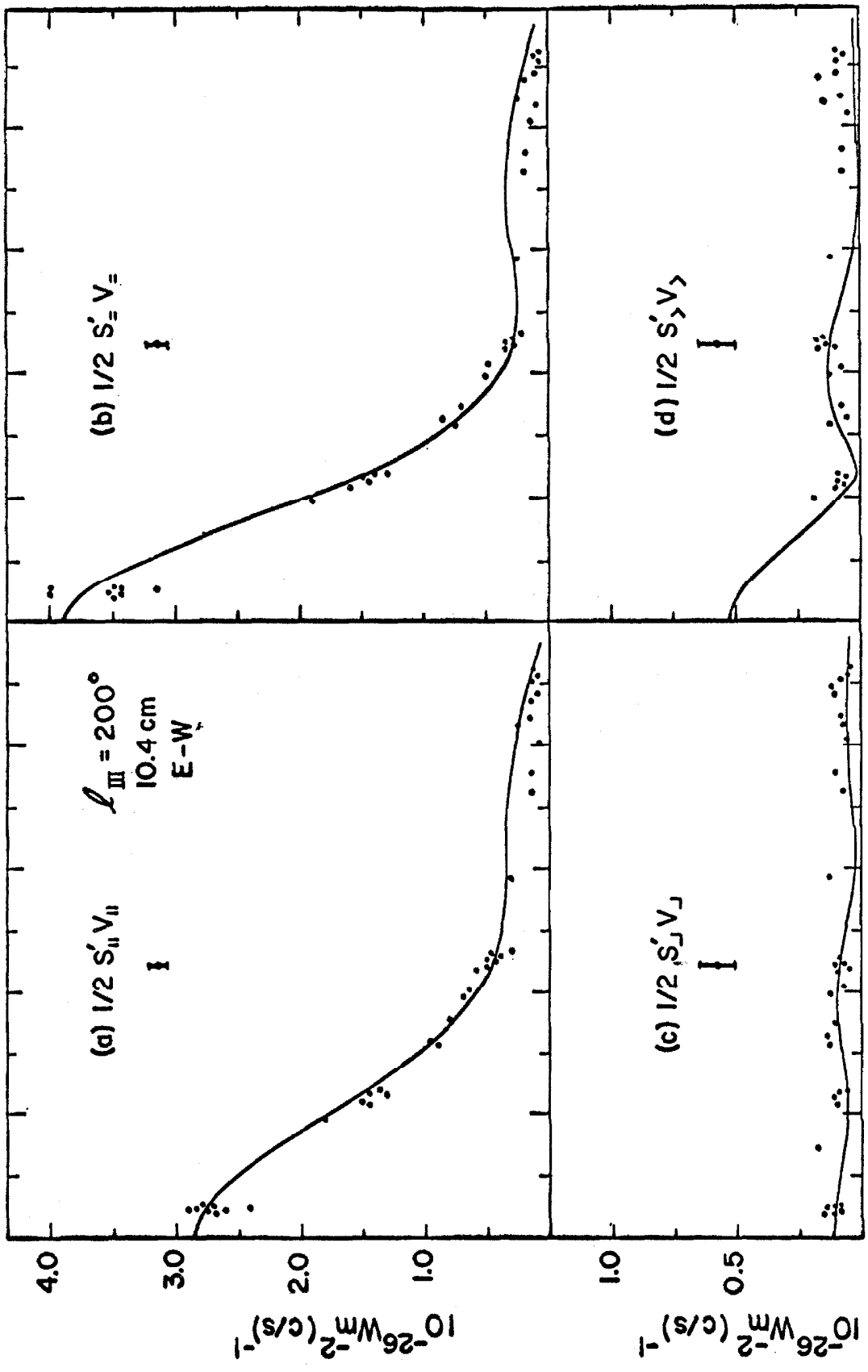

Figure 12. Visibility amplitudes for $\ell_{III}=200°$ at 10.4 cm(E-W baseline, Oct.-Nov., 1963.)

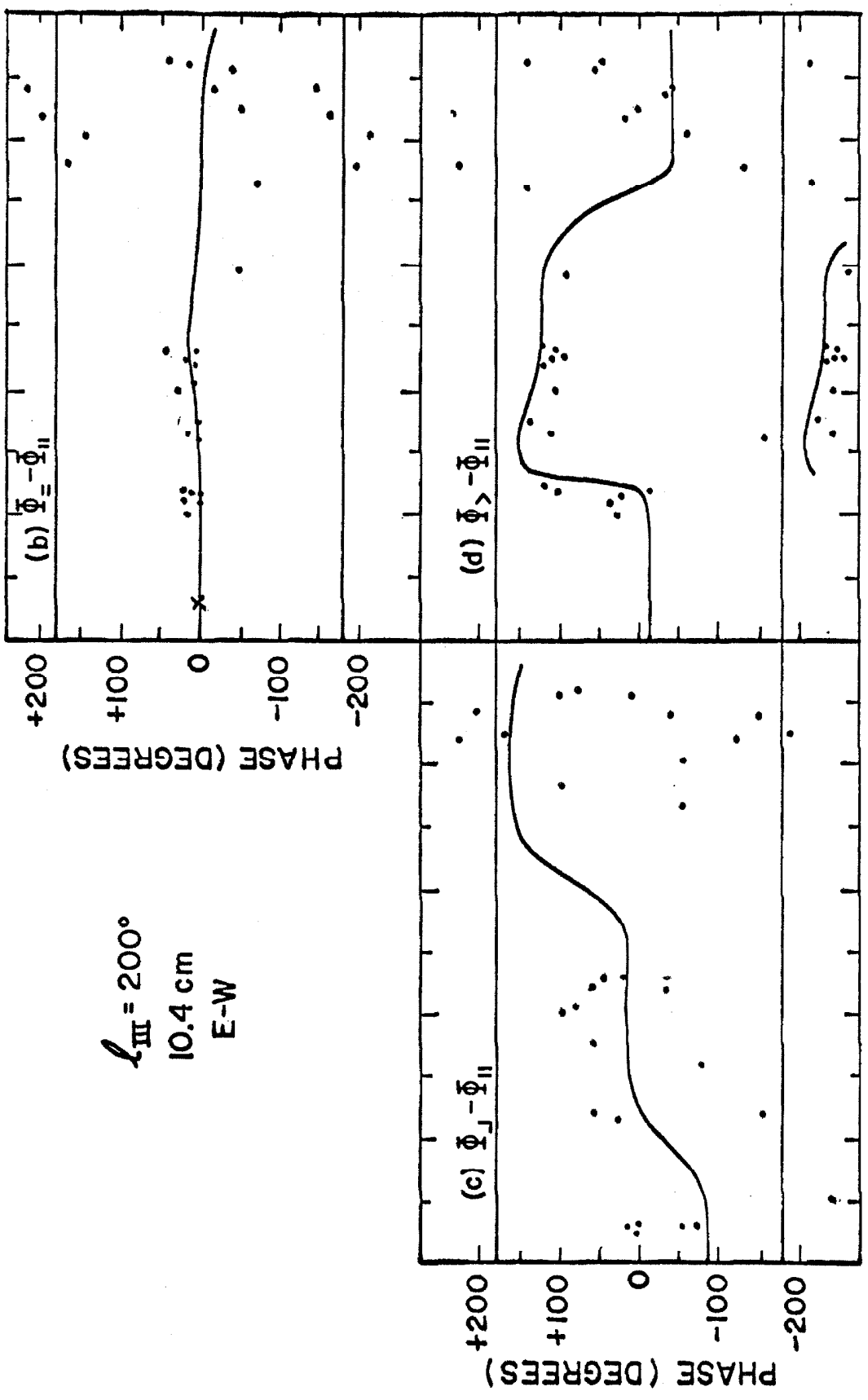

Figure 13. Relative visibility phases for ℓ_{III}=200° at 10.4 cm(E-W baseline, Oct.-Nov.,1963.)

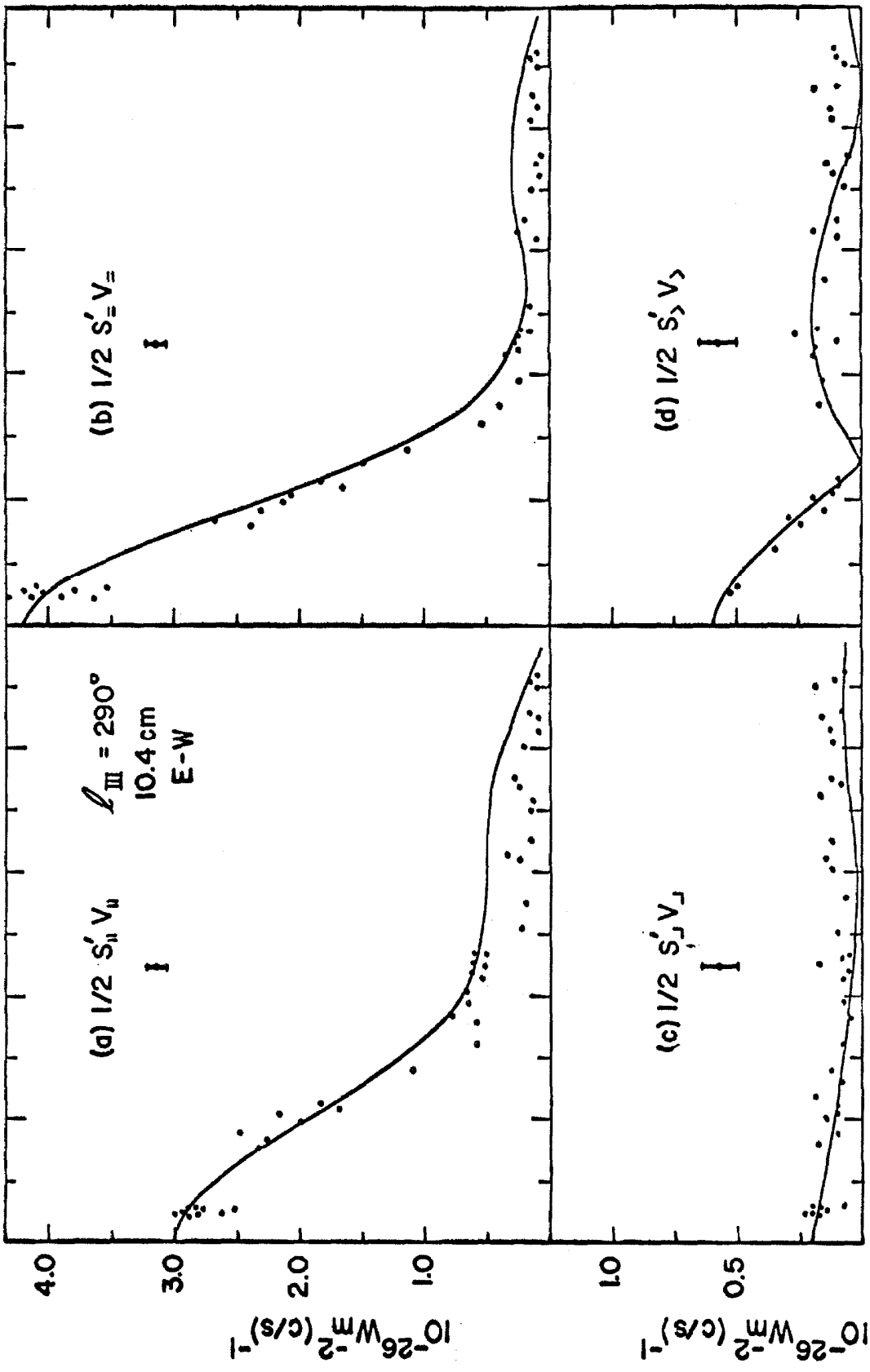

Figure 14. Visibility amplitudes for $\ell_{III}=290°$ at 10.4 cm(E-W baseline, Oct.-Nov., 1963.)

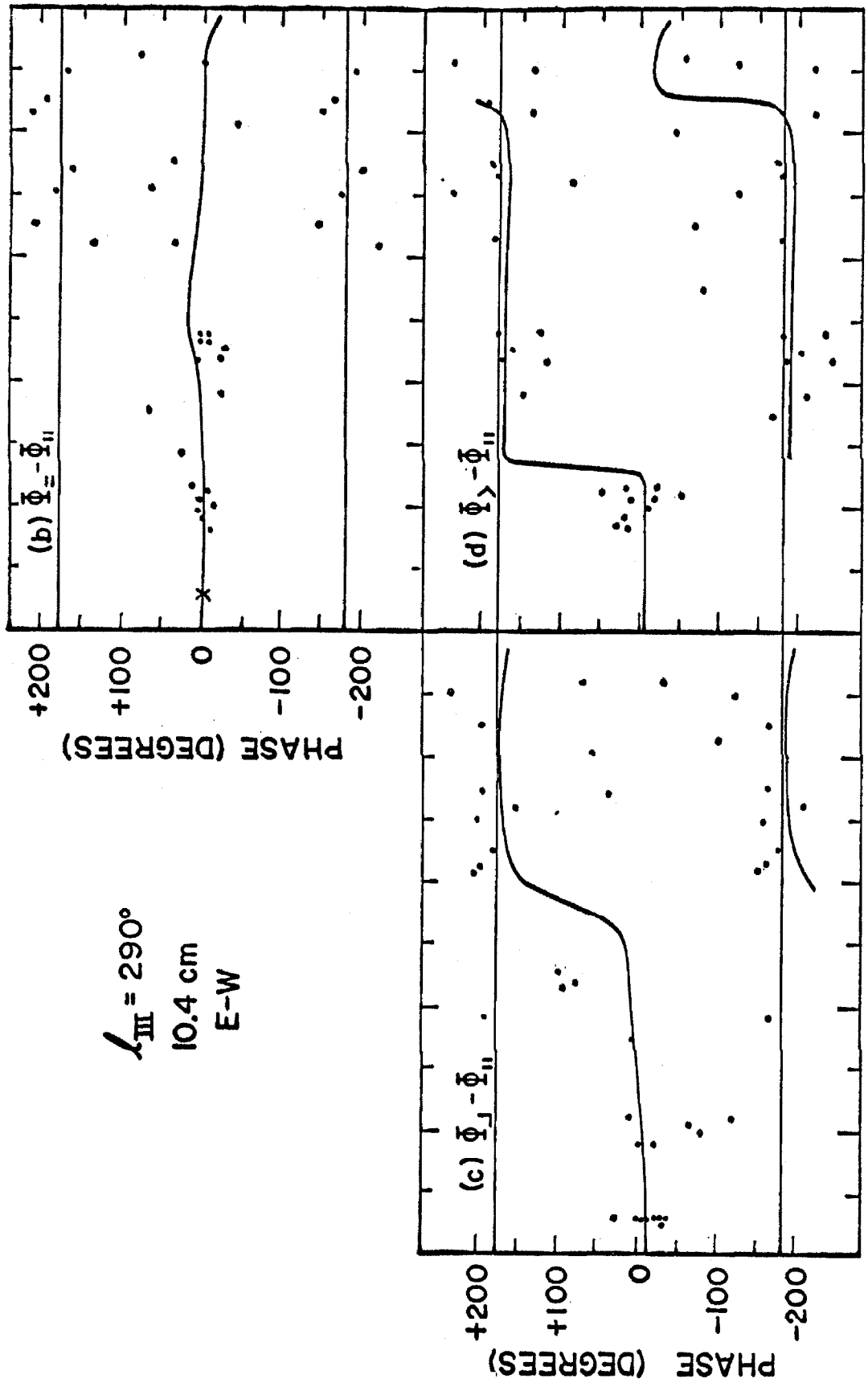

Fig. 15 Relative visibility phases for $\ell_{III}=290°$ at 10.4 cm (E-W baseline, Oct.-Nov., 1963).

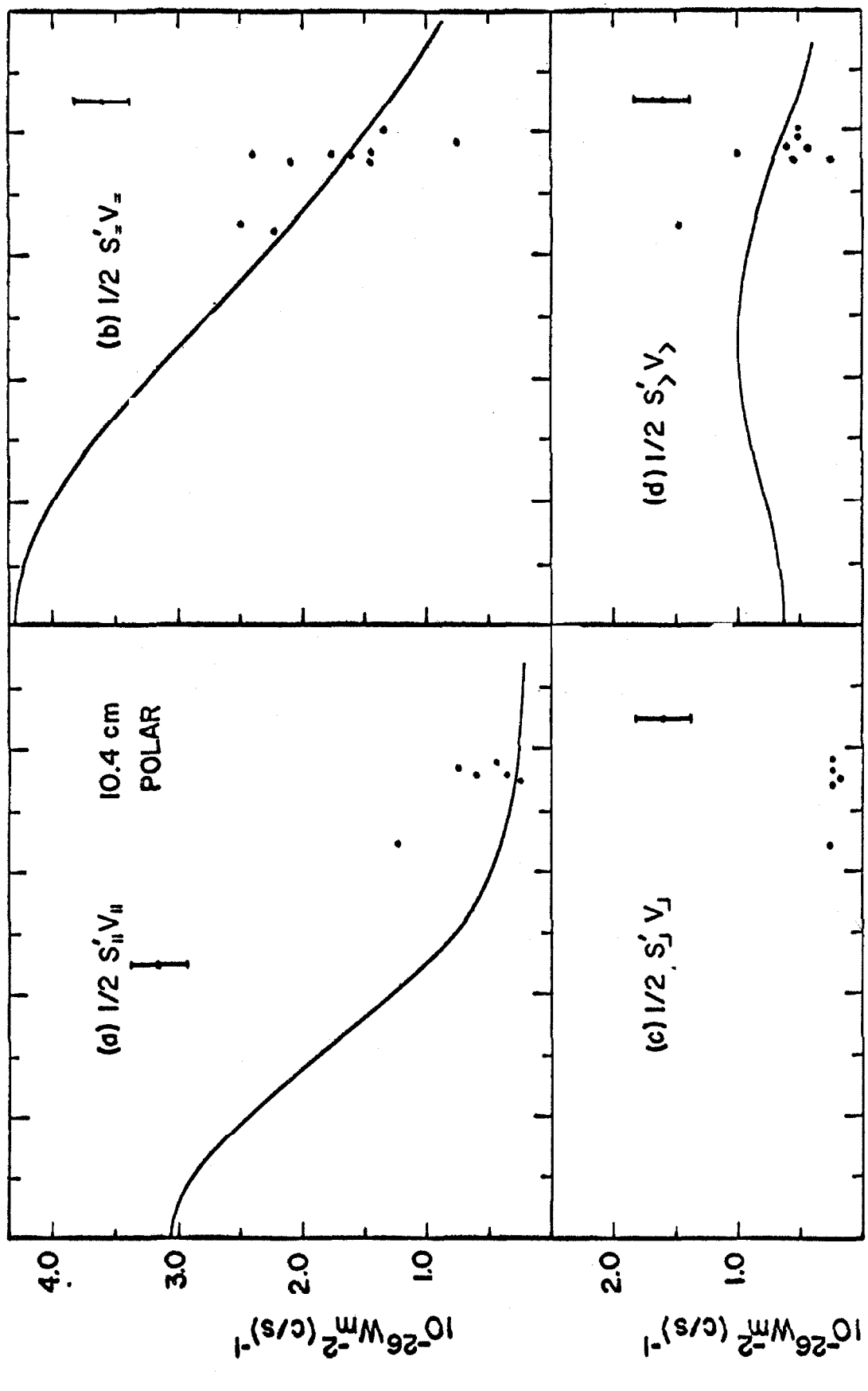

Figure 16. Visibility amplitudes at 10.4 cm. (Polar baseline, July, 1964).

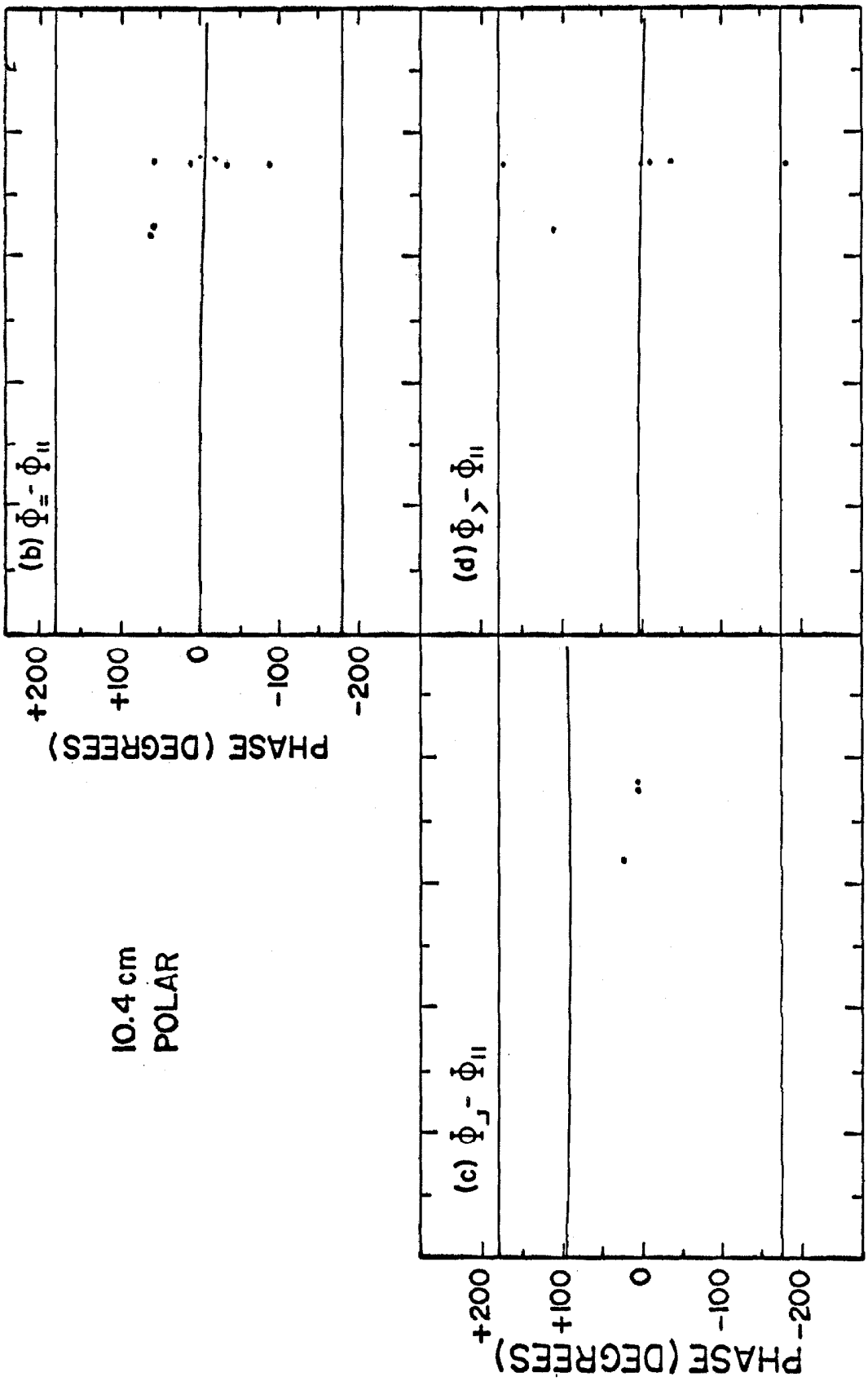

Figure 17. Relative visibility phases at 10.4 cm. (Polar baseline, July, 1964).

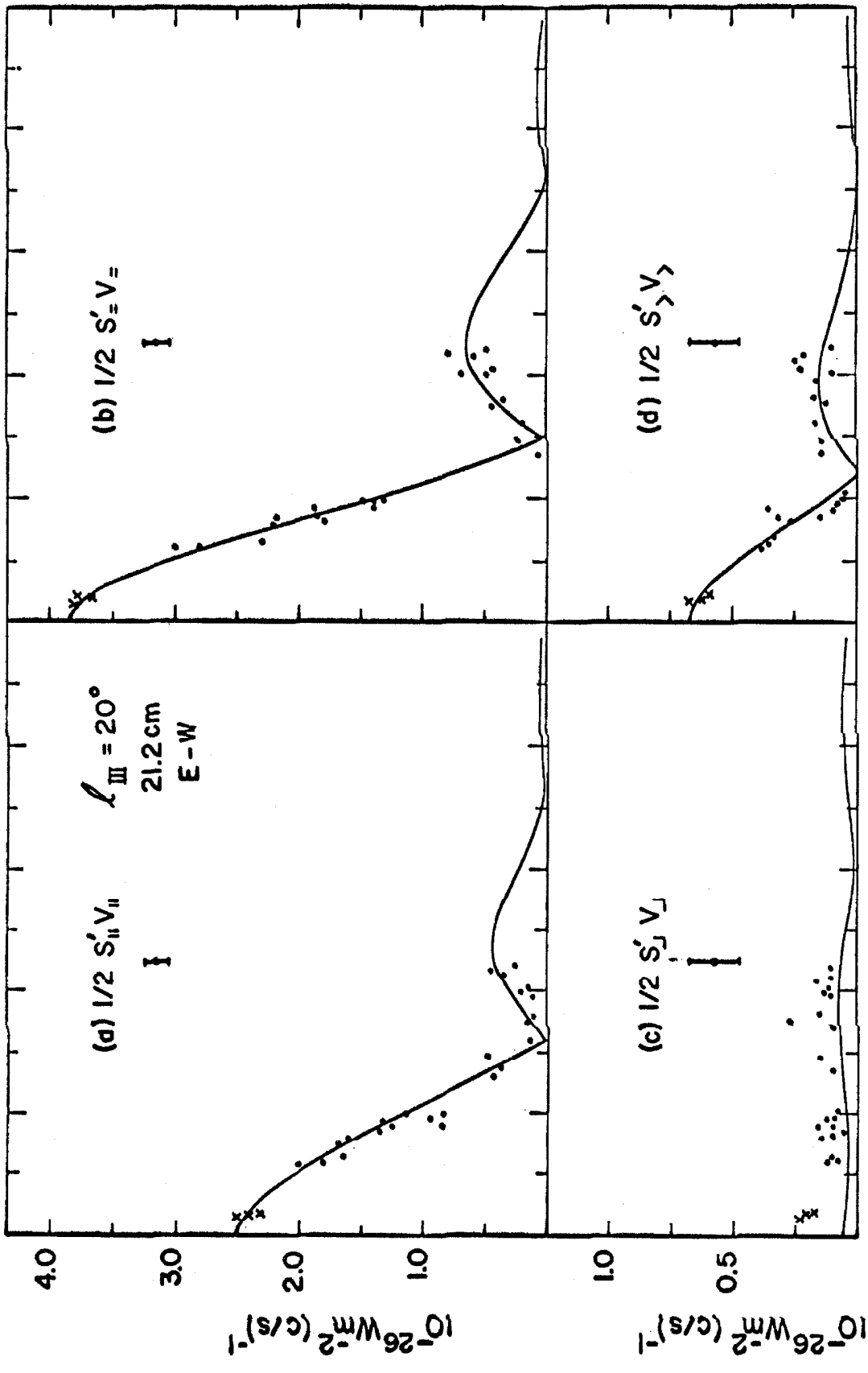

Fig. 18. Visibility amplitudes for $\ell_{III}=20°$ at 21.2 cm(E-W baseline, Nov., 1963-Feb.,1964).

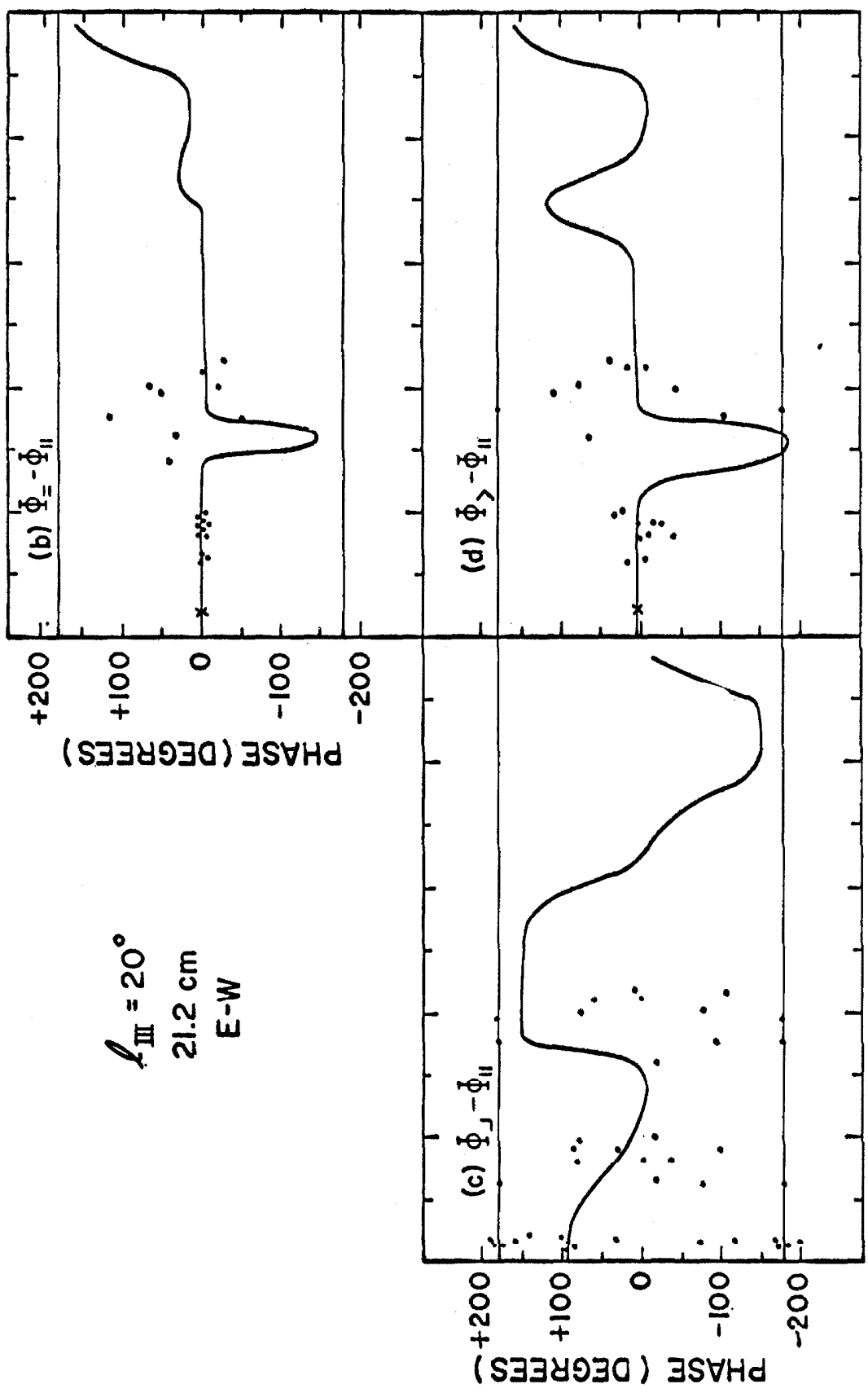

Fig. 19. Relative visibility phases for $\ell_{III}=20°$ at 21.2 cm(E-W baseline, Nov. 1963-Feb.,1964).

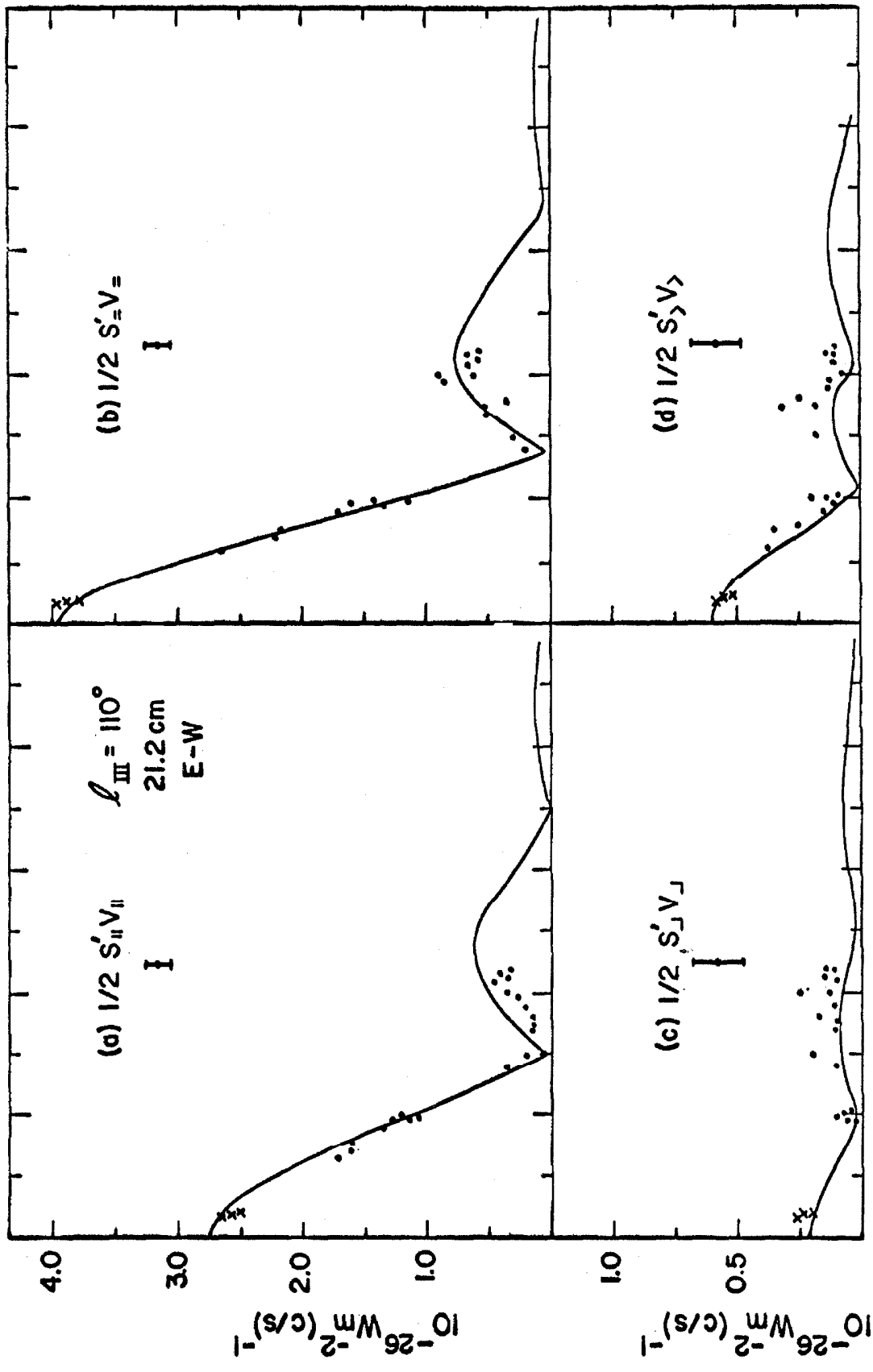

Fig. 20. Visibility amplitudes for $\ell_{III}=110°$ at 21.2 cm (E-W baseline, Nov., 1963-Feb., 1964).

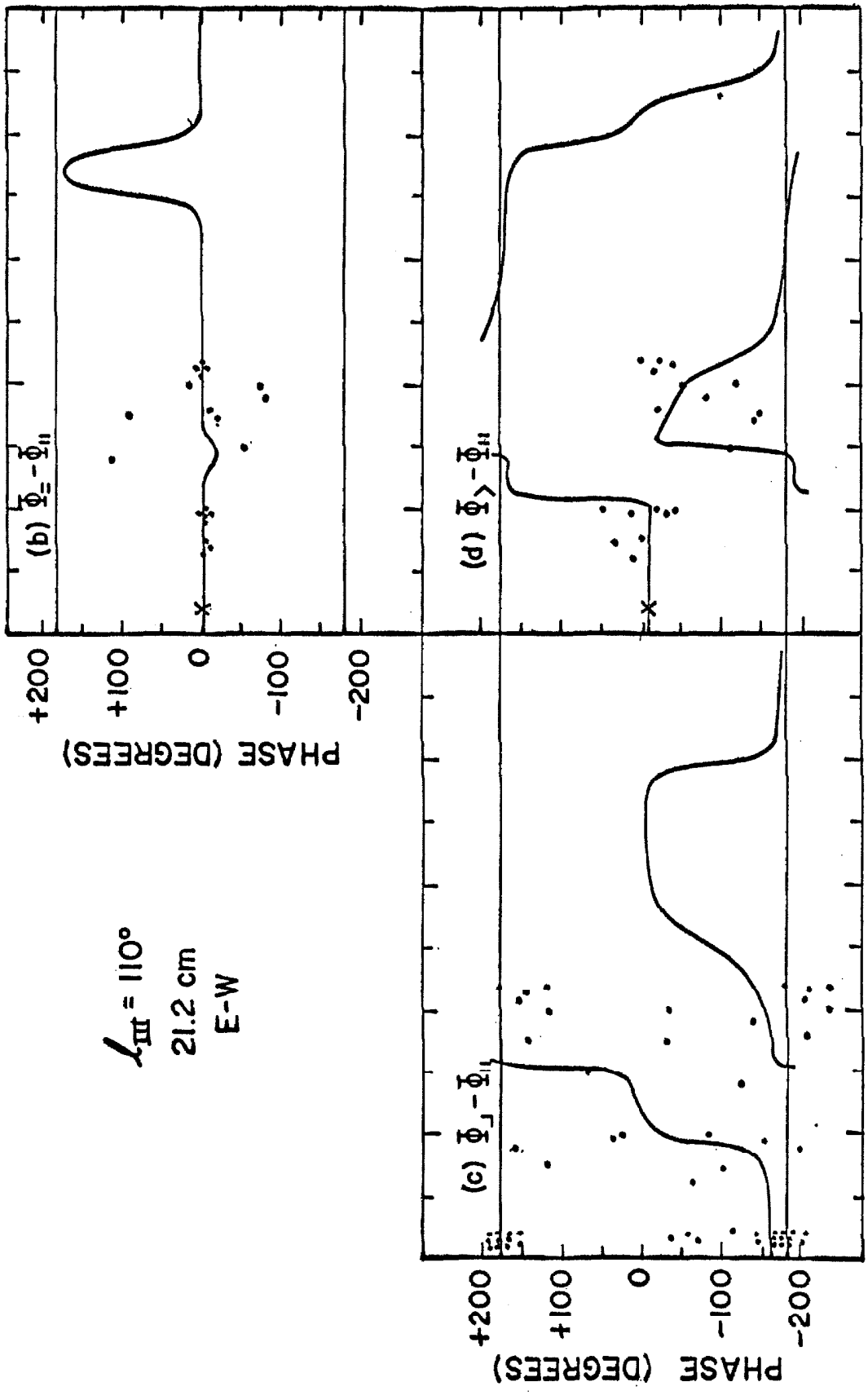

Fig. 21. Relative visibility phases for $l_{III}=110°$ at 21.2 cm(E-W baseline, Nov.,1963-Feb.,1964).

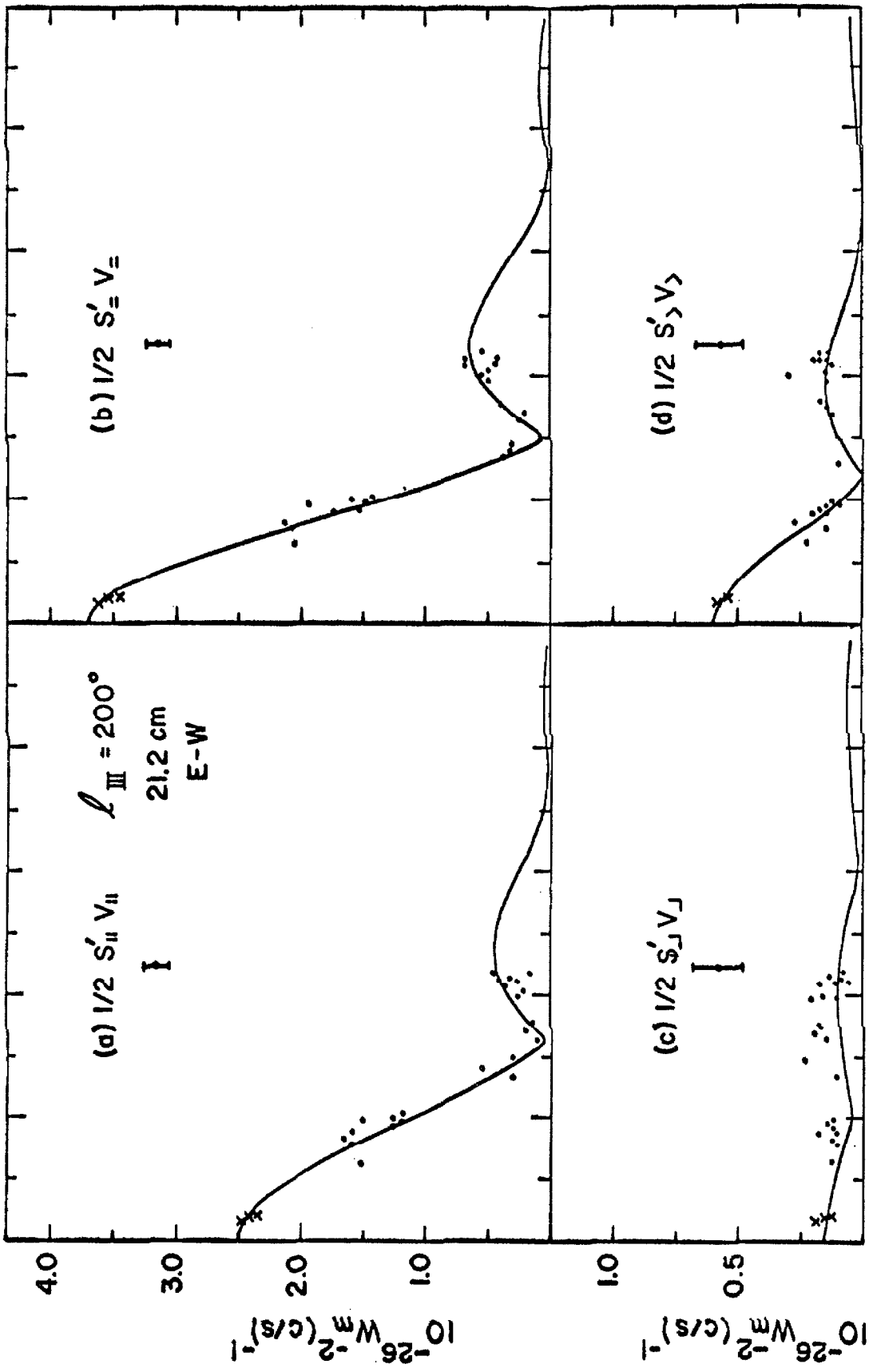

Fig. 22. Visibility amplitudes for $\ell_{III}=200°$ at 21.2 cm (E-W baseline, Nov., 1963-Feb., 1964).

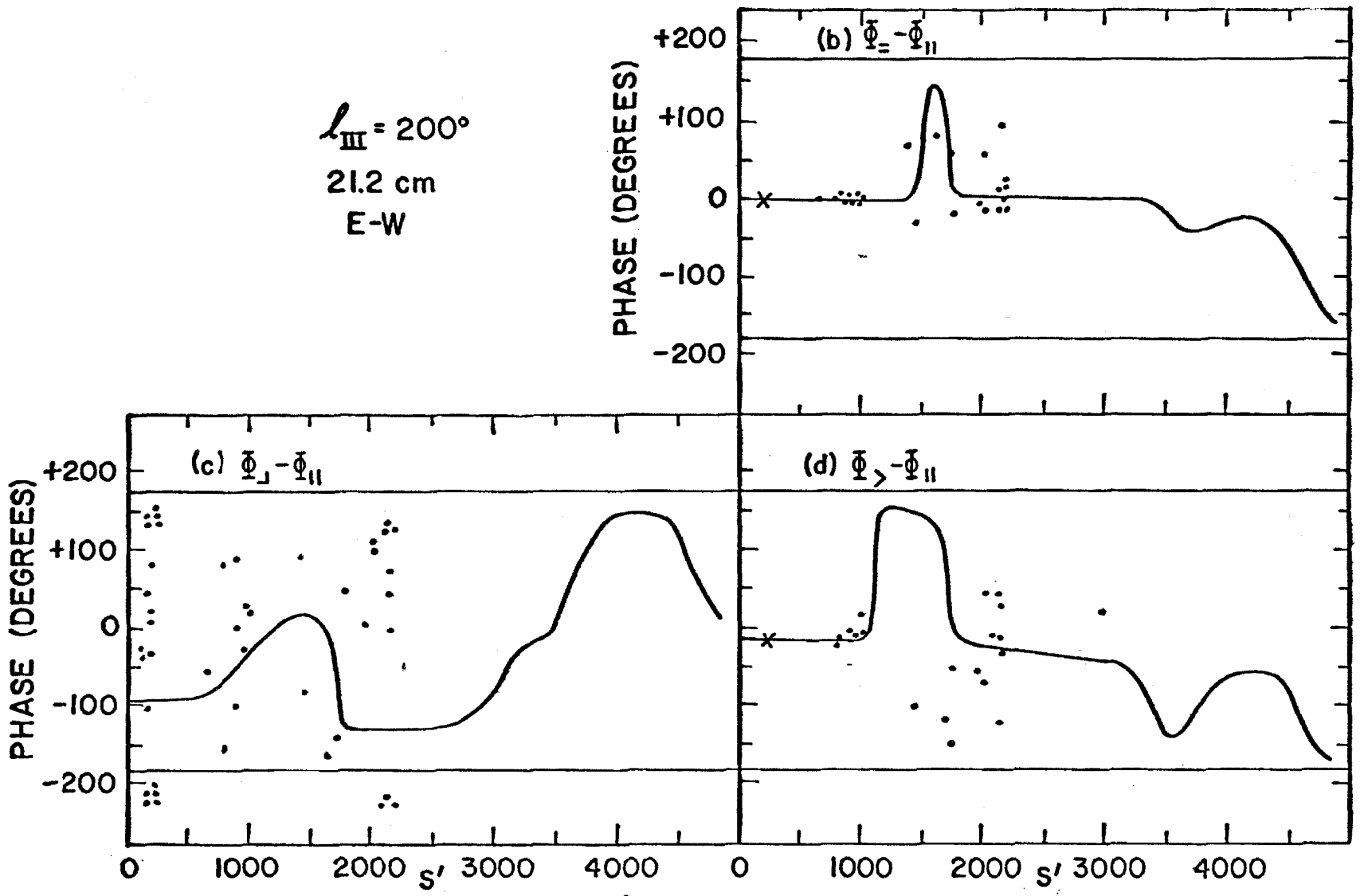

Fig. 23. Relative visibility phases for ℓ_{III}=200° at 21.2 cm(E-W baseline, Nov.,1963-Feb.,1964).

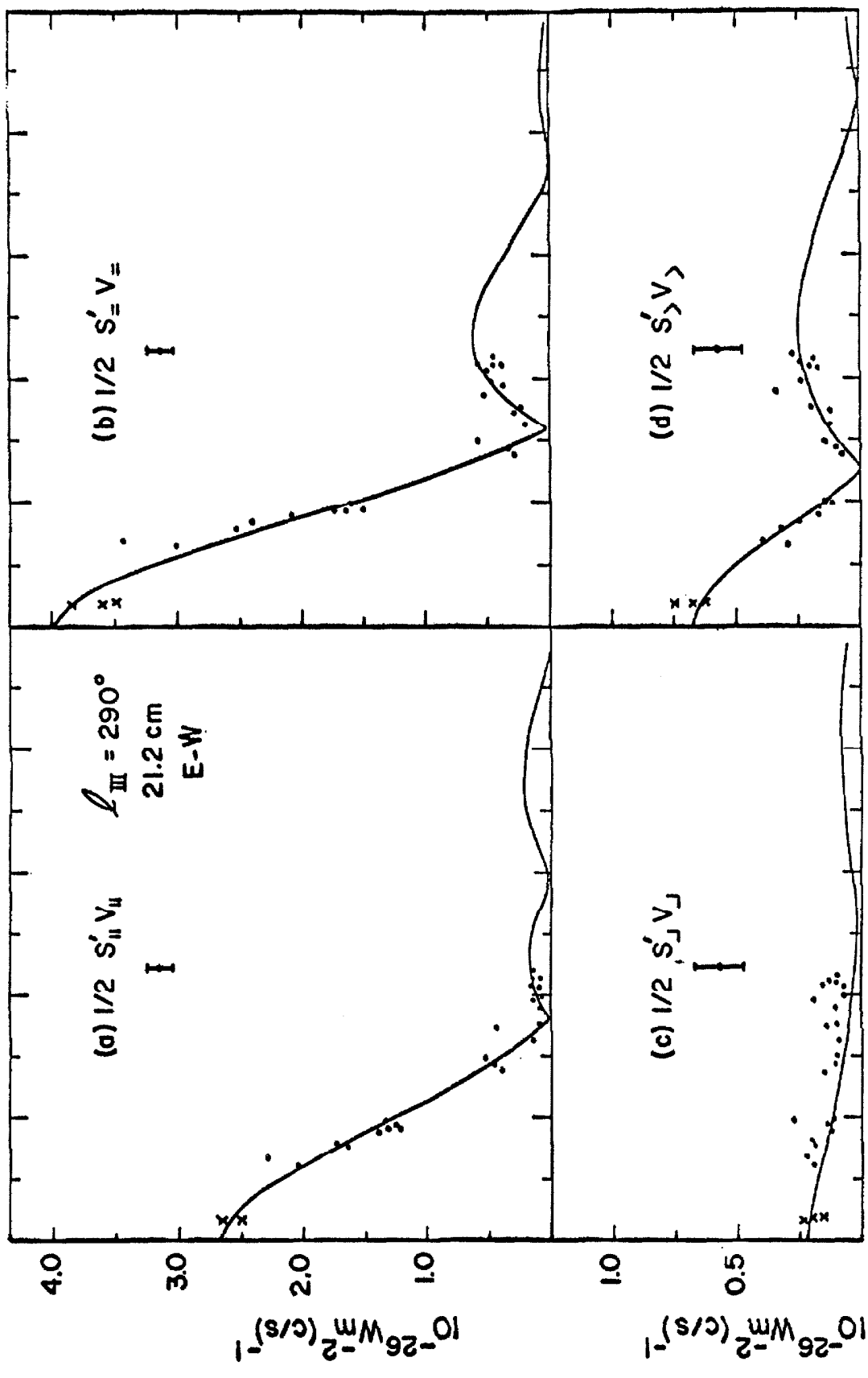

Fig. 24. Visibility amplitudes for $\ell_{III}=290°$ at 21.2 cm (E-W baseline, Nov., 1963-Feb., 1964).

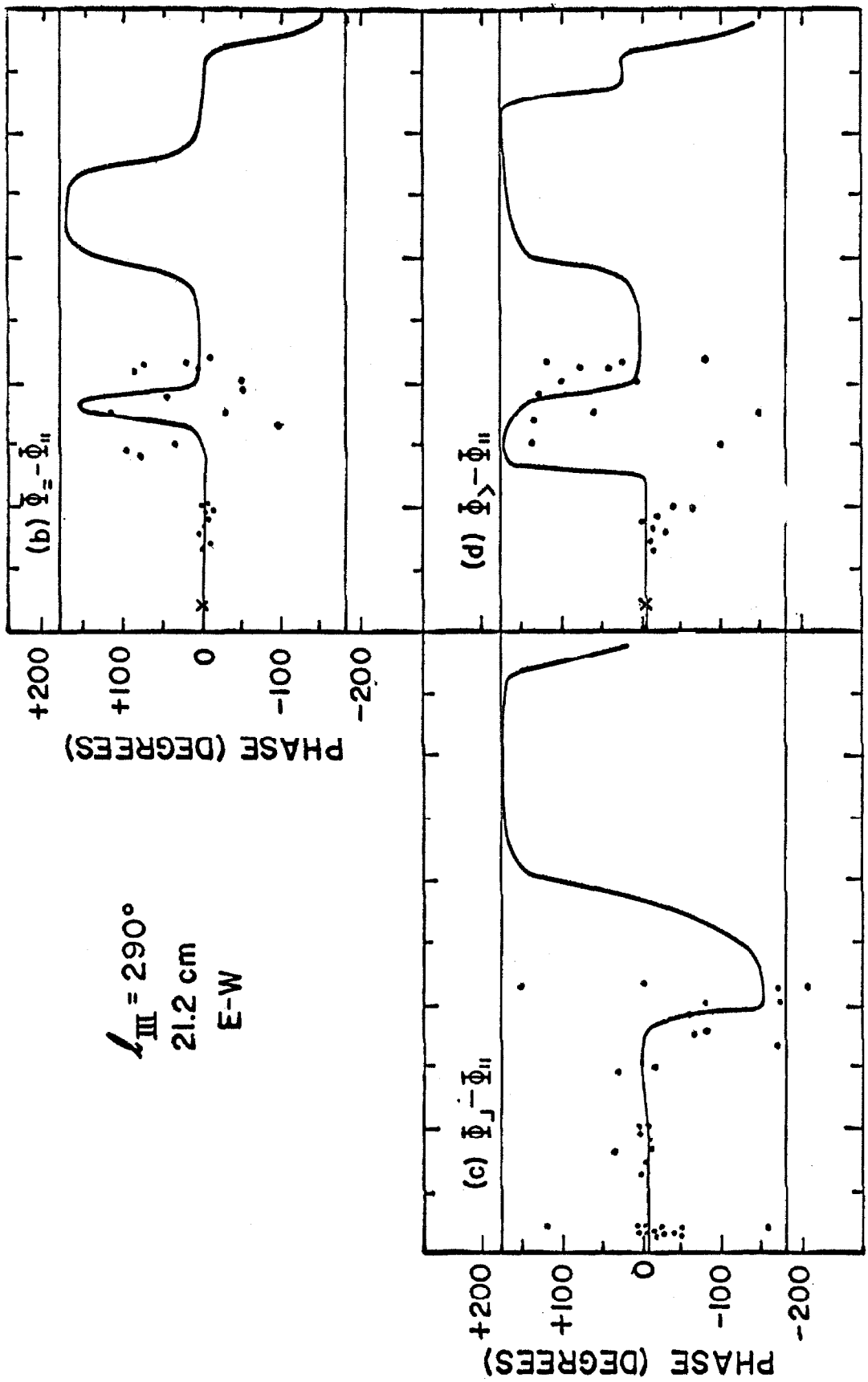

Fig. 25. Relative visibility phases for $l_{III}=290°$ at 21.2 cm(E-W baseline, Nov.,1963-Feb.,1964).

most useful. The solid curves sketched in the figures will be explained in the next chapter and, for the moment, can be ignored.

Each of the figures represents a range of 90° in ℓ_{III}, centered on the given value. Each of the visibility amplitude plots shows an error bracket which represents the typical RMS error due to system noise. The errors associated with the phases vary wildly because they depend on the visibility amplitudes. In some cases the density of data points is too great to allow them to be plotted individually. An x is then used to represent the average of several data points.

A casual inspection of the visibility functions, without any detailed analysis, reveals several gross features of the brightness distribution. In the first place, the earlier size measurements, which gave one and three Jupiter diameters for the polar and equatorial dimensions respectively, are roughly confirmed. The parallel horn measurements at 10.4 cm., particularly the one with horns parallel to the polar axis, reveal the behavior one finds for "halo-core" objects. The halo is resolved rather quickly, but the core contribution still lingers on at long baselines. This behavior is not evident at 21.2 cm., however, and this suggests that the core is produced by thermal emission from the disk, which is important at the shorter wavelength, but relatively unimportant at the

longer wavelength.

The 21.2 cm. observations reveal that the non-thermal emission must have a very symmetric distribution in the plane of the sky. This is because the first "null" of the visibility functions is very nearly a true null. The visibility amplitudes drop to at least the level of the noise at this point.

The measurements with a polar baseline at 10.4 cm. indicate another interesting detail. The visibility amplitude for crossed horns shown in Figure 16d is larger at 3200λ than the zero baseline value and then decreases quickly at longer baselines. This is what one would expect if the radiation near the equator were polarized with the plane of polarization in the equatorial direction and the radiation in each of the polar regions were polarized with the plane of polarization in the polar direction. This reveals the magnetic field orientation because the plane of polarization should be perpendicular to the apparent magnetic field direction. The result is consistent with a dipole magnetic field.

There are other features which could also be mentioned, but we may as well proceed directly with a more elegant analysis which will produce the detailed brightness distribution more accurately.

VI INTERPRETATION OF THE VISIBILITY FUNCTIONS

To analyze the results of the last chapter, a model fitting procedure was adopted. It is possible, in principle, to directly invert the visibility functions, each of which is the Fourier transform of a one-dimensional brightness distribution. In practice, however, it would have been difficult to get accurate results. This is due to the scatter of the points, the fact that in the limited range of baselines (spatial frequencies) there were places with a scarcity of points to determine the curve, and also the lack of absolute phase information. Another complication is that each visibility function in the present study contains only a small fraction of the total information, and it is mainly by comparing and combining them that one extracts the information. Because of these difficulties, model fitting seemed to be the best course of action.

The procedure was to start with a generalized model for the two-dimensional brightness distribution of Jupiter which contained a number of unknown parameters. A computer program was prepared for computing and plotting the interferometer response to the model as a function of baseline for different baseline orientations and different feed combinations. The parameters were varied to obtain

the best agreement between the computed and observed visibility functions.

The generalized model chosen was not, in fact, completely general. In order to simplify the problem somewhat, certain features were built into the model. These features are things which were known previously or expected from theoretical and geometrical considerations.

First, the assumption was made that the total emission, brightness distribution, and polarization properties remained nearly constant throughout the period during which the observations were made (Oct., 1963 to July, 1964), except for the apparent changes associated with Jupiter's rotation. The Caltech observations do not show any sizeable long term variations in the equivalent disk temperature, nor do those of Bash, et al (35) or Roberts and Komesaroff (9).

Symmetry of the nonthermal emission about its major and minor axes was assumed and was built into the model. We have already seen that the visibility functions, especially those for 21.2 cm., show this to be approximately true. However, allowance is made for a possible small displacement between the positions of the thermal and nonthermal contributions. Chang (59) estimated that Jupiter's magnetosphere has a radius fifty times the planet's radius. Hence, we may be justified in expecting that the solar

wind will not cause much distortion in the emitting region.

The assumption was also made that Jupiter's magnetic field is roughly a dipole field so that the apparent field orientation can be determined, at least crudely, for each point of the source. This leads to two important simplifications:

(a) Because the plane of polarization is perpendicular to the field direction, one can predict the polarization direction in any given region.

(b) Because of the beaming properties of synchrotron radiation, one can predict in a crude fashion which regions will beam their emission, if any, toward the earth.

A uniform circular disk without polarized limbs was assumed for the thermal emission from the planet. At 10.4 cm. the thermal emission should be well below the non-thermal emission, but its contribution is still important. For the present, secondary effects are ignored. These include the known flattening of the disk, possible latitude effects in the brightness distribution of the disk, possible limb darkening, and possible linear polarization of the limbs (in the case where part of the thermal emission comes from the planetary surface).

Figure 26 shows schematically the generalized model. The region D is the uniform disk representing the

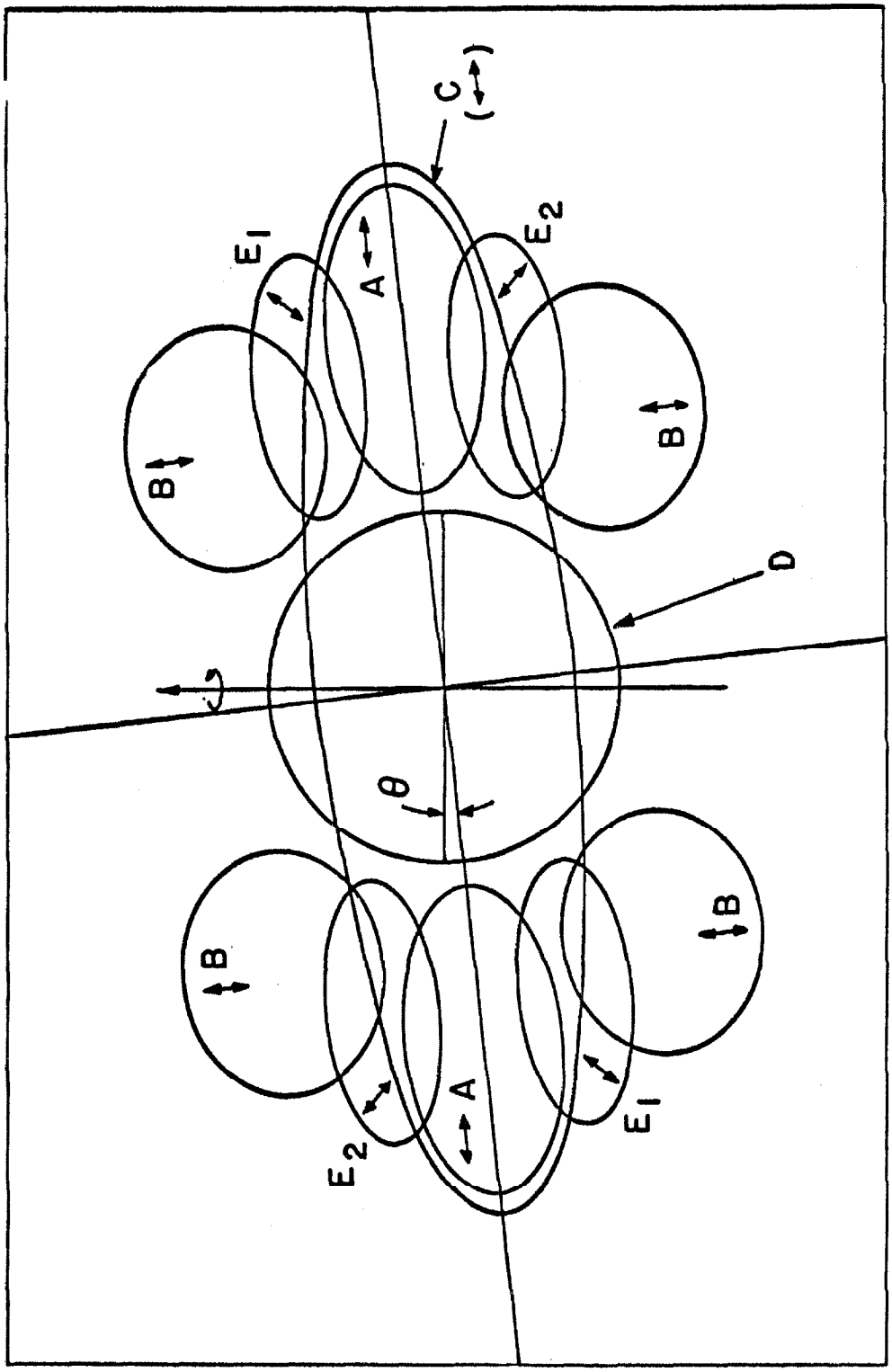

Figure 26. The generalized model. The dimensions are variable parameters. The specific ones shown are somewhat similar to the ones determined by fitting.

thermal contribution. All the others are for the non-thermal contribution and are taken to be elliptical gaussians. The unknown parameters to be found by fitting are the contributions from each region (flux parameters), two dimensions for each region which determine the size of the ellipse, and additional parameters which specify the position of the region. In addition, there is a parameter (p_o) which specifies the degree of linear polarization for each element (assumed to be the same for each region). As an approximation, each region except D is assigned one of four possible orientations for its plane of polarization as shown in Figure 26. The radiation from D is randomly polarized.

Region C represents radiation in the equatorial part of the source. To this are added the A regions to allow for the expected limb brightening of the synchrotron emission. (There must be limb brightening along the equator because we are dealing with a shell of emission. There is obviously no emission in the volume occupied by the planet. Moreover, the planet obscures the radiation behind it.) The B regions represent radiation to the sides of the poles which is polarized oppositely to that of the equatorial regions. The E regions are intermediate between the two extremes. As an approximation, the circularly polarized radiation

is all assigned to the A regions.

The integrated flux density associated with the Stokes parameters originates as follows:

$$\begin{aligned} S'_I &= A+B+C+D+E \\ S'_Q &= p_o\ (A+C-B) \\ S'_U &= p_o\ (E_1-E_2) = 0 \\ S'_V &= p'A \end{aligned} \qquad (6\text{-}1)$$

where A is the total flux density of the A regions and so forth for B, C, D, and E.

$E_1 = E_2 = 1/2\ E$

p' is a function of ℓ_{III} and was determined on the basis of the short baseline observations.

These equations can be generalized to give the unnormalized complex visibility functions of the Stokes parameters.

$$\begin{aligned} \underline{I} &= \underline{A}+\underline{B}+\underline{C}+\underline{D}+\underline{E} \\ \underline{Q} &= p_o\ (\underline{A}+\underline{C}-\underline{B}) \\ \underline{U} &= p_o\ (\underline{E}_1-\underline{E}_2) \\ \underline{V} &= p'\underline{A} \end{aligned} \qquad (6\text{-}2)$$

where $\underline{A} = \underline{A}\ (s_x, s_y, \ell_{III})$ and so forth for $\underline{B}$, $\underline{C}$, $\underline{D}$, $\underline{E}_1$, and $\underline{E}_2$.

These are the unnormalized complex visibility functions for the various regions.

The calculation of the interferometer response to the model, as a function of baseline for different feed combinations is straightforward. We find from equations (2-2) and (2-3) combined with (6-2) that

$$\frac{\underline{R}_{\shortparallel}}{k} = \tfrac{1}{2}(\underline{A}+\underline{B}+\underline{C}+\underline{D}+\underline{E}) - \tfrac{1}{2}p_o\ (\underline{A}+\underline{C}-\underline{B})\cos 2\theta$$

$$+\tfrac{1}{2}p_o\ (\underline{E}_1-\underline{E}_2)\sin 2\theta$$

$$\frac{\underline{R}_{=}}{k} = \tfrac{1}{2}(\underline{A}+\underline{B}+\underline{C}+\underline{D}+\underline{E}) + \tfrac{1}{2}p_o(\underline{A}+\underline{C}-\underline{B})\cos 2\theta$$

$$- \tfrac{1}{2}p_o(\underline{E}_1-\underline{E}_2)\sin 2\theta \qquad (6\text{-}3)$$

$$\frac{\underline{R}_{\lrcorner}}{k} = -\tfrac{1}{2}p_o(\underline{A}+\underline{C}-\underline{B})\sin 2\theta - \tfrac{1}{2}p_o(\underline{E}_1-\underline{E}_2)\cos 2\theta$$

$$+ \tfrac{1}{2}ip'\underline{V}$$

$$\frac{\underline{R}_{>}}{k} = \tfrac{1}{2}p_o(\underline{A}+\underline{C}-\underline{B})\cos 2\theta - \tfrac{1}{2}p_o(\underline{E}_1-\underline{E}_2)\sin 2\theta$$

$$+ \tfrac{1}{2}ip'\underline{V}$$

where $\underline{R}_{\shortparallel} = \underline{R}_{\shortparallel}(s_x, s_y, t, \ell_{III})$ and so forth for

$\underline{R}_{=}$, $\underline{R}_{\lrcorner}$ and $\underline{R}_{>}$

$$k = GA \exp\left[i(-2\pi s_x \Omega t + \psi)\right]$$

$\underline{A}$, $\underline{B}$, $\underline{C}$, $\underline{D}$, $\underline{E}_1$, and $\underline{E}_2$ are the unnormalized complex visibility functions for a double elliptical gaussian, two double elliptical gaussians, an elliptical gaussian, a uniform disk, a double elliptical gaussian, and a double elliptical gaussian respectively, each with its proper orientation.

θ = P.A. of the plane of polarization -P.A. of equator (as in Chapter III).

Moffet (79) describes the visibility functions for simple configurations such as these. The sizes and separations are given by the parameters being attempted. By the assumed symmetry, $\underline{B}$, $\underline{C}$, $\underline{E}_1$, and $\underline{E}_2$, and the real part of $\underline{A}$ have phase 0° (+) or 180° (-) and can be added algebraically. However, D may be centered differently, and thus $\underline{D}$, as well as the imaginary part of $\underline{A}$, must be added in with regard to the phase.

Although the calculation of the interferometer response is straightforward, it is extremely laborious and must be done many times to try different values for the parameters. It was for this reason that the calculations were carried out using a computer. The computed visibility functions were displayed in tabular form and also in graphical form where the scales were suitable for comparing directly with the plotted data.

The difference in position between the non-thermal

and thermal emission was handled by expressing it as a phase difference composed of the sum of a constant term (representing a position difference in Jupiter's polar direction) and a term which varies sinusoidally with ℓ_{III} (representing a position difference perpendicular to the polar direction). The constants in this relation were not input parameters, but they could be easily changed. p', which describes the imaginary part of A (circular polarization), was represented by a similar relation.

In addition to the input parameters representing the quantities to be determined by fitting, the computer was also given, for each calculation, the value of ℓ_{III} and the position angles of the polar axis and magnetic axis with respect to the interferometer baseline. For all of the present east-west observations, the position angle of the polar axis with respect to the baseline was 65°.

The single dish observations of flux density and percentage of linear polarization provide two constraints which the flux parameters must satisfy through equations (6-1). In addition, certain constraints are put on the dimension parameters by the requirement that each region lie in that part of the magnetic field which will give its emission the correct plane of polarization. One would not expect the dimension parameters to vary

much because of beaming differences as Jupiter rotates. Therefore, for each likely combination of p_o and the dimension parameters, the interferometer response was calculated for each ℓ_{III} with an east-west baseline and for a single ℓ_{III} with a polar baseline, adjusting only the flux parameters to satisfy the single dish constraints at each ℓ_{III}.

The best model which has been found for the two-dimensional brightness distribution of Jupiter at 10.4 cm. is shown in Figure 27. The diagram shown is for $\ell_{III} = 20°$. The value found for p_o was 0.7. The calculated east-west interferometer response to this model, with the orientation it had while the observations were made, is shown by the solid curves drawn in Figures 8 and 9. The models for $\ell_{III} = 110°$, 200°, and 290°, which differ only because of slight changes in the flux parameters, are very similar to Figure 27, and hence are not shown separately. Their computed east-west interferometer responses are given by the solid curves in Figures 10 to 15. The response for a baseline along the direction of Jupiter's magnetic axis is given by the curves in Figures 16 and 17. It is shown for $\ell_{III} = 20°$ although that is unimportant considering the inexactness of the polar data.

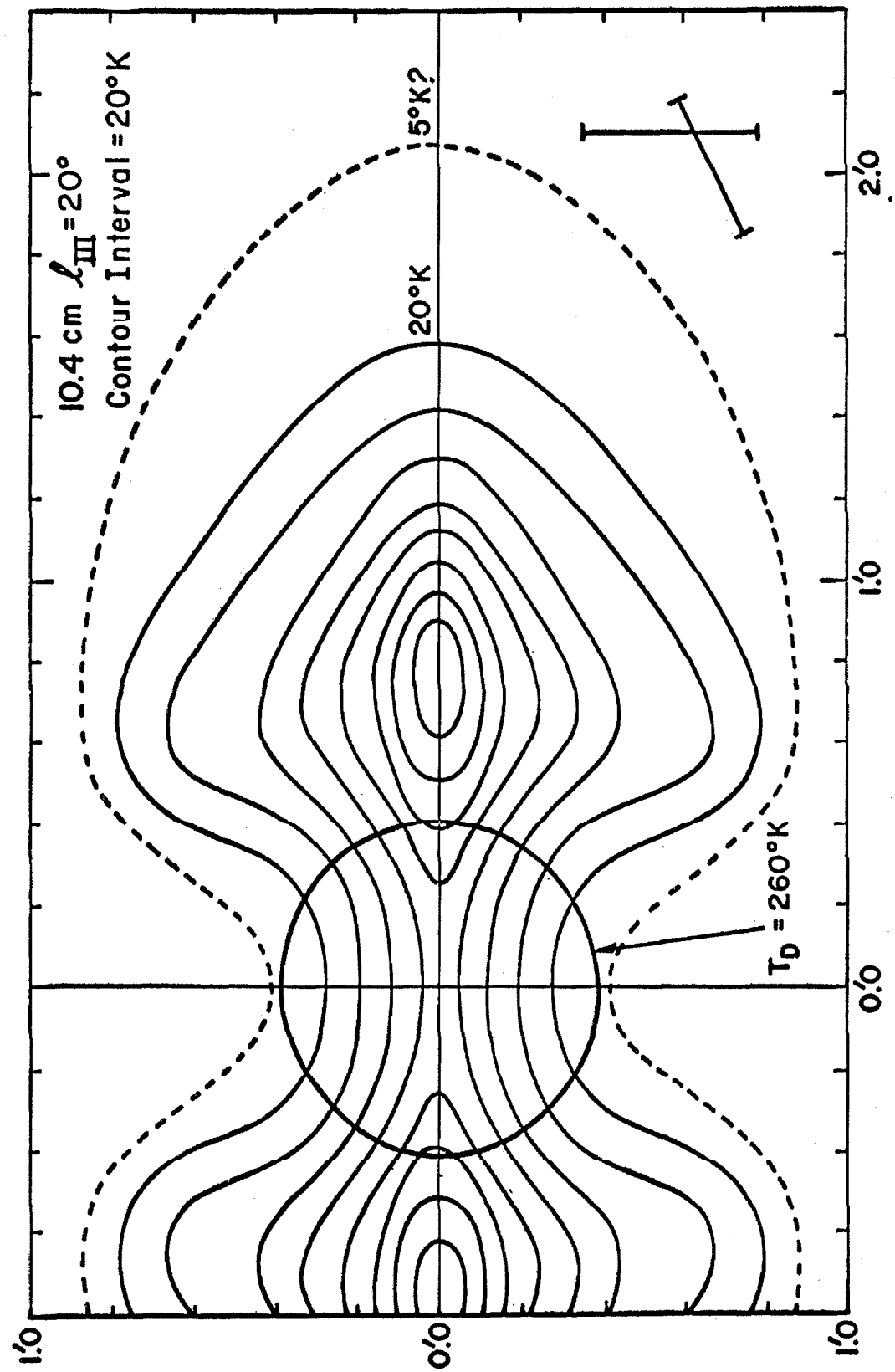

Figure 27. The 10.4 cm. brightness distribution determined for $\ell_{III}=20°$. The scale, in minutes of arc, refers to a distance of 4.04 A.U.

It is much harder to obtain a detailed brightness distribution at 21.2 cm. because there is less information available. The baseline range was smaller than at 10.4 cm., and there were no measurements with polar baselines. However, it was found that the best fit to the data was obtained by using the same dimension parameters and same p_o as the 10.4 cm. model and taking D one-fourth as large. The other flux parameters had to be changed some to satisfy the single dish measurements. The resulting model is shown in Figure 28 for $\ell_{III} = 20°$. The calculated interferometer response for this and the other longitudes is shown by the curves drawn in Figures 18 to 25.

In general, the visibility functions for the model fit the observation quite well and account for the changes observed as Jupiter rotates. For any given visibility function the fit can usually be improved easily by a minor change in the model. However, this generally upsets the fit of several others. The point is to fit all the visibility functions as well as possible with one model. There are some noteworthy disagreements between the calculated curves and the data. These cases should be mentioned together with their effects on the fitted model.

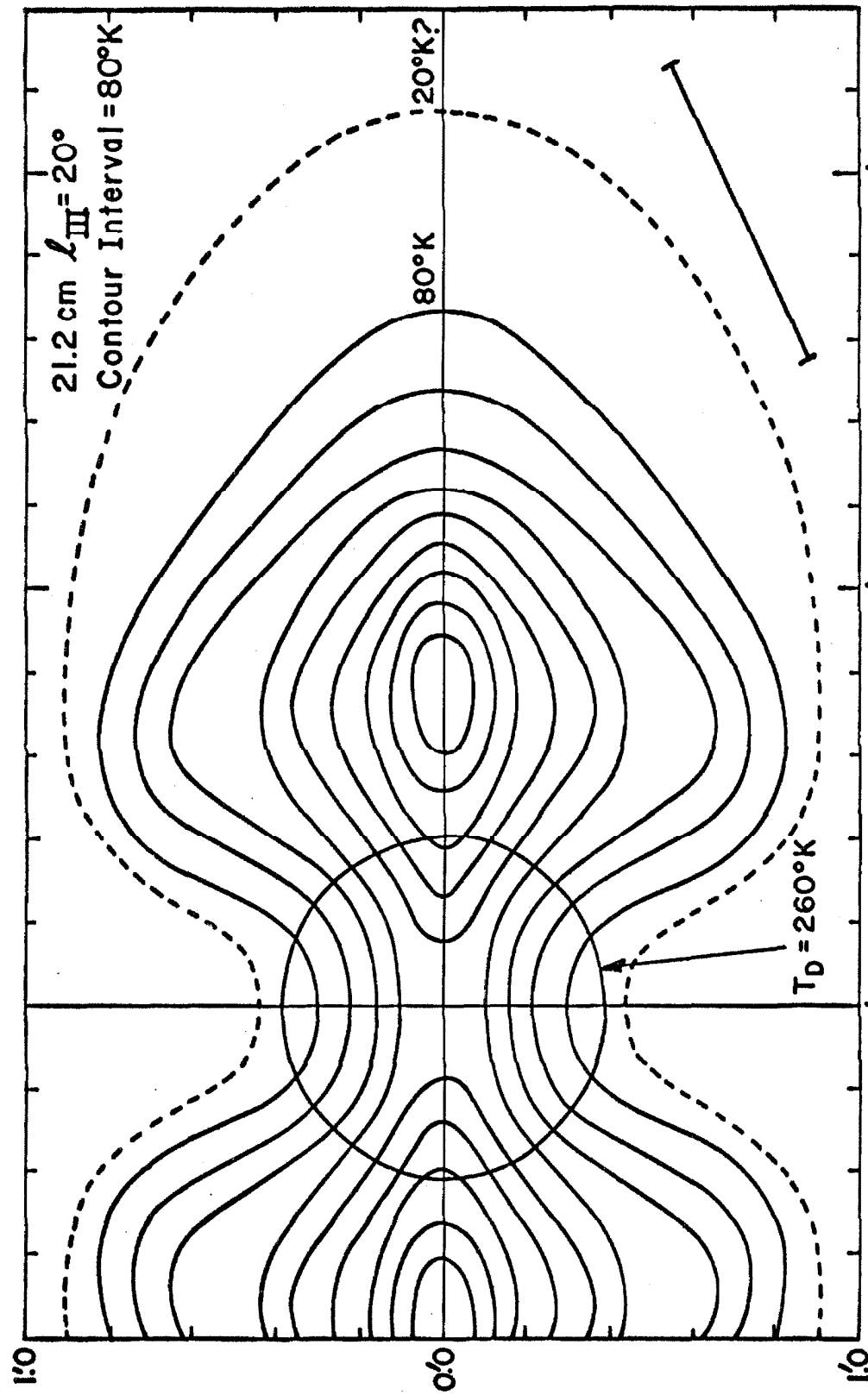

Figure 28. The 21.2 cm. brightness distribution determined for $\ell_{III}=20°$ The scale, in minutes of arc, refers to a distance of 4.04 A.U.

First let us consider the 10.4 cm. visibility functions. With parallel horns in the equatorial direction, the computed visibility amplitudes [curves (b)] are invariably high in the region of 3500 λ. It seems that no reasonable change in the parameters can correct this without producing worse effects elsewhere. This is probably due to an intrinsic flaw in the general model. Because of the assumed gaussian shape of the A regions, it is impossible to fill in enough radiation close to the planet near the equatorial plane. If this could be done, then the disagreement could be corrected. However, it would have only a minor effect on Figure 27.

A similar disagreement between the calculations and the data exists for the visibility amplitudes with parallel horns in the polar direction, but it is only for a couple longitudes, especially $\ell_{III} = 290°$. It is still not clear what causes this. It can be corrected with only minor changes in the model, but the same changes make the fit worse elsewhere.

The curves (c) and, to a lesser extent (d), are often systematically lower than the data points. This does not necessarily mean a disagreement between the model and the observations. According to the appendix, if the signal is low (zero or well below noise), then the data should be systematically high. In such cases

the fringe amplitudes do not give much information, and the signal level must be estimated from the consistency of the phase data.

For the measurements with a polar baseline, curves (a) and (d) are both low at 3200 λ. It seems impossible to correct one without making the other worse. However, the data are incomplete and the errors are large so that it is quite probably the fault of the data. Much of the information about the polar dimensions comes from the east-west measurements. This is possible because the polar axis was 25° away from celestial north.

At 10.4 cm. the phase function calculations agree well with the data, considering the problems involved. One must remember that when the signal is low the phase points will have a large scatter, and moreover, the calculations of the phase functions will be very sensitive to the model and to ℓ_{III}.

At 21.2 cm. the calculated visibility amplitudes agree well with the data except that at $\ell_{III} = 110°$ the second maximum of curve (a) is a bit high. The phase functions show some disagreements, but they are not too serious. At this wavelength the visibility functions for parallel horns have second maxima and thus go through a rapid phase reversal at some baseline. The reason that the calculated phase functions do not, in general,

reverse instantly as the baseline passes the critical point and do not reverse exactly (that is, change by 180°) is because of the circular polarization and the small position difference between the thermal and non-thermal contributions built into the model. At 21.2 cm. the phase functions often go through several rapid changes and the positions and senses of the changes are very sensitive to the model and to ℓ_{III}. Much of the scatter and apparent disagreement can be traced to the fact that each plot contains data from quite a large range of ℓ_{III}.

One very interesting result of the present study is that the disk temperature for the thermal radiation appears to be quite high; in fact, about twice as high as the temperature inferred from infrared measurements and from 3 cm. measurements. This result was obtained as follows: As explained earlier, one expects limb brightening for the emission from Jupiter's radiation belt because it is a shell structure, and moreover, the disk obscures the back part. It is possible to calculate roughly what the limb brightening should be, or at least to set a lower limit for it. If the flux parameters in the model are made to satisfy this condition, then at 10.4 it is impossible to fit the parallel horn measurements if the emission from the disk corresponds to only 130°K.

In particular, at baselines of 2000-2400λ one gets a well defined second maximum with a phase reversal for the calculated transforms and this obviously isn't true. The only way to solve the problem is to put much more radiation in the central region. At 21.2 cm., however, this fitting problem was hardly noticeable, and the conclusion is that the extra central emission has a thermal spectrum. Thus it was identified with the thermal disk emission, making a disk temperature of at least 260°K. (If it is much larger, other fitting problems arise.)

As we have seen, the present investigation has provided a rather detailed two-dimensional brightness distribution for Jupiter's decimeter radio emission, certainly much more detailed than what was previously available. This is because both the sensitivity and the range of baselines was much larger than in previous work. Something should also be said about the accuracy of the model. If any of the assumptions made for the generalized model were seriously violated, it should have shown up as a serious fitting problem. The distribution of the emission among the various regions and the overall dimensions are probably quite accurate. However, the smaller details are not as accurately determined. The available resolution is indicated by the brackets shown

in Figures 27 and 28. They represent the separation of a double source, in the direction of the baseline orientations used, whose visibility function would be at its first null at the largest baseline used. The resolution at 21.2 cm. is obviously much lower than at 10.4 cm. At 21.2 cm. the finer details were provided by using the same dimension parameters as at 10.4 cm.

The model found here can be easily tested with future observations. The last half of the calculated visibility functions for 21.2 cm. in Figures 18 to 25 are really predictions of what should be observed at longer baselines with the source and the baseline in the same relative orientation as in the present study. For other examples, see Figures 29 and 30. The first is a prediction of the visibility amplitude function with the baseline perpendicular to the magnetic axis of the source, and the other is for the baseline at 30° to the magnetic axis of the source.

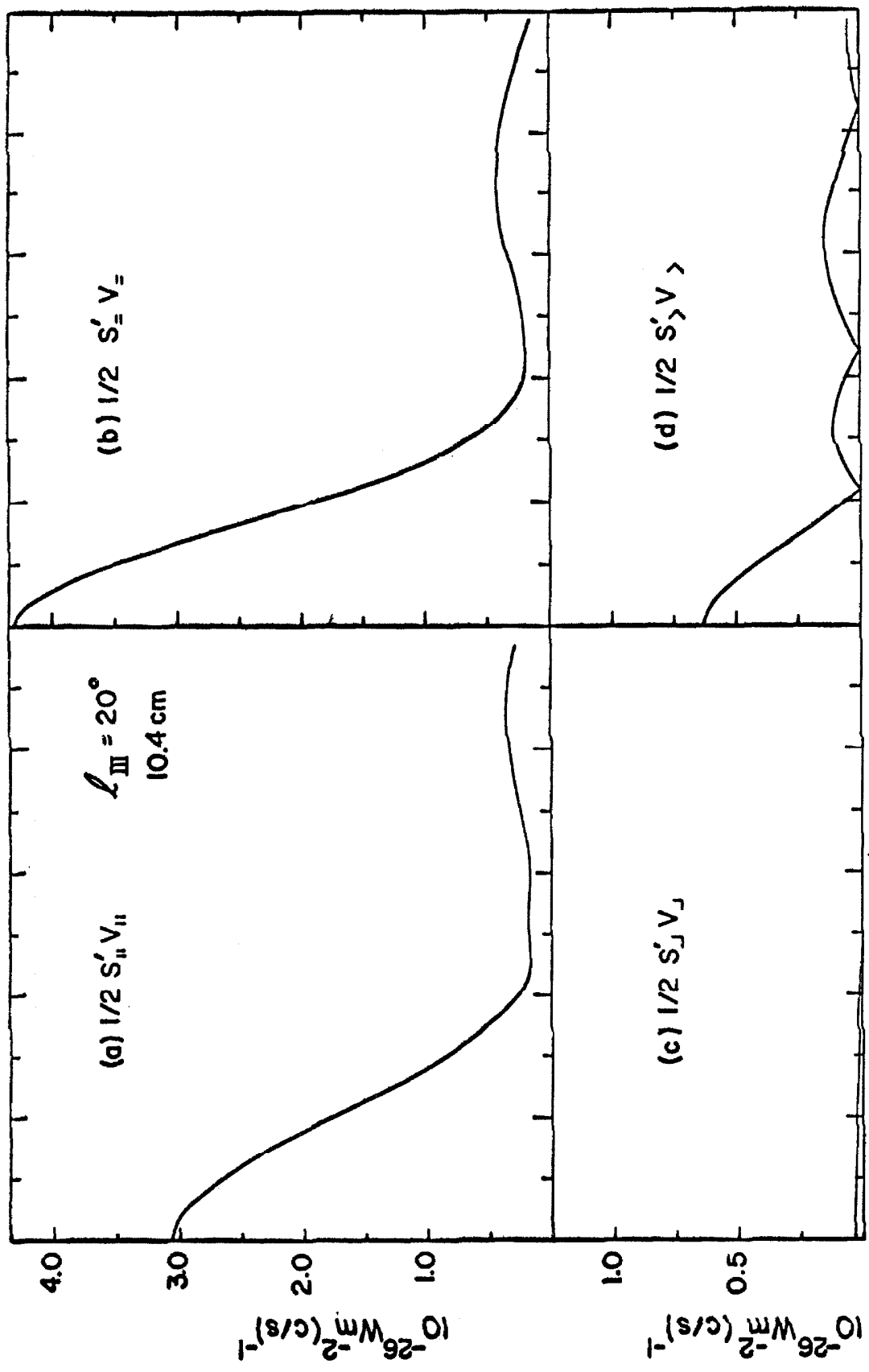

Fig. 29. The predicted 10 cm. visibility amplitude functions for $\ell_{III}=20°$ with the baseline in the equatorial direction.

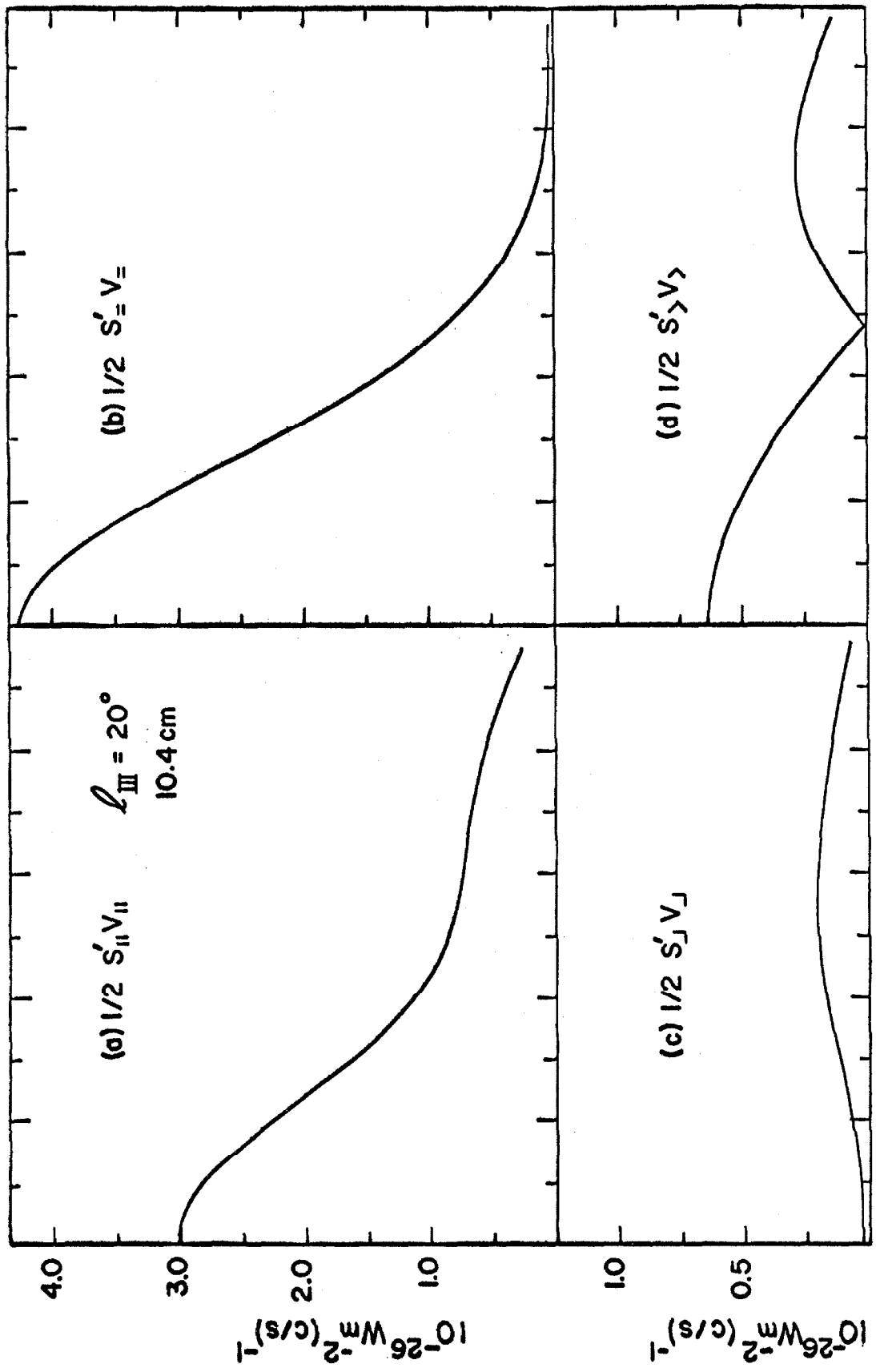

Fig. 30. The predicted 10 cm. visibility amplitude functions for $\ell_{III}=20^{\circ}$ with the baseline 30° from the magnetic axis direction.

VII DISCUSSION

A. Single Dish and Short Baseline Observations

It was pointed out earlier that several observers have studied Jupiter's integrated radiation and have discussed the subject at some length. In particular Roberts and Komesaroff (9), whose measurements were very accurate, have thoroughly considered the implications of their results. The present short baseline observations do not permit much additional speculation, but perhaps some of the important points should be reviewed and expanded a bit.

Davis and Chang (55) pointed out that if Jupiter's decimeter emission is the result of synchrotron radiation in a dipole field, then the electrons must be confined mainly to flat helices near the equatorial plane in order to explain the high degree of linear polarization in the direction of the equatorial plane. Roberts and Komesaroff (9) have found an even more severe restriction on the electron pitch angle distribution. It is imposed by the beaming properties of the radiation. By taking observations at 11 and 21 cm., of the sort shown in Figures 2b and 2c, and fitting them with calculations made by Thorne (61), which give the flux density and percentage polarization as a function of the magnetic

latitude of the earth, they find that the equatorial pitch angle distribution goes as

$$0.8 \sin^2 \alpha_E + \sin^{18} \alpha_E \quad .$$

The second term is to provide sufficiently sharp beaming in the equatorial plane, and the first term is to keep the percentage polarization from being too high. At longer wavelengths the beaming is not so sharp.

Another point they make is that the observed spectrum, which is very flat, suggests a power law spectrum for the electrons of the form

$$N(E)dE = kE^{-1}dE \qquad \text{between cutoffs.}$$

This is implied by the well-known fact that, in a synchrotron emission source, an electron spectrum of the form $N(E)dE = kE^{\gamma}dE$ yields an emission spectrum of the form ν^{α} where $\gamma = 2\alpha - 1$ and ν is between the critical frequencies for the cutoff energies.

The asymmetry found by Roberts and Komesaroff (9), (43) in the curve giving direction of polarization vs. l_{III} (corresponding to Figures 2a and 3a) is still a mystery. They suggested an asymmetry in the magnetic field to explain it. The present investigation showed that the brightness distribution of the radiation is quite symmetric, but perhaps only a small asymmetry is

needed to explain the effect. Warwick (69) proposed that it is due to shading by the planet. This would require that the centroid of the radio emission be displaced well away from the center of the planet, and it now appears that the displacement is quite small. Roberts and Komesaroff (9) pointed out that, according to theoretical models, the shading is small (less than 6 percent), but for a realistic thick-shell model the shading should be more. The geometrical models of the last chapter indicate more than 6 percent, but in view of the small displacement, the explanation of Warwick is still in difficulty.

The asymmetry of the curve was found to be less pronounced at 11 cm. than at 21 cm. and this suggests some wavelength dependent mechanism such as Faraday rotation of the plane of polarization. For example, if there is Faraday rotation within the source then the plane of polarization of radiation near the equator at the rear of the source could undergo a rotation which varied and changed sense as the magnetic axis rocked to and fro. However, for a small rotation in a dipole field it would simply add a small sine term 90° out of phase with the expected sine dependence on l_{III}. This would change the curve but would not produce an asymmetry unless there is an asymmetry of the field.

Also, the electron density required to produce the rotation is quite large. (For a one gauss field the electron density must be about 10^4 cm.$^{-3}$ to produce a 10° rotation when the tilt toward the earth is maximum.)

B. Circular Polarization

Field (77) and Roberts and Komesaroff (9) have both pointed out that the detection of circular polarization in a synchrotron emission source can, in principle, pin down the magnetic field strength and electron energy as well as the field direction. The latter point was discussed in connection with the circular polarization results of Chapter IV. The conclusion was that the polarity of Jupiter's magnetic field is opposite that of the earth's. It is of great interest to attempt some determination of the field strength and electron energy as well.

Chang (59) and Chang and Davis (60) have made some calculations of relevant quantities in Jupiter's radiation belt using an average field strength, an electron energy spectrum with a minus one exponent as given above between cutoffs having critical frequencies of 100 and 10,000 Mc/s. They assumed a source volume ten times that of Jupiter and a total radiated power of 2.8×10^{16} ergs/sec. By several indirect arguments they find that the field strength is probably of the order of

1 gauss. Then the cutoff energies are 25 and 2.5 Mev.

Unfortunately no one has made accurate calculations for the circular polarization from an assembly of electrons having some given energy and pitch angle distributions. Roberts and Komesaroff (9) carried out an approximate analysis for single energy electrons. They assumed that, although the pitch angle distribution was variable over the width of the emission cone, it would not vary by much. This assumption may be a bit too severe, but the result should still be useful. They find

$$\text{Degree of Circ. Pol.} = \frac{V}{I} = 0.61 \frac{N'(\theta)}{N(\theta)} \xi \qquad (7\text{-}1)$$

where ξ measures the width of the beaming cone, θ is the angle between the observation direction and the field direction, and $N(\theta)$ is the electron pitch angle distribution evaluated at $\alpha = \theta$. (This is different from the equatorial pitch angle distribution mentioned earlier.) Thus the degree of circular polarization depends on the emission cone size relative to the scale of variation of the pitch angle distribution, and gives a condition on the electron energy because $\xi = Mc^2/E$.

If the observation frequency is at the frequency of maximum emission for the electrons ($\nu = \nu_c/3$) and if we use the relation between the critical frequency,

field strength, and electron energy, we get

$$\text{Degree of Circ. Pol.} = 0.72 \frac{N'(\theta)}{N(\theta)} \left(\frac{B_o \sin\theta}{\nu} \right)^{\frac{1}{2}} \quad (7\text{-}2)$$

where B_o is in gauss and ν is in Mc/s. If there is some distribution of electron energies then the bulk of the circular polarization may come from energies slightly different from that used above and this would change the numerical factor.

Trapped electrons spend most of their time near their mirror points, and, as Chang and Davis (60) point out, most of the emission comes from electrons near their mirror points. Thus we expect a rather sharp distribution of pitch angles centered on 90°. It should be more sharply peaked at 90° than the distribution function for equatorial pitch angles because an electron's equatorial pitch angle is the smallest pitch angle it will have. It spends most of its time with its pitch angle closer to 90°. The distribution should be symmetric about 90° because the number of electrons approaching their mirror points equals the number being reflected. Hence,

$$N'(90°)/N(90°) = 0$$

as Roberts and Komesaroff (9) imply. However, when θ

goes slightly to one side or the other of 90° it reaches the steep part of the $N(\alpha)$ vs. α curve and $N'(\theta)/N(\theta)$ is large in magnitude. This seems to have been overlooked by Roberts and Komesaroff, who concluded that for Jupiter one might not expect much circular polarization. For the equatorial pitch angle distribution given previously, the first derivative divided by the function is about 2 for $\alpha_E = 80°$ or $100°$. For the general pitch angle distribution, which is more sharply peaked around 90° the value is probably larger, say $N'(\theta)/N(\theta) \approx 4$ at $\theta = 80°$ or $100°$.

According to the results of Chapter IV, the circular polarization seems to come mainly from each side of the planet near the equatorial plane. In these regions the magnetic field is parallel to the magnetic axis so the angle θ for this case is 90° plus the magnetic latitude of the earth. When the earth is at the magnetic equator, $\theta = 90°$ and $N'(\theta)/N(\theta) = 0$ so there should be no circular polarization. This agrees roughly with the result. When the magnetic axis is tilted toward or away from us (for the present observations that would be $\theta = 102°$ or $82°$) then $N'(\theta)/N(\theta)$ is large and has opposite signs for the two cases, and the degree of circular polarization is large and has opposite senses for the two cases. This agrees with

the observational result as well. This qualitative result would be expected without the preceding analysis, but hopefully we can get some quantitative information as well.

The maximum degree of circular polarization obtained from the small baseline observations at 10.4 and 21.2 cm. gives the correct frequency dependence as shown by equation (7-2), but in view of the errors, this may be accidental. In fact, if the thermal component had been subtracted out so that the degree of circular polarization referred only to a fraction of the non-thermal component, then the frequency dependence wouldn't be as correct.

For estimating the electron energies and field strength, let's use $N'(102°)/N(102°) \approx 5$. For 21.2 cm. the degree of circular polarization for the whole source is 0.045 at $\theta = 102°$, but for just that part of the source which yields the circular polarization it might be 0.100. Then using equations (7-1) and (7-2) we find an electron energy of 15 Mev and a magnetic field strength of 1.1 Gauss. There are rather large uncertainties involved, but we see that the results agree roughly with those of Chang and Davis (60).

It is not difficult to see why the brightness distribution of the circularly polarized component appears

as it does. There should not be much coming from the polar regions because the front half tends to cancel the back half. Thus it comes mainly from the equatorial regions. It is double partly for the same reason that the rest of the radiation belt emission is double. There is no radiation from the volume occupied by the planet and the planet obscures the back side. Moreover, in the front center, the magnetic lines of force are curved so they do not tilt in the same way as the lines of force at the sides when the magnetic axis rocks to and fro. The result is that θ varies along the lines of force and does so in such a way as to reduce the circular polarization.

C. The Brightness Distribution

Figure 27 looks vaguely like a plot of electron fluxes in the earth's Van Allen belt. Of course it must be remembered that the figure represents a completely different thing. It shows the synchrotron radiation from the electrons as projected on the plane of the sky. Mixed into it are the beaming properties of the emission from each electron, the dependence of emission rate on field strength, and the electron energy, density, and pitch angle distributions as a function of position in the source.

The interferometric work of Radhakrishnan and Roberts (10) with a baseline in the equatorial direction showed that the response with crossed horns (one 45° on each side of the equatorial direction) was resolved sooner than that for parallel horns. The same effect was found in the present investigation. Chang (59) and Chang and Davis (60) suggested that to explain this one could have the proportion of electrons with steep helices increase as one gets closer to the planet. Figures 27 and 28 seem to show the opposite effect, if anything, because the polar emission must arise from far-out electrons with steep helices at the equator. The observational effect is obtained because the polar emission, which is quite close to the axis and doesn't become resolved as quickly as the equatorial emission, has the opposite plane of polarization.

The value found for the parameter p_o might, in principle, yield some useful information about the source. However, there are some difficulties. The accuracy of the determination is not too great and the value found ($p_o = 0.7$) may easily be off by 0.05. Also, p_o does not really represent the degree of linear polarization in a small element of area because the model was formed by superposing several overlapping regions, each with different planes of polarization. Therefore, the degree

of linear polarization in each area element of the model is somewhat less than p_o.

Eventually a physical model should be fitted to the results of this investigation; that is, a model which includes the physical parameters describing the electrons and the magnetic field in the source. A great deal has been found out about these parameters, but it would be very interesting to have a physical model which would duplicate the behavior of the source as it has been observed. The models of Chang (59) and Chang and Davis (60), while providing a great deal of insight into the problem, now seem inadequate for determining a sufficiently detailed model. By superposing their models having the correct electron energy distribution but different pitch angles, one could perhaps obtain a thin-shell model with the proper pitch angle distribution and then superpose such models with different sizes to obtain a thick shell model. Choosing the correct combinations would be a matter of trial and error. However, this might be too crude, and there are other problems as well. In any case, for the purposes of this thesis, only a geometrical model for the brightness distribution has been determined.

D. ' The Disk Radiation

The large disk emission found by the present brightness distribution work was an unexpected result, and it would be nice if it could be accounted for. As a matter of fact, an explanation may already exist. Field (52) tried several ways to explain Jupiter's enhanced radiation toward longer wavelengths, and one was to suppose that the opacity in Jupiter's atmosphere was decreasing toward longer wavelengths and that the temperature in the atmosphere increased toward greater depths. Then one would see to lower, hotter depths with increasing wavelength. He used an atmospheric model of Kuiper (80) and assumed that all the opacity in this wavelength region was due to ammonia. His result was not successful in explaining most of the enhanced radiation (which is now explained by synchrotron emission), but it might explain the extra disk emission found by the present investigation.

Another possible explanation is that the extra radiation from the disk is due to free-free emission in a Jovian ionosphere. However, in order to get the observed thermal spectrum for this extra radiation, one requires an ionosphere which is optically thick at these wavelengths and has an electron temperature of only 260°K. This seems unlikely. If the ionosphere is optically

thin then the spectrum would be flat and there would be limb brightening. This sort of ionosphere would not satisfy the necessary conditions for the extra radiation.

E. Relation to Decameter Results

The most direct relation between the decimeter and decameter emission has been the rotation period. The System III period, found from the repetition of the decameter burst pattern as Jupiter rotates, was based on observations made before 1961. As explained in Chapter III, the decimeter period (obtained from the rocking of the plane of polarization) found at Caltech during the period July, 1961, to February, 1964, and by Roberts and Komesaroff (9) during the period August, 1962 to August, 1963, agrees with the System III period to within $\pm 0^{s}.5$. The odd thing is that, beginning in 1960, the decameter period began to increase by about 1^{s} per year according to Douglas and H. J. Smith (81) and A. G. Smith, et al (82). Thus it appears that the decameter and decimeter periods no longer agree very well, although this should be checked by newer decimeter observations. Presumably the decimeter period is more closely related to the rotation period of the magnetic field, and the change in the decameter period, if real, is caused by something other than the magnetic field.

One theory for explaining the origin and

nature of the decameter activity is that of Warwick (83), which requires that the magnetic dipole be displaced well away from the planet's center. Another is that of Ellis and McCulloch (84), which requires a local anomaly in a centered dipole field. The results of the present investigation show no indication that such conditions exist. However, they do not rule out the possibility of some small asymmetry in the field. Indeed, the observations of Roberts and Komesaroff (9), (43) of the plane of polarization vs. ℓ_{III} indicate some asymmetric effect at work.

An interesting new development in regard to the decameter emission is the discovery that the time at which bursts are likely to occur is strongly correlated, not only with ℓ_{III}, but also with the position of the satellite Io; the probability being much higher when Io is to one side or the other of Jupiter. The discovery by Bigg (85) has been confirmed by Dulk (86). According to Bigg (87), Io may also have some effect on the decimeter emission. Io's orbit, lying in Jupiter's equatorial plane and having a radius of 6 Jovian radii, probably puts Io in the outer parts of the radiation belt. The data from the present investigation were not carefully checked for such an effect. The main problem was that at none of the antenna spacings used did the

observations cover more than one revolution of Io about Jupiter. Dickel (88) has reported a lack of any effect by Io at 3.75 cm.

F. Future Observations

If nothing else, the present study had indicated what future observations would be most interesting and useful. There are certain routine observations which will continue to be of interest such as additional checks of the decimeter rotation period and additional checks for long-term changes in the flux density or percentage of linear polarization. However, let us consider only those things which are especially suited for an interferometer; in particular, the one in the Owens Valley.

The brightness distribution models found in the present study should not be considered final, and additional observations should be made to check and refine them. The project with perhaps the greatest priority is the extension of the 10 cm. observations with north-south or diagonal antenna spacings giving a baseline oriented in the polar direction of the source. The only observations of this type in the present study were for baselines between 3000 and 4000 λ . In addition to this range, observations should be made at some smaller baselines and, especially, at somewhat longer baselines. The latter can be achieved

with the present instrument by observing when Jupiter is at a higher declination and also by making the observations when Jupiter is closer, that is, near opposition. (Observing near opposition would also give a much better signal-to-noise ratio than was available for the polar measurements in the present study.) For example, for the opposition of December, 1965, Jupiter's declination will be $+23^{\circ}$. There is not much point in making 21 cm. observations with this baseline orientation because the available baseline is not large enough.

Additional observations with east-west spacings will be of interest mainly when Jupiter's orientation in the sky and/or the baseline rotation bring the two into a greatly different relative orientation than in the present study. In planning future observations it should be remembered that at 10 cm. the fringe amplitudes for Jupiter were comparable to or less than noise at the largest baselines. That is, the measurements were noise limited. At the largest 21 cm. baseline the fringe amplitudes were often quite large and in that case shouldn't be severely limited by noise nor confusion, both of which are about equally important at this wavelength.

It will be useful to continue making measure-

ments of the circular polarization and to try to take out any possible instrumental effects. It may prove helpful to make the feed horn position angles follow the plane of polarization as it rocks back and forth.

It would also be useful to include Jupiter in the regular position measurement runs made with the interferometer. The accuracy in measuring absolute positions has reached the point where a rather small position difference between the radio source and the optical disk could be detected. Occultations of Jupiter by the moon are potentially of great value and should not be neglected. However there are no promising ones for the Owens Valley in the near future.

These suggestions are made in reference to the existing instrument at the Owens Valley Observatory. The future promises to bring lower noise receivers, higher frequency operation, better stability, longer baselines, and more collecting area. All of these will, of course, greatly increase the capability for studying Jupiter's radio emission.

APPENDIX

From the sine and cosine channels of the integrator one can determine the amplitude and relative phase of the interferometer fringes during the integration. The system noise produces a degree of uncertainty in the result. In addition, the noise produces a systematic error in the amplitude when this integration method is used. We will now examine this error and the uncertinty produced by the noise.

Several integration runs were made without a signal in order to measure the magnitude of the noise and to determine its behavior. It seems to be well behaved in that it exhibits a random phase and that the integral increases as the square root of the integration time. Thus the integral per unit time decreases as the square root of the observing time. It is probably valid to consider the noise in each channel as being normally distributed about the signal value for that channel with a standard deviation which can be determined by the noise measurements made and which goes as the square root of the observing time.

Let s be the reading of the sine channel for some given integration time, c the cosine reading, r the computed amplitude ($r = \sqrt{s^2+c^2}$),

and Φ the computed phase. Let s_o, c_o, r_o, and Φ_o be the corresponding quantities which would have been obtained if there were no noise. s and c are distributed as

$$P(s) = \frac{1}{\sqrt{2\pi}\sigma} e^{-s^2/2\sigma^2} , \quad P(c) = \frac{1}{\sqrt{2\pi}\sigma} e^{-c^2/2\sigma^2} .$$

The standard deviation is the same for each because the two channels are identical except for phase. It is clear that the vector result, $\underline{r} = re^{i\Phi}$, will have a circular gaussian distribution on the sc-plane. However, r will have the distribution

$$P(r) = \frac{r}{\sigma^2} e^{-r^2/2\sigma^2}$$

in the absence of a signal. This is often called the Rayleigh distribution. If there is a signal r_o then the form will be

$$P_1(r) = \frac{r}{\sigma^2} e^{-(r^2+r_o^2)/2\sigma^2} I_o(rr_o/\sigma^2)$$

where $I_o(x)$ is the Bessel function of zero order and purely imaginary argument. [See, for example, Lawson and Uhlenbeck (89).]

The expectation value (or mean) of the measured amplitude can be found for a given signal r_o.

$$\overline{r} = \int_o^\infty r P_1(r) dr$$

This can be integrated using the standard form

$$\int_0^\infty t^{\mu-1} e^{-p^2 t^2} I_\nu(at)\, dt = \frac{\Gamma\left(\frac{\mu+\nu}{2}\right)\left(\frac{a}{2p}\right)^\nu}{2p^\mu \Gamma(\nu+1)} e^{\frac{a^2}{4p^2}} \cdot {}_1F_1\left(\frac{\nu-\mu}{2}+1, \nu+1; -\frac{a^2}{4p^2}\right)$$

where ${}_1F_1(a,b;z)$ is the confluent hypergeometric function. We find

$$\bar{r} = \sigma\sqrt{\frac{\pi}{2}}\ {}_1F_1\left(-\tfrac{1}{2}, 1; -\frac{r_o^2}{2\sigma^2}\right)$$

This is shown in Figure 31a. We see that for r_o comparable to or smaller than σ, the integrator gives a result which is systematically large. Moreover, for $r_o \lesssim \sigma$, the mean value of the integrated amplitude is fairly constant and therefore does not contain much information about the true amplitude. However, for such low signals, the measured phase (which will have a large random error, but no corresponding systematic error) still provides valuable information about the signal.

The preceding discussion gives us information about the measured amplitude if we know the true amplitude, but our problem is the reverse of this. Let A be the event that the true value is in a certain element dr_A, B the event that it is in another element dr_B, and E the event of a certain experimental result dr. We have seen that the probability of E given A is

$$P(E|A) = P_1(r)dr = (r/\sigma^2)e^{-(r^2+r_o^2)/2\sigma^2} I_o(rr_o/\sigma^2)dr \quad .$$

According to Bayes' Theorem

$$\frac{P(A|E)}{P(B|E)} = \frac{P(A)}{P(B)} \frac{P(E|A)}{P(E|B)} \quad .$$

If we are to be completely objective, then we have no a priori knowledge about the true value so that $P(A) = P(B)$. Thus

$$P(A|E) = P_2(r_o)dr_o = KP(E|A)$$

where K is a normalization factor determined by

$$1 = K\int_o^\infty P(E|A)dr_o = K\int_o^\infty (r/\sigma^2)e^{-(r^2+r_o^2)/2\sigma^2} I_o(rr_o/\sigma^2)dr_o .$$

This can be integrated by using the standard form. The result is

$$K = \frac{\sigma}{r}\sqrt{\frac{2}{\pi}} \left[{}_1F_1(\tfrac{1}{2},1;-r^2/2\sigma^2)\right]^{-1} \quad .$$

Our answer then is that for the distribution of r_o we have

$$P_2(r_o) = \frac{1}{\sigma}\sqrt{\frac{2}{\pi}}\left[{}_1F_1(\tfrac{1}{2},1;-r^2/2\sigma^2)\right]^{-1} e^{-(r^2+r_o^2)/2\sigma^2} I_o(rr_o/\sigma^2)$$

The final step is to find the expectation value of r_o.

$$\bar{r}_o = \int_o^\infty r_o P_2(r_o) dr_o \quad .$$

We can use the same standard form as before to obtain

$$\bar{r}_o = \sigma\sqrt{\frac{2}{\pi}} \left[{}_1F_1(\tfrac{1}{2},1;-r^2/2\sigma^2) \right]^{-1} {}_1F_1(0,1;-r^2/2\sigma^2) \quad .$$

Then, since ${}_1F_1(0,1;-r^2/2\sigma^2) \equiv 1$ we have

$$\bar{r}_o = \sigma\sqrt{\frac{2}{\pi}} \left[{}_1F_1(\tfrac{1}{2},1;-r^2/2\sigma^2) \right]^{-1} = Kr$$

This is plotted in Figure 31b. When $\frac{r}{\sigma} >> 1$, $\bar{r}_o \longrightarrow r$, but when r and σ are of comparable size the expectation value of the true result can differ significantly from the measured value.

Let us now examine briefly the uncertainty in $\bar{r}_o$ by considering the standard deviation σ_o of r_o.

$$\sigma_o^2 = \int_o^\infty (r_o - \bar{r}_o)^2 P_2(r_o) dr_o$$

$$= \int_o^\infty r_o^2 P_2(r_o) dr_o - \bar{r}_o^2$$

By using our previous integration formula we have

$$\sigma_o = \left\{ \bar{r}_o \sigma \left[\sqrt{\frac{\pi}{2}}\, {}_1F_1(-\tfrac{1}{2}, 1; -r^2/2\sigma^2) - \bar{r}_o/\sigma \right] \right\}^{\frac{1}{2}}$$

This is shown by the dashed line in Figure 31b. When r is small it is not quite right to use σ_o to determine an error bracket about $\bar{r}_o$ because the error distribution about $\bar{r}_o$ is very asymmetric. However, σ_o does provide a feeling for the size of the uncertainty.

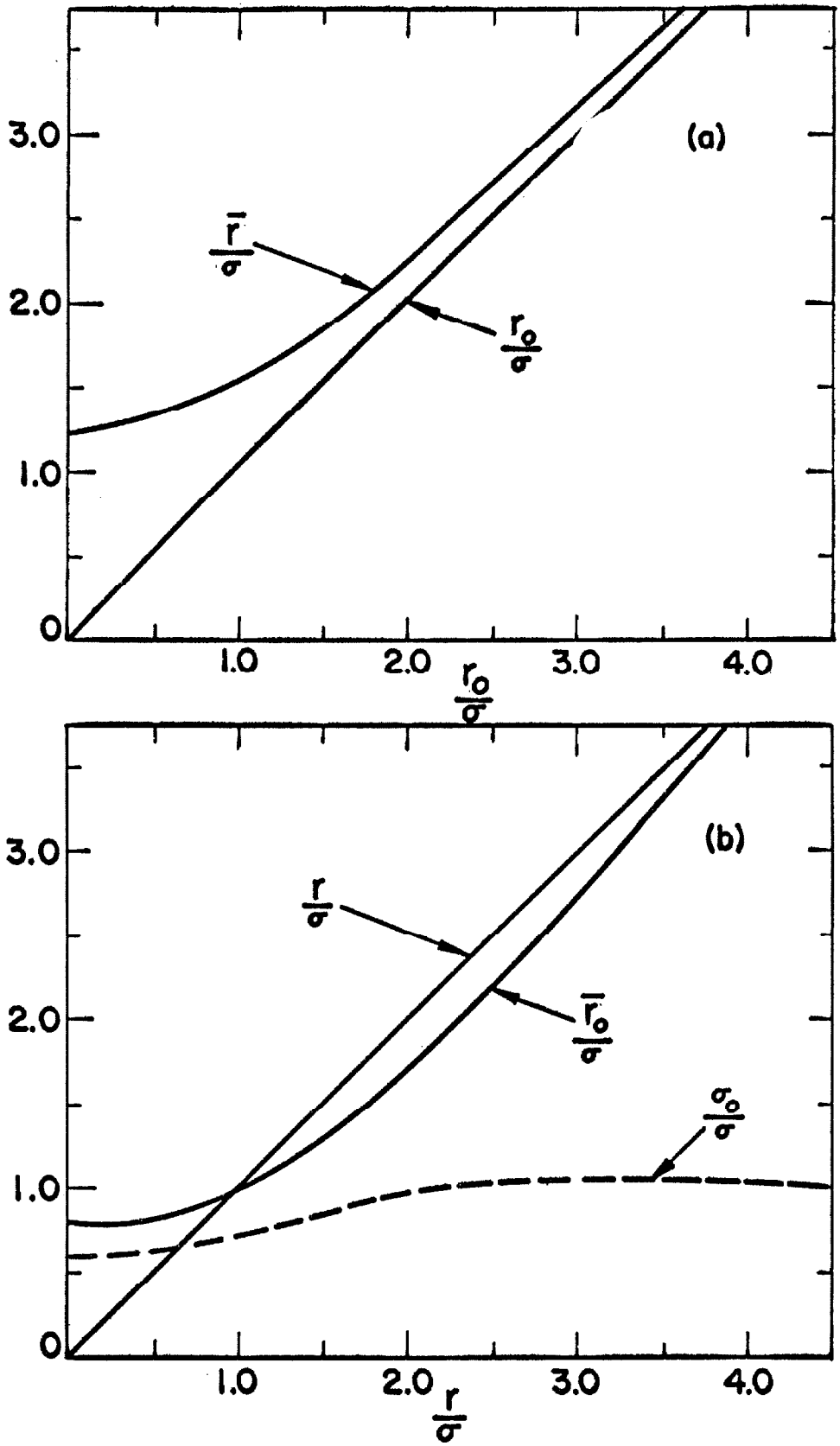

Fig. 31. a) The expected measured amplitude for a given true amplitude. b) The expected true amplitude and standard deviation for a given measured amplitude.

REFERENCES

1. D. H. Menzel, W. W. Coblentz, and C. O. Lampland, Ap. J., 63, 177, 1926.

2. B. F. Burke and K. L. Franklin, Jour. Geophys. Res., 60, 213, 1955.

3. C. H. Mayer, T. P. McCullough, and R. M. Sloanaker, Ap. J., 127, 11, 1958.

4. C. H. Mayer, T. P. McCullough, and R. M. Sloanaker, Proc. IRE, 46, 260, 1958.

5. E. F. McClain and R. M. Sloanaker, Proc. IAU Symp. No. 9 - URSI Symp. No. 1, ed. R. N. Bracewell (Stanford: Stanford University Press), p. 61, 1959.

6. R. M. Sloanaker, A. J., 64, 346, 1959.

7. G. L. Berge and D. Morris, Ap. J., 140, 1330, 1964.

8. G. L. Berge, A.J., 70, 132, 1965.

9. J. A. Roberts and M. M. Komesaroff, submitted to Icarus, December, 1964.

10. V. Radhakrishnan and J. A. Roberts, Phys. Rev. Letters, 4, 493, 1960.

11. D. Morris and G. L. Berge, Ap. J., 136, 276, 1962.

12. F. J. Kerr, Sky and Telescope, 24, 254, 1962.

13. C. H. Mayer, A. J. 64, 43, 1959.

14. F. D. Drake and H. I. Ewen, Proc. IRE, 46, 53, 1958.

15. B. Y. Mills, A. G. Little, K. V. Sheridan, and O. B. Slee, Proc. IRE, 46, 67, 1958.

16. L. E. Alsop, J. A. Giordmaine, C. H. Mayer, and C. H. Townes, Proc. IAU Symp. No. 9 - URSI Symp. No. 1, ed. R. N. Bracewell (Stanford: Stanford University Press), p. 69, 1959.

17. J.A. Giordmaine, L. E. Alsop, C. H. Mayer, and C. H. Townes, Proc. IRE, 47, 1062, 1959.

18. J. A. Giordmaine, L. E. Alsop, C. H. Townes, and C. H. Mayer, A. J., 64, 332, 1959.

19. J. A. Giordmaine, Proc. Nat. Acad. Sci., 46, 267, 1960.

20. R. M. Sloanaker and J. W. Boland, presented at XIIIth General Assembly, URSI, September 1960.

21. R. M. Sloanaker and J. W. Boland, Ap. J., 133, 649, 1961.

22. J. A. Roberts and G. J. Stanley, PASP, 71, 485, 1959.

23. E. F. McClain, A. J. 64, 339, 1959.

24. E. F. McClain, J. H. Nichols, and J. A. Waak, presented at the XIIIth General Assembly, URSI, September 1960.

25. E. F. McClain, J. H. Nichols, and J. A. Waak, A. J., 67, 724, 1962.

26. E. Epstein, Nature, 184, 52, 1959.

27. F. D. Drake, presented informally at URSI meeting, May, 1959.

28. F. D. Drake and H. Hvatum, A. J., 64, 329, 1959.

29. F. D. Drake and H. Hvatum, presented at XIIIth General Assembly, URSI, September, 1960.

30. R. J. Long and B. Elsmore, The Observatory, 80, 112, 1960.

31. D. Morris and G. L. Berge, Proc. XIIth International Astronautical Congress, ed. R. M. L. Baker, Jr. and M. W. Makemson (Academic Press, New York) p. 681, 1963.

32. M. S. Roberts, A. J., 67, 280, 1962.

33. M. S. Roberts, IRE Trans., Antennas and Propagation, AP-10, 494, 1962.

34. M. S. Roberts and G. R. Huguenin, La Physique des Planetes, 11th Colloque International d'Astrophysique, Liege. Mem. Soc. Roy. Sci., Liege, 7, 569, 1962.

35. F. N. Bash, F. D. Drake, E. Gundermann, and C. E. Heiles, Ap. J. 139, 975.

36. A. C. Miller and B. L. Gary, presented at Washington meeting of URSI, 1962.

37. A. C. Miller and B. L. Gary, A. J., 67, 727, 1962.

38. A. C. Miller and B. L. Gary, presented at XIVth General Assembly URSI, September, 1963.

39. A. Boischot, M. Ginat, and I. Kazes, C. R. Acad. Sc., 254, 2527, 1962.

40. A. Boischot, M. Ginat, and I. Kazes, Ann. d'Astro., 26, 385, 1963.

41. D. Morris and J. F. Bartlett, La Physique des Planetes, 11th Colloque International d'Astrophysique, Liege, Mem. Soc. Roy. Sci., Liege, 7, 564, 1962.

42. J. G. Bolton, Proc. IRE Aust. 24, 106, 1963.

43. J. A. Roberts and M. M. Komesaroff, Nature, 203, 827, 1964.

44. W. K. Rose, J. M. Bologna, and R. M. Sloanaker, A. J., 68, 78, 1963.

45. W. K. Rose, J. M. Bologna, and R. M. Sloanaker, presented at XIVth General Assembly URSI, September, 1963.

46. D. V. Korolkov, Yu N. Parijsky, and G. M. Timofeeva, Astronomical Circular of the Astronomical Council, USSR Academy of Sciences, No. 283, 1964.

47. Yu N. Parijsky, Astronomical Circular of the Astronomical Council, USSR Academy of Sciences, No. 285, 1964.

48. B. L. Gary, A. J., 68, 568, 1963.

49. B. L. Gary, presented at XIVth General Assembly URSI, September, 1963.

50. F. T. Haddock and J. R. Dickel, presented at Third Western National Meeting AGU, 1963. Trans. AGU, 44, 886, 1963.

51. J. F. R. Gower, Nature, 199, 1273, 1963.

52. G. B. Field, Jour. Geophys. Res., 64, 1169, 1959.

53. G. B. Field, Jour. Geophys. Res., 65, 1661, 1960.

54. G. B. Field, Jour. Geophys. Res., 66, 1395, 1961.

55. L. Davis, Jr. and D. B. Chang, Jour. Geophys. Res., 66, 2524, 1961.

56. L. Davis, Jr. and D. B. Chang, Jour. Geophys. Res., 67, 1634, 1962.

57. L. Davis, Jr. and D. B. Chang, Jour. Geophys. Res., 67, 2169, 1962.

58. D. B. Chang, Boeing Scientific Laboratories Document D1-82-0060, 1960.

59. D. B. Chang, Ph. D. Thesis, Calif. Institute of Technology, 1962. Reprinted as Boeing Scientific Document D1-82-0129, 1962.

60. D. B. Chang and L. Davis, Jr., Ap. J., 136, 567, 1962.

61. K. S. Thorne, Ap. J. Supp. 8, 1, 1963.

62. A. A. Korchak, Geomag. and Aeronom., 3, 394, 1963; also Soviet Astronomy (A.J.), 7, 764, 1964.

63. C. H. Mayer, The Solar System: ed. G. P. Kuiper and B. M. Middlehurst, U. of Chicago Press, p. 442, 1961.

64. C. H. Mayer, La Physique des Planetes, 11th Colloque International d' Astrophysique, Liege. Mem. Soc. Roy. Sci., Liege, 7, 99, 1962.

65. F. D. Drake, Physics Today, 14, No. 4, 30, 1961.

66. J. A. Roberts, Planetary and Space Science, 2, 221, 1963.

67. R. Wildt, H. J. Smith, E. E. Salpeter, and A. G. W. Cameron, Physics Today, 16, No. 5, 19, 1963.

68. A. G. Smith and T. D. Carr., Radio Exploration of the Planetary System, Van Nostrand, Princeton, N.J., 1964.

69. J. W. Warwick, Annual Reviews of Astronomy and Astrophysics, ed. L. Goldberg, 2, 1, 1964.

70. B. G. Clark and A. D. Kuz'min, Obs. of the Owens Valley Radio Obs. No. 1, 1965 (Submitted to Ap. J.).

71. B. Anderson, W. Donaldson, H. P. Palmer, B. Rowson, Nature, 205, 375, 1965.

72. K. I. Kellermann, A. J. 69, 205, 1964.

73. A. T. Moffet, Ap. J. Supp., 7, 93, 1962.

74. D. Morris, V. Radhakrishnan, and G. A. Seielstad, Ap. J., 139, 551, 1964.

75. S. Chandrasekhar, Radiative Transfer (London: Oxford University Press), pp. 24-35, 1950.

76. B. Morrison, U. S. Naval Obs. Circular No. 92, 1962 and No. 94, 1964.

77. G. B. Field, Private Communication, 1964.

78. J. W. Warwick, Ap. J., 137, 1317, 1963.

79. A. T. Moffet, Ph. D. Thesis, Calif. Institute of Technology, 1961.

80. G. Kuiper, The Atmospheres of the Earth and Planets, ed. G. Kuiper, U. of Chicago Press, pp. 306-405, 1952.

81. J. N. Douglas and H. J. Smith, Nature, 199, 1080, 1963.

82. A. G. Smith, G. R. Lebo, N. F. Six, Jr., and T. D. Carr, Ap. J., 141, 457, 1965.

83. J. W. Warwick, Ap. J., 137, 41, 1963.

84. G. R. A. Ellis and P. M. McCulloch, Aust. J. Phys., 16, 380, 1963.

85. E. K. Bigg, Nature, 203, 1008, 1964.

86. G. A. Dulk, A. J., 70, 137, 1965.

87. E. K. Bigg, Private Communication, 1964.

88. J. R. Dickel, Paper presented at AAS meeting, March 1965.

89. J. L. Lawson and G. E. Uhlenbeck, Threshold Signals (M.I.T. Radiation Lab Series), Chap. 7, 1949.